Micro-CT and Micro-FE Analysis of Stress Transfer of Femoral Stems

Fanxiao Liu

SIGILL. UNIVERSITAT. LUDOVIC. MAXIM.

München 2021

Aus der Klinik und Poliklinik für
Orthopädie, Physikalische Medizin und Rehabilitation

Klinik der Ludwig-Maximilians-Universität München

Vorstand: Prof. Dr. med. Dipl.-Ing. V. Jansson

Micro-CT and Micro-FE Analysis of Stress Transfer of Femoral Stems

Dissertation
zum Erwerb des Doktorgrades der Medizin
an der Medizinischen Fakultät der
Ludwig-Maximilians-Universität zu München

Vorgelegt von

Fanxiao Liu
aus
Shandong

Jahr
2021

Mit Genehmigung der Medizinischen Fakultät der Universität München

Berichterstatter:	Prof. Dr. med. Peter E. Müller
Mitberichterstatter:	Prof. Dr.med. Stefan Piltz PD Dr. med. Lucas Geyer
Mitbetreuung durch die promovierten Mitarbeiter:	Dr. techn. Yan Chevalier
Dekan:	Prof. Dr. med. dent. Reinhard Hickel
Tag der mündlichen Prüfung:	21.01.2021

To my family

Eidesstattliche Versicherung

Liu Fanxiao

Name, Vorname

Ich erkläre hiermit an Eides statt,

dass ich die vorliegende Dissertation mit dem Thema

Micro-CT and Micro-FE Analysis of Stress Transfer of Femoral Stems

selbständig verfasst, mich außer der angegebenen keiner weiteren Hilfsmittel bedient und alle Erkenntnisse, die aus dem Schrifttum ganz oder annähernd übernommen sind, als solche kenntlich gemacht und nach ihrer Herkunft unter Bezeichnung der Fundstelle einzeln nachgewiesen habe.

Ich erkläre des Weiteren, dass die hier vorgelegte Dissertation nicht in gleicher oder in ähnlicher Form bei einer anderen Stelle zur Erlangung eines akademischen Grades eingereicht wurde.

22.01.2021 Shandong	Fanxiao Liu
Ort, Datum	Unterschrift Doktorandin/Doktorand

Table of Contents

1 Background

1.1 Motivation

While hip arthroplasty is still the gold standard for the treatment of pain and function of patients with end-stage arthritis and femoral head necrosis (Learmonth et al., 2007), long-term behavior of implantation remains challenging due to polyethylene wear, with resultant osteolysis and/or aseptic loosening (Berry et al., 2002). Initial primary stability is necessary for uncemented femoral stems in order to ensure bone ingrowth and secondary stability, which is crucial in the long-term behaviors of these implants.

The implant design and metaphyseal fit are decisive factors of primary fixation stability of cementless hip stems (Malchau et al., 1997). A femoral implant should ideally maintain the physiological load distribution in the proximal femur; however, the metallic stem inserted into the femur alters its natural stress distribution that may lead to bone resorption, which is detrimental to mechanical stability (Jayasuriya et al., 2013; Stucinskas et al., 2012). Femoral stem press-fit fixation depends on optimal proximal fit and stress transfer for long-term function (Stiehl, 1993). The implantation of a metallic stem may result in the shaft bone fractures at the tip of the femoral stem and the possible migration of femoral stems. Moreover, in some cases, it was seen that even small geometrical differences in stem designs (such as between Taperloc and Excia® T) might have an impact on fixation, or induce increased risks of periprosthetic fractures right after implantation. These concerns motivated research work by our collaborators and further involved us in the development of appropriate methodologies.

In particular, biomechanical tests can help quantify migration for different designs, but lack the capabilities to assess primary contact interface or risks of fractures at implantation. Recently, high resolution numerical models have been proposed to evaluate the fixation of implanted devices such as screws (Steiner et al., 2017; Steiner et al., 2015; Wirth et al., 2011) and bone anchors (Chevalier, 2015; Sano et al., 2013; Yan, 2019) in trabecular bone. Some of these models rely on the use of micro finite element (μFE) analyses, based on μCT scanning, that allow an accurate representation of bone microstructures and their interfaces with the implant (Chevalier, 2015; Steiner et al., 2017; Torcasio et al., 2012; Wirth et al., 2011). These methods not only provide alternatives, reducing the need for the invasive mechanical testing and replacing it with computational biomechanics to simulate in-vivo bone-loading conditions, but also give the chance to assess bone strength through non-invasive methods, thus reducing the cost, time, and number of experiments. To our knowledge, such methods have yet to be used to quantify implant-to-bone contact surface of implanted femoral stems and to evaluate their internal load transfer. Therefore, this project is the first to use high-resolution micro-CT-based technology to evaluate the contact properties and bone tissue stresses around femoral stems.

1.2 Thesis outline

This thesis starts with an introduction that describes the anatomy of the hip joint and current procedures for hip arthroplasty, methods of finite element analysis. This is then followed by the objectives and hypotheses of this study, then the required material and methods, presentation of results and an overall discussion.

2 Introduction

This chapter mainly focused on the anatomy of the hip joint, current procedures for hip arthroplasty, the modular structure of the artificial hip joint implants, and the osseous integration of cementless total hip arthroplasty (primary and secondary stability), as well as the stress shielding and stress transfer of cementless total hip arthroplasty. Meanwhile, this part also describes the characteristics of finite element analysis (finite element model, types, creation of process, and the micro-FE analysis using micro-CT image), to provide general information about the methodologies used in this doctoral work.

2.1 Anatomy of a Healthy Hip Joint

The hip joint, called articulation coxae in anatomy, is a ball-and-socket joint which is the second largest weight-bearing joint in the body. The hip joint forms the connection between the thighbone (femur) and the acetabulum. The acetabulum is a cup-shaped socket or concave surface in the pelvis consisting of the ilium, ischium and pubis that provides a resting place for the rounded head of the femur (femoral head) and allows free rotation of the femur. In a healthy hip joint, the surfaces of the femoral head and acetabulum are composed of a durable layer of articular cartilage, whose principal function is to provide a smooth, lubricated surface for articulation and to facilitate the transmission of loads with a comparatively low friction coefficient (Roache, 2012; Sophia Fox et al., 2009) (**Figure 1**).

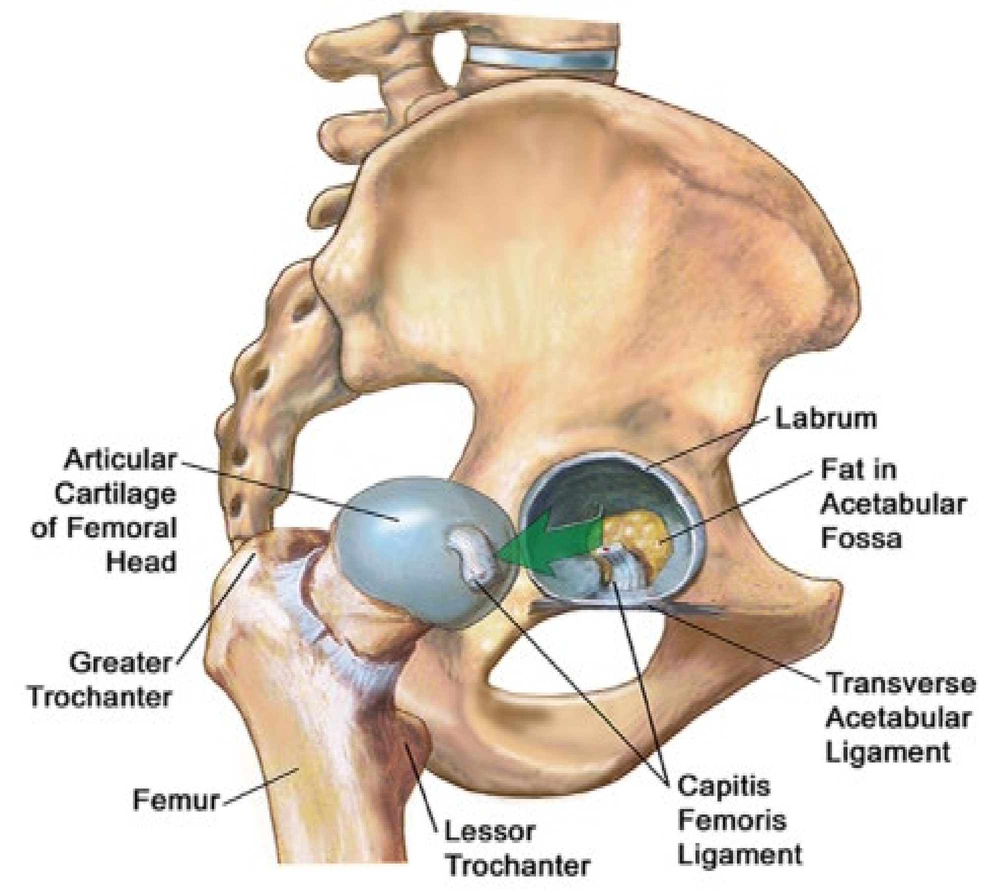

Figure 1. Diagrammatic sketch of a normal hip joint (Roache, 2012)

The hip joint capsule is composed of the fibrous membrane and synovial membrane, which nourish and lubricate the joint, thereby providing better conditions for a high range of movement (Schünke et al., 2015). The tremendous stability of a healthy hip joint relies not only on the fit between the femoral head and the acetabulum but also on the strong ligaments around a healthy hip joint, including the iliofemoral ligament and pubofemoral ligament in the anterior of the hip joint and the ischiofemoral ligament in the posterior of the hip joint (**Figure 2**), as well as multiple muscles (**Figure 3**), including the gluteal muscles, quadriceps, iliopsoas, hamstrings and groin muscles, which generate the pronation, extension, adduction, abduction, and internal and external rotation of the hip (Lumen, 2008; Roache, 2012; Whittle, 2003).

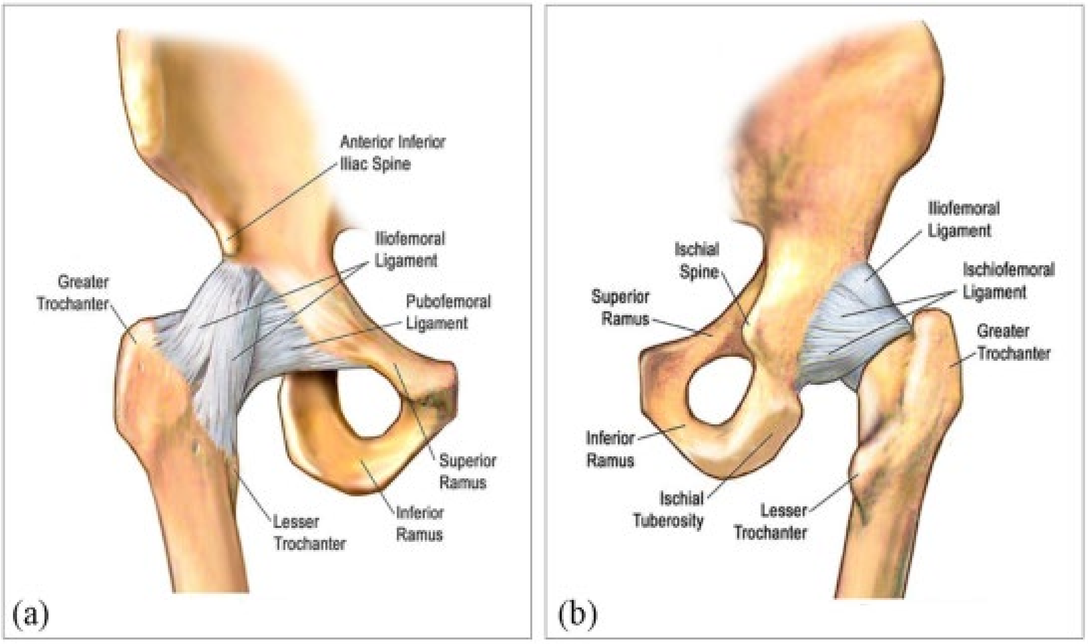

Figure 2. Diagrammatic sketch of the ligaments around a healthy hip joint (Roache, 2012)

(a) Diagrammatic sketch of a right hip joint in an anterior view;

(b) Diagrammatic sketch of a right hip joint in a posterior view.

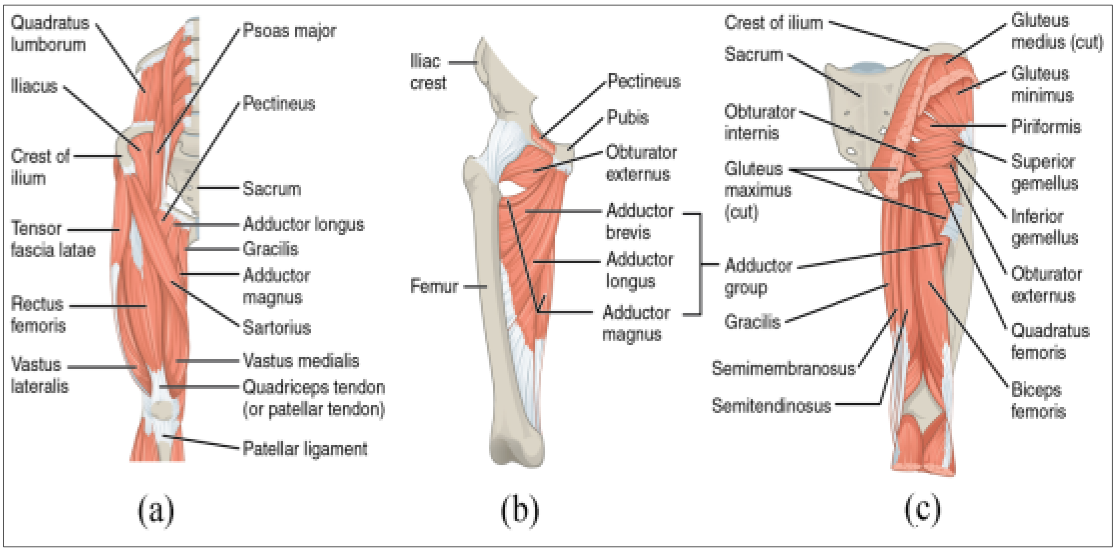

Figure 3. Diagrammatic sketch of the muscles around hip joint (Lumen, 2008)

(a) Anterior view of superficial pelvic and thigh muscles of right leg;

(b) Anterior view of deep pelvic and thigh muscles of right leg;

(c) Posterior view of pelvic and thigh muscles of right leg.

2.2 Hip Osteoarthritis

The hip joint is a frequent site for osteoarthritis (Abate et al., 2008). As a result of the increase in life expectancy, the incidence of hip osteoarthritis has progressively increased and has become one of the major causes of disability in the elderly people (Jordan et al., 2009; Kim et al., 2014; Oliveria et al., 1995; Woolf et al., 2012). Hip osteoarthritis is a slowly evolving process characterized by the degradation and destruction of articular cartilage, narrowing of the joint space, and the formation of osteophytes, subchondral sclerosis, and bone spurs (Dallari et al., 2016; Sokolove and Lepus, 2013) (**Figures 4 and 5**). These characteristic changes resulting from hip joint osteoarthritis often lead to the exposure of subchondral bone and bone-on-bone friction that impede the physiological function of the hip due to pain, stiffness, and physical function and neuromuscular pattern deterioration (Dawson et al., 2004; Steultjens et al., 2000, 2001; Tsertsvadze et al., 2014). Therefore, hip osteoarthritis is a prevalent and costly chronic musculoskeletal condition that imposes a significant global burden ((Bennell et al., 2014; Cross et al., 2014).

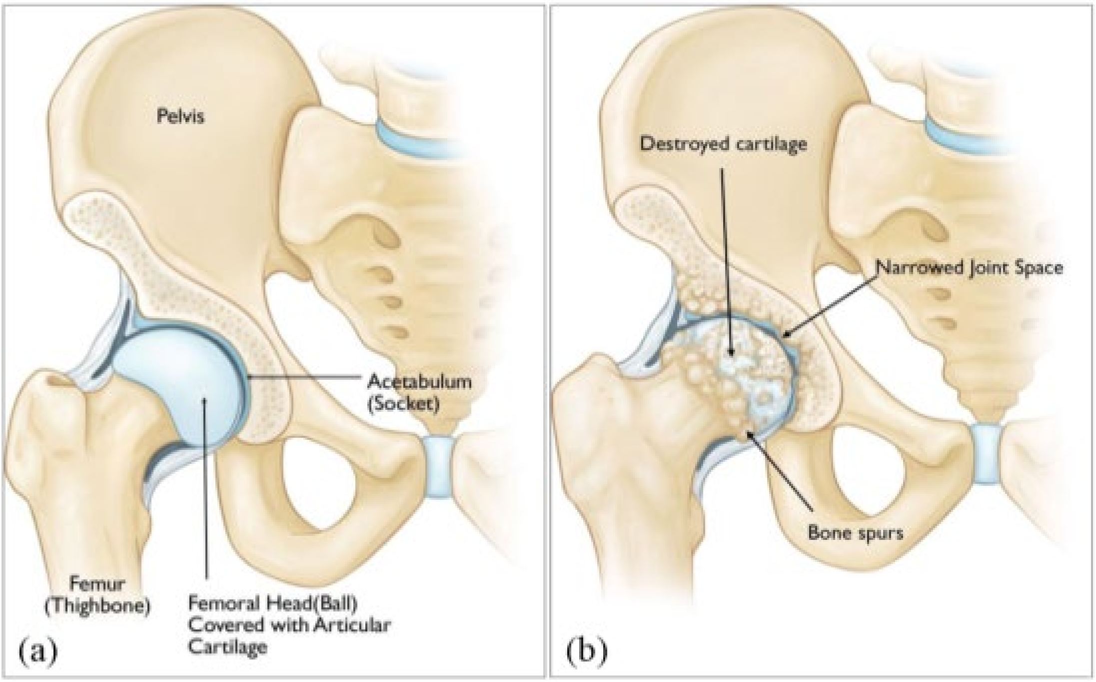

Figure 4. Diagrammatic sketch of a healthy hip joint and an arthritic hip joint (OrthoInfo, 2019)

(a) Diagrammatic sketch of a healthy hip joint indicates the healthy cartilage and the normal joint space between femoral head and acetabulum;

(b) Diagrammatic sketch of a hip joint with osteoarthritis indicates the destroyed cartilage, bone spurs, narrowed joint space between femoral head and acetabulum.

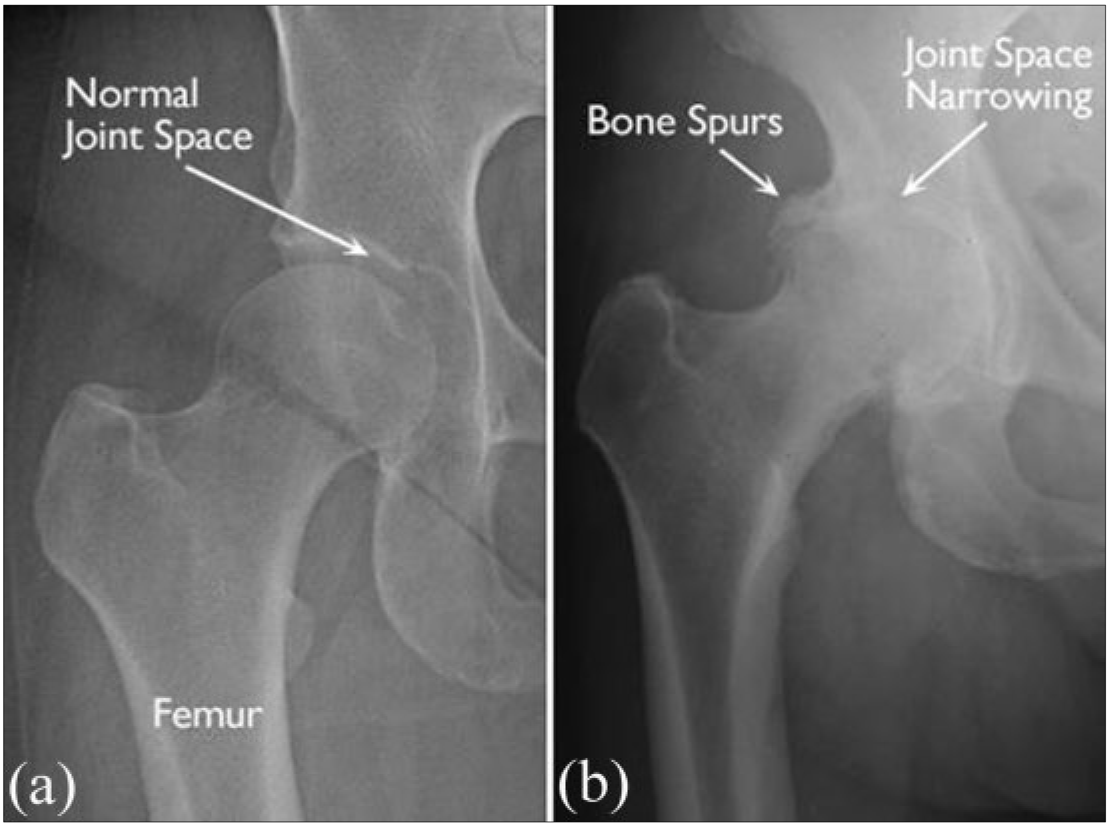

Figure 5. Clinical X-ray imaging of a normal hip joint and a hip joint with osteoarthritis (OrthoInfo, 2019)

(a) Clinical X-ray imaging of a healthy hip joint indicates the healthy cartilage and the normal joint space between femur and acetabulum;

(b) Clinical X-ray imaging of an arthritic hip indicates the destroyed cartilage, bone spurs and the severe narrowing of hip joint space between femur and acetabulum.

2.3 Artificial Hip Arthroplasty

Artificial hip arthroplasty is defined as the surgical procedure that replaces the femoral head and/or acetabulum damaged by hip disease or trauma using artificial devices (Steinberg et al., 1999). Hip arthroplasty is often divided into total hip arthroplasty (THA) and hemiarthroplasty (Mariconda et al., 2017). The main difference between these two surgical procedures is that THA replaces both the femoral head and acetabulum using an artificial device, whereas hemiarthroplasty replaces only the femoral head (Nichols et al., 2017).

Surgical indications of artificial hip arthroplasty include primary or secondary osteoarthritis, aseptic necrosis of the bone (femoral head necrosis), trauma (femoral neck fracture, traumatic hip arthritis), rheumatoid hip arthritis, benign and malignant bone tumours of the femur bone, and ankylosing spondylitis (Kabukcuoglu et al., 1999; Lee et al., 2017; Pang et al., 2013; Pyda et al., 2015; Stirton et al., 2019; Wang and Bhattacharyya, 2017; Yuasa et al., 2016).

In recent decades, artificial hip arthroplasty has developed into a reliable surgery procedure, and the therapeutic effectiveness of this technique has been fully confirmed through long-term follow-up analyses in clinical practice (Ancelin et al., 2016; Hemmila et al., 2019; Ravi et al., 2019). While hip arthroplasty is treated as gold standard for pain relief and functional recovery in patients with end-stage arthritis and femoral head necrosis (Learmonth et al., 2007), the long-term behaviour of implantation remains challenging due to many complications after implantation. One complication in THA is aseptic loosening; however, the underlying mechanisms of aseptic loosening are very complicated. At present, a view accordant with present-day ideas is that abrasive particles generated from polyethylene wear at the prosthesis interface are the dominant factors, followed by stress shielding after implantation. Both of these factors result in osteolysis and bone absorption and ultimately lead to the failure of artificial hip joint replacements (Berry et al., 2002).

In Germany, primary hip arthroplasty is one of the most frequent surgical procedures: approximately 230,000 of these procedures are performed each year. In addition, more than 53,000 hip revision surgeries are performed each year, which imposes a significant socio-economic burden (Statistisches Bundesamt, 2005 to 2016) (**Figure 6**).

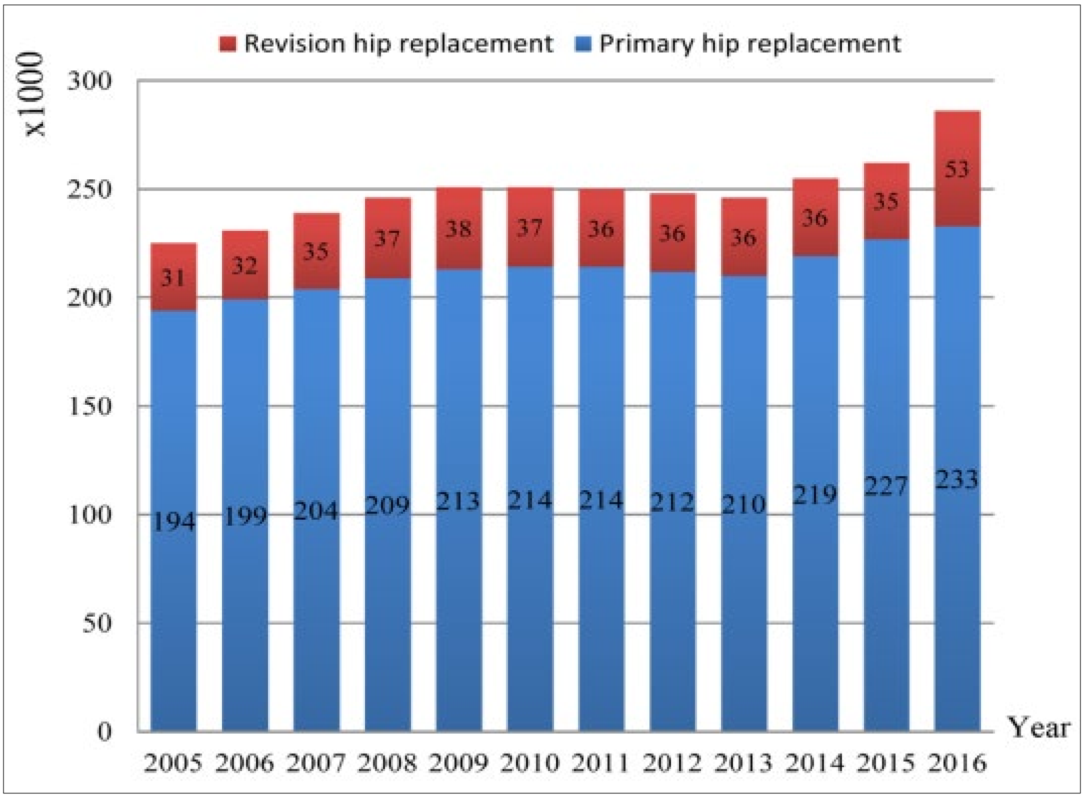

Figure 6. Data of hip joint replacements in Germany (Statistisches Bundesamt, 2005 to 2016)

2.4 Modular Structure of the Artificial Hip Joint Implants

The artificial hip joint implants in THAs usually consist of a femoral stem, a femoral head and an acetabular cup, which includes a liner (inlay) and an acetabular shell (**Figure 7**). A femoral stem, typically made of cobalt-chromium-molybdenum or titanium alloy, was inserted into the proximal medullary cavity of the femur, providing great support for the femoral head and complete mechanical conduction for the hip joint. The femoral head, which is usually made with metal or ceramic materials (e.g., Co-Cr-Mo-cast alloys (stainless steel), alumina and zirconia), connects the femoral stem and acetabular shell and provides a bearing surface for the artificial hip joint. The acetabular shell, which is usually made from the same materials listed above, is fixed to the pelvic acetabulum. The liner, made of polyethylene, ceramic and metal, is located inside the shell, thereby providing another bearing surface for the artificial hip joint.

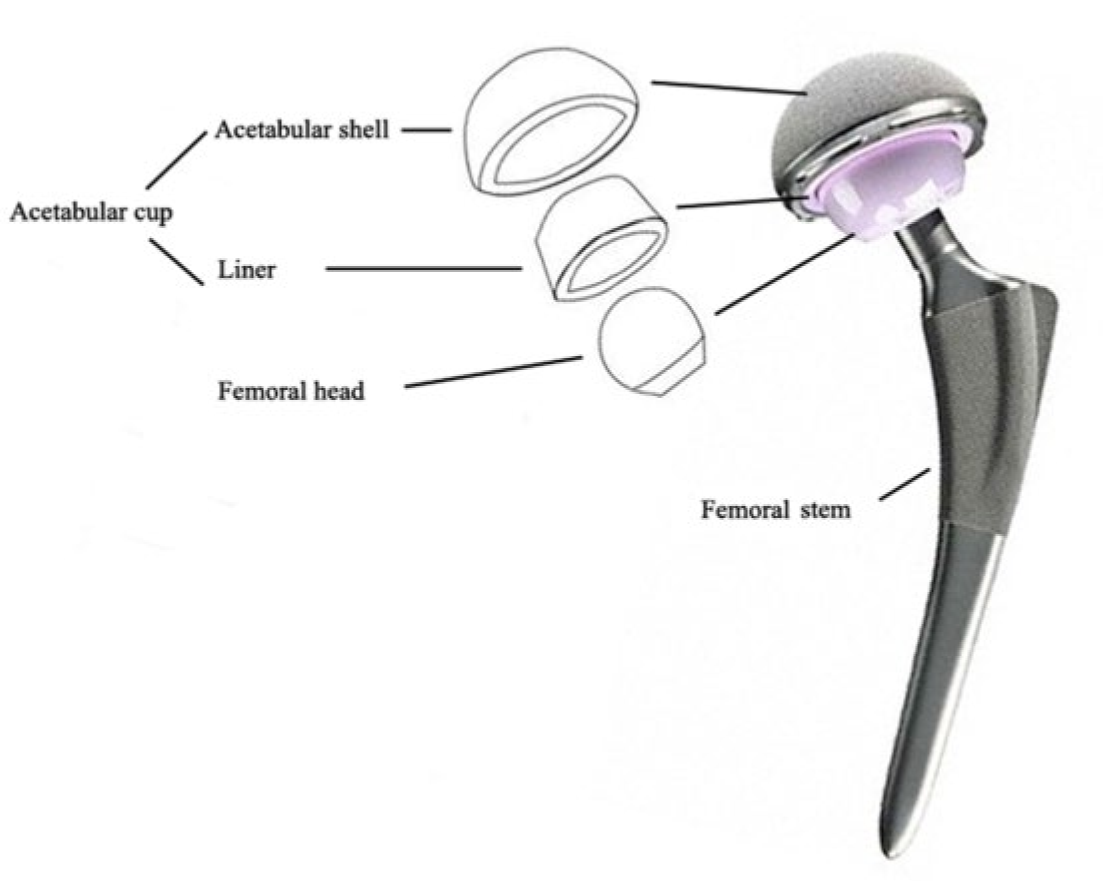

Figure 7. Diagrammatic sketch of the structure of artificial hip joint prosthesis (Yan, 2019)

2.5 Cemented and Uncemented Total Hip Arthroplasty

The underlying mechanical interlocking of the fixation between a patient's hip endoprosthesis and bone (femur and acetabular bone) has a strong influence on the service life of hip joint prosthesis. Cemented and uncemented fixation methods are commonly used in THA (Rolfson et al., 2016; Schmidler, 2018) (**Figure 8**). The cemented fixation method relies on a well-known fast-handeuring 'bone cement' based on polymethylmethacrylate (PMMA), which is a rigid thermoplastic material, to achieve ultimate stability directly after implantation (Limongi et al., 2016). In 1961, Dr. John Charnley first introduced PMMA into hip arthroplasty operations (Charnley, 1961). Although the cemented fixation method creates important disadvantages of osteolysis association with cement disease, such as inflammation, fillers and allergies (Harris and McGann, 1986; Huddleston, 1988; Limongi et al., 2016), cemented fixation is still widely used for implant fixation (Jameson et al., 2015; Unnanuntana et al., 2009) because it can provide ultimate stability directly after implantation and has reliable clinical effectiveness on long-term follow-up (Bordini et al., 2007; Smith et al., 2012; Unnanuntana et al., 2009).

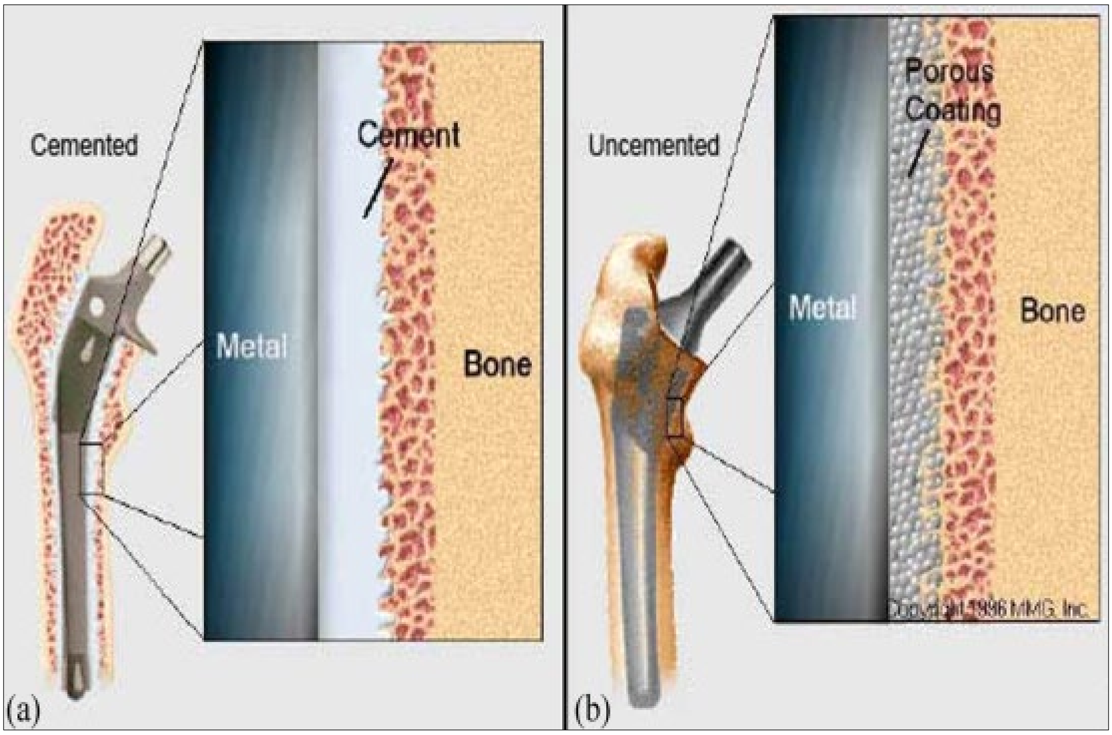

Figure 8. Diagrammatic sketch of cemented and cementless THA (Schmidler, 2018)

(a) Cemented THA;

(b) Cementless THA.

In contrast to cemented hip endoprosthesis that achieves ultimate stability directly after implantation with the direct help of PMMA, cementless hip endoprosthesis relies on its mechanically press fit and lock between the implant and bone for primary stability and the biological osseous integration of the implant for secondary stability (Ruben et al., 2012, Yan, 2019).

The uncemented femoral stem, which is typically made of titanium alloy, has a variety of geometrical designs and prosthesis surface layers (Kim and Yoo, 2016). To achieve permanent stability, the surface of the femoral stem is often coated with titanium pure or hydroxyapatite (HA), which is an osteoinductive and osteoconductive material that stimulates and allows bone ingrowth. HA, which largely consists of calcium and phosphorous, has great biocompatibility and can form excellent bone bonding with bone tissue, which is beneficial to the fixation of implants and femurs. Hence, HA is commonly used as a synthetic bone substitute to promote osseointegration between bone and various orthopaedic implants, such as hip, knee and dental implants. A prospective study (Tudor et al., 2015) involving 219 patients was conducted to compare porous and HA-coated sleeves of a modular cementless femoral stem (SROM) in THA, and the results demonstrated that both HA-coated and porous sleeves had excellent long-term outcomes. Numerous studies (Aksakal et al., 2014; Garcia Araujo et al., 1998; Soballe et al., 1993) have demonstrated that HA coatings precipitate strong osseointegration in a short period of time and have shown faster pain relief and bone ingrowth, thereby reducing the recovery period in patients with implant replacements. The use of uncemented stems with HA coatings has produced good clinical and radiological results that were well supported in three other studies regarding long-term follow-up (Capello et al., 2006; Geesink, 2002; Lazarinis et al., 2011).

Multiple published studies have attempted to quantitatively compare the effectiveness, survival time and revision rates of uncemented and cemented femoral stems in primary hip replacements; however, the results of such studies remain inconclusive. Two studies confirmed that THA using cement or cementless methods had higher survival times and similar revision rates (Smith et al., 2012; Unnanuntana et al., 2009). A multivariate survival analysis involving a total of 4,750 primary THAs demonstrated that the type of prosthesis was the only factor that affected survival time of implants and can be amended, which was partially in disagreement with studies reporting that cemented femoral stems were used more often than cementless ones (Bordini et al., 2007).

In contrast, Hailer et al. conducted a study comparing uncemented with cemented primary THAs using the evaluations of 170,413 operations from the Swedish Hip Arthroplasty Register, and the results showed that cementless THA had a lower survival time than cemented THA due to the relatively worse performance of cementless acetabular cups (Hailer et al., 2010). A pooled analysis of 50,968 primary THAs from the Finnish Arthroplasty Registry revealed that in patient's ≤ 55 or ≥ 75 years old, there were no significant differences regarding the long-term survival between uncemented and cemented THAs; whereas in patients 55-74 years old, the survival of uncemented THA was superior to that of cemented THA (Makela et al., 2008).

Due to the versatility of materials and designs for artificial hip prostheses, each design and material has its own characteristics and exhibits its own advantages and disadvantages under different conditions, which indicates no single implant is suitable for all patients with hip diseases. Hence, it is still impractical to define which fixation method is better for the final clinical decision. To make a final decision, clinical orthopaedic surgeons need to consider their own experience along with various conditions, such as the characteristics of various prostheses and the age and needs of the patients, including anticipation, service life, activity level, body mass, hip joint bone quality, and surgical history.

However, with the development of the surgical techniques and improvements in the materials and designs of implants, cementless hip prosthesis has become increasingly popular over the past few years (Belmont et al., 2008; Engh et al., 2002; Khanuja et al., 2011; McNally et al., 2000; Meding et al., 2004; Meding et al., 2000; Streit et al., 2013).

2.6 Cementless Femoral Stem Prosthesis

Although conventional straight stem femoral prostheses exhibited several undesirable side effects, such as resultant osteolysis and/or aseptic loosening, bone loss and proximal stress shielding (Berry et al., 2002; Brown et al., 2002; Bugbee et al., 1997; Engh et al., 2003; Stukenborg-Colsman et al., 2012), numerous published studies confirmed their excellent clinical outcomes at short-, mid- or long-term follow-ups (Bordini et al., 2007; Dolhain et al., 2002; Giliberty, 1983; Hozack, 1998; Keisu et al., 2001a; Khanuja et al., 2011; McGrory et al., 1995; McLaughlin and Lee, 2008; Parvizi et al., 2004) (**Figure 9**).

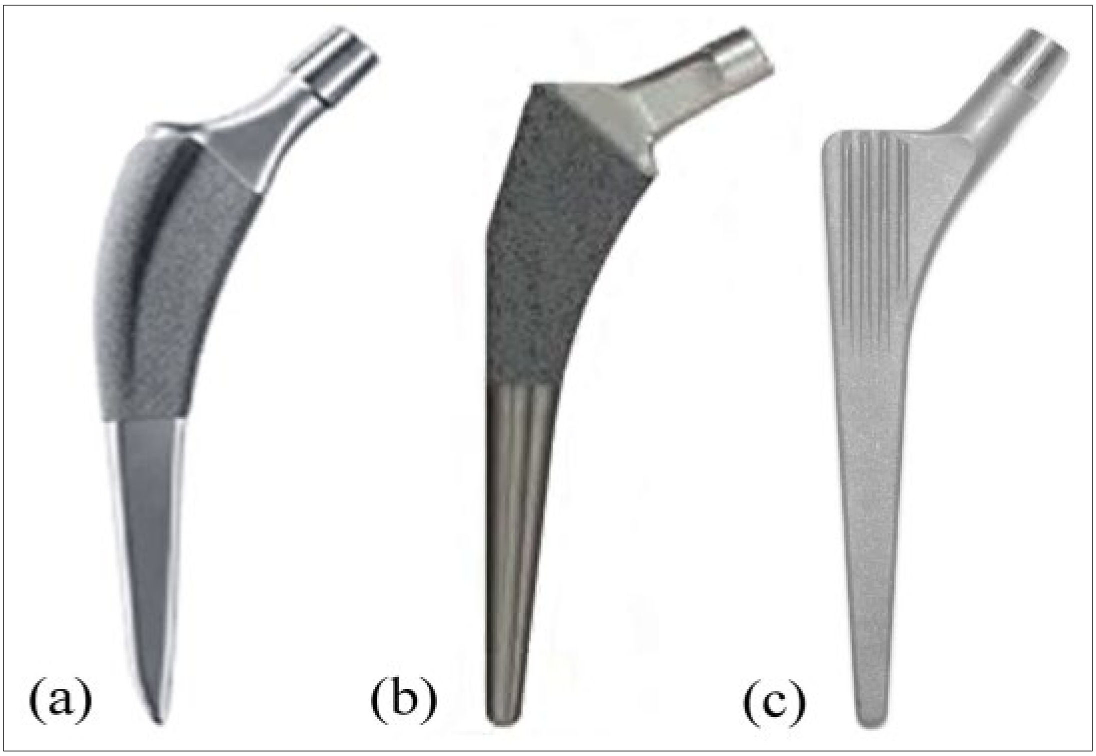

Figure 9. Examples of several commonly used standard straight-stem femoral implants in a front view

(Aesculap Implant Systems, 2015; Biomet, 2013; Yan et al., 2017)

(a) Excia® T Standard Hip Stem Prosthesis (Aesculap, Germany);

(b) Taperloc® Complete Hip Stem Prosthesis (Zimmer, USA);

(c) CLS Spotorno Hip Stem Prosthesis (Zimmer, USA).

The Taperloc® cementless hip stem was designed using a titanium substrate with the following features: wedge-shaped, straight, collarless and proximally circumferential titanium porous plasma sprayed. It took a long time for the Taperloc® hip stem to be used as a clinically referenced hip stem with proven good long-term clinical outcomes for rheumatoid arthritis, obese and non-obese patients, patients 50 years old or order, and patients 80 years old or order (Dolhain et al., 2002; Giliberty, 1983; Hozack, 1998; Keisu et al., 2001a; McGrory et al., 1995; McLaughlin and Lee, 2008; Parvizi et al., 2004).

The Excia® T Standard Hip Stem has many advanced features such as a minimal rounded shoulder design that provides probability for bone conservation, a microporous Ti-plasma rough coating for secondary stability of cementless hip stem, and the dual-taper combined with proximal flanges design, which reduces the difficulty of the THA procedure for clinicians.

Recently, short stem femoral implants have gained increasing popularity because they can meet the growing demand for bone conservation at the proximal part of the femur, provide substantial physiological stress transfer, and give a chance for revision with a standard stem (Falez et al., 2008; Khanuja et al., 2011; Morrey, 1989; Schmidutz et al., 2012; Tahim et al., 2012; Yan, 2019). Commonly used short femoral stems including Metha®, Fitmore® and Nanos®, have been introduced into clinical environments with reliable survival at long-term follow-up (Kaipel et al., 2015; Khanuja et al., 2014; Morrey, 1989; Morrey et al., 2000; Pipino, 2004; Pipino et al., 2000; Schnurr et al., 2017; Toni et al., 2017; van Oldenrijk et al., 2014; Yan, 2019) (**Figure 10**).

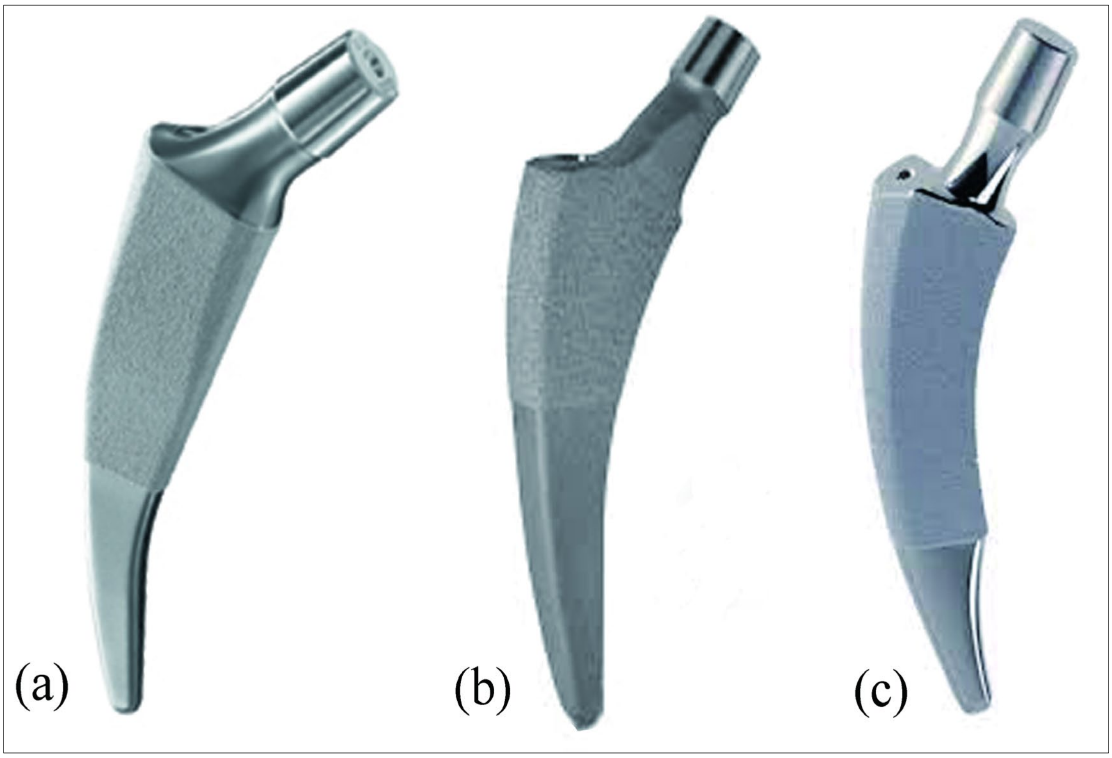

Figure 10. Examples of several commonly used short-stem femoral implants in a front view (Acklin et al., 2016; Brinkmann et al., 2017; Gustke, 2012)

(a) Metha Short-stem Hip Prosthesis (Aesculap, Germany);

(b) Fitmore Short-stem Hip Prosthesis (Zimmer, USA);

(c) Nanos Short-stem Hip Prosthesis (Smith & Nephew, UK).

2.7 Osseous Integration of Cementless Total Hip Arthroplasty

The process of osseointegration is a key point for the survival of uncemented femoral stem prostheses and can be distinguished as two main steps: primary stability and secondary stability. First, the initial primary stability of uncemented femoral stem prostheses is achieved by relying on their mechanically press fit and lock between the implant and the bone (Ostbyhaug et al., 2010). The initial primary stability provides a steady environment for bone ingrowth, which is necessary and crucial to the long-term behaviour of a cementless femoral implant. The secondary stability of cementless femoral stem prostheses, also called biological osseous integration, is obtained when new bone gradually grows into the implant-bone interface, which is the area between the bone and an artificial stem (Ruben et al., 2012). To achieve good long-term implant survival, an indispensable prerequisite for biological osteogenesis is adequate primary stability with little movement at the bone-implant interface (Jasty et al., 1997; Pilliar et al., 1986).

2.7.1 Primary Stability of Cementless Femoral Stem Prosthesis

In contrast to cemented hip endoprosthesis, which achieves ultimate stability directly after implantation, the primary stability of cementless hip endoprosthesis relies on the underlying mechanical interlocking of the femoral stem by press-fitting into the proximal femoral cavity. The metaphyseal fit and implant geometrical design are decisive factors of primary fixation stability of uncemented femoral stems, and these factors directly affect the long-term survival rate of uncemented femoral stems (Malchau et al., 1997). An ideal implant should maintain the natural stress distribution in the proximal part of the femur; however, after implantation, the artificial femoral stem could affect the physiological load distribution, which would result in damage to mechanical stability by regional bone resorption (Jayasuriya et al., 2013; Stucinskas et al., 2012). Insufficient primary fixation stability of a cementless femoral stem may result in the formation of a fibrous membrane between the femoral stem and the femoral bone, preventing the process of bone ingrowth and consequently leading to main failure of fixation or implant loosening (Jasty et al., 1997; McKellop et al., 1991; Pilliar et al., 1986; Yan, 2019) (**Figure 11**).

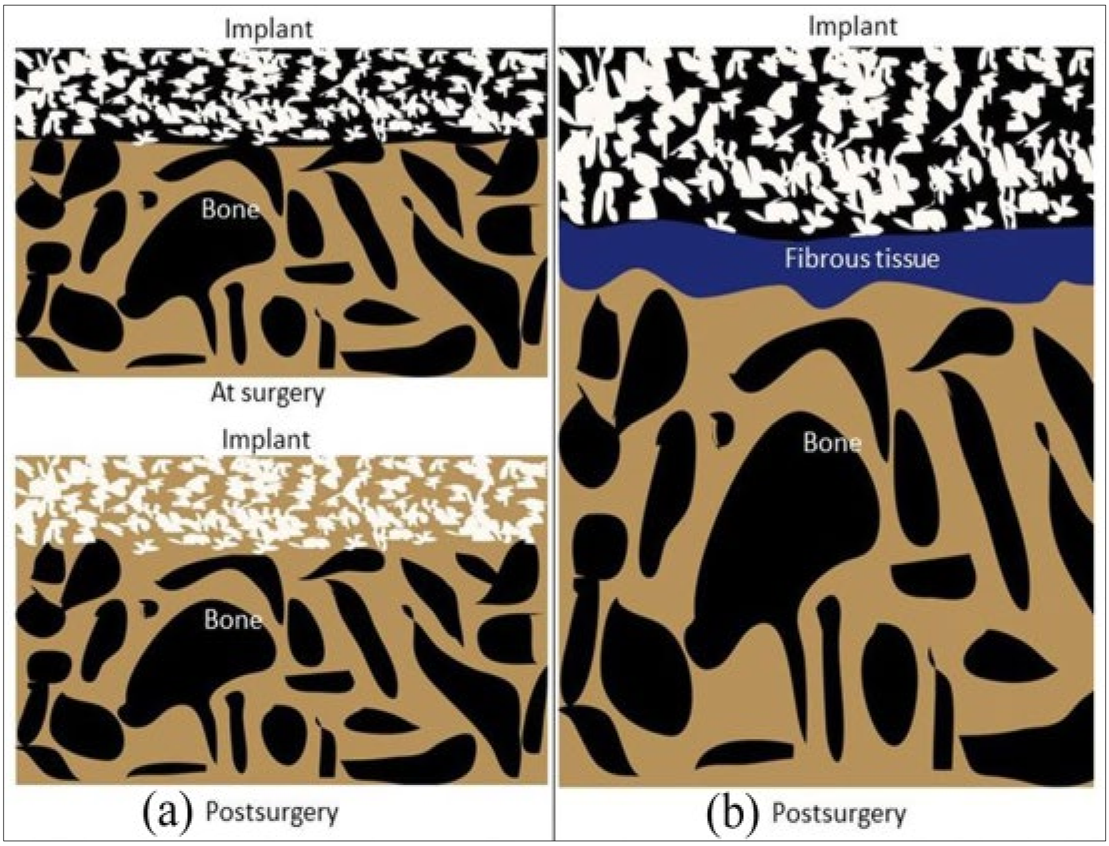

Figure 11. Diagrammatic sketch of osseous integration at the implant-bone interface (Yan, 2019)

(a) After implantation, the newly formed bone grows into the porous structure of the artificial femoral stem;

(b) After implantation, the formation of a fibrous membrane around the femoral stem prevents the process of bone ingrowth and consequently lead to the failure of fixation or implant loosening

After the artificial prosthesis is subjected to vertical or rotating loads, the inducible movements at the bone-implant interface are defined as micromotions (Burke et al., 1991). Micromotion is the permanent movement of the artificial femoral hip prosthesis relative to the femur. Several studies confirmed that micromotion with a value of 28 μm between the implant interface and host bone was compatible with the process of osseous integration. Small amounts of micromotions were reported to be a must for bone ingrowth. However, reversible micromotions exceeding 150 μm lead to the generation of a fibrous membrane around the femoral stem, which is harmful for bone ingrowth and finally results in the failure of osseous integration (Bragdon et al., 1996; Isaacson and Jeyapalina, 2014; Jasty et al., 1997; Pilliar et al., 1986; Soballe et al., 1992a; Soballe et al., 1992b).

2.7.2 Secondary Stability of Cementless Femoral Stem Prosthesis

Secondary stability refers to the osseous integration between the uncemented femoral stem and femur bone and cannot be achieved if insufficient primary stability is obtained. Therefore, secondary stability is essential for successful osseous integration after implantation (Westphal et al., 2006; Yan 2019).

2.8 Stress Shielding and Stress Transfer of Cementless THA

The forces on the hip are mainly composed of partial body weight force (BWF), abductor muscle force (AMF) and hip joint contact force (JCF) (Dickinson et al., 2010; Roache, 2012; Yan, 2019) (**Figure 12**).

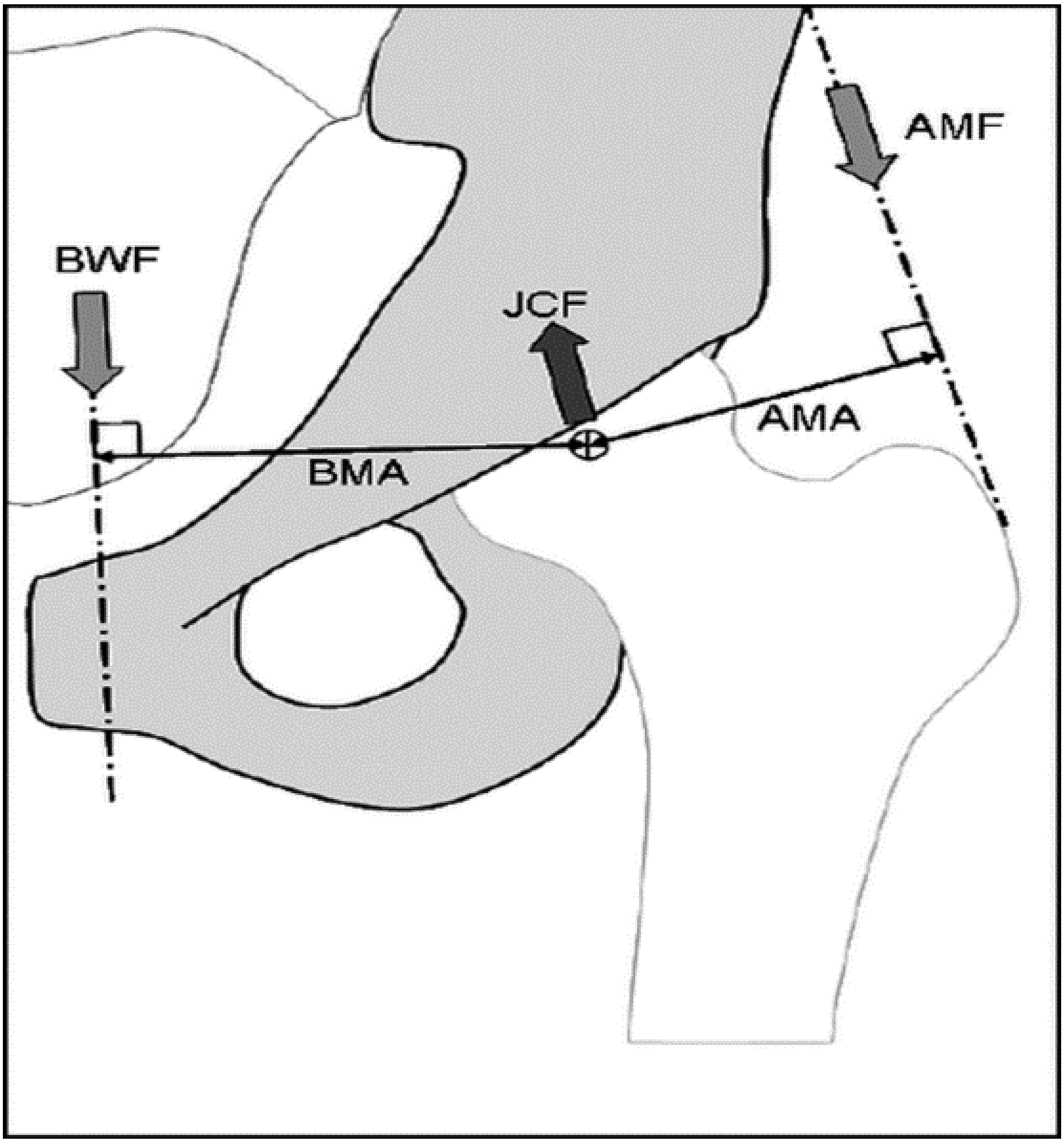

Figure 12. Diagrammatic sketch of different forces on the femoral head (Dickinson et al., 2010)

AMA, abductor moment arm; AMF, abductor muscle force; BMA, body weight moment arm; BWF, body weight force; JCF, joint contact force.

These forces on a healthy femoral head are transmitted through the femoral neck and intertrochanteric region to the regional cortex bone in the proximal part of the femur. The normal stress distribution in the proximal part of the femur can be altered after implanting a stiffer femoral hip prosthesis (Arifin et al., 2014; Jayasuriya et al., 2013;

Stucinskas et al., 2012) (**Figure 13**). Glassman et al. noted that the proximal bone of the femur was shielded or protected from loading after implantation surgery (Glassman et al., 2006). The phenomenon where stress transfer through that bone is reduced after implantation is known as stress shielding (Ibrahim et al., 2017; Ridzwan et al., 2007). This phenomenon occur because of Wolff's law (Wolff, 1886), which was developed by a German anatomist and surgeon named Julius Wolff. Wolff's law is a theory that bone in a healthy person or animal will remodel in response to changes in corresponding loads. If the loads on a part of the bone decrease, the bone will remodel itself to become thinner and weaker because of insufficient stimuli required for continued bone remodeling; likewise, if the loading on a part of the bone increases, the bone will become stronger and thicker to bear the increased loading (Frost, 1994; Ruff et al., 2006). Stress shielding seems to be impacted by the fixation methods (e.g., cemented or cementless fixation), material properties (e.g., contact surface), the stem designs (e.g., geometry and length), and individual patient-related factors (Aamodt et al., 2001; Enoksen et al., 2016; Ruben et al., 2012; Wilkinson et al., 2003).

Numerous studies have evaluated the stress distribution using experiments (Bieger et al., 2012; Decking et al., 2008; Fottner et al., 2009; Gronewold et al., 2014; Schmidutz et al., 2017; Westphal et al., 2006) or finite element (FE) methods (Pettersen et al., 2009). A biomechanical study was reported to record the stress distribution of composite femurs, and the results demonstrated that the highest stress reduction in a composite femur implanted with an uncemented femoral stem was achieved in the lesser trochanter (Schmidutz et al., 2017). Bieger et al. (Bieger et al., 2012) measured the stress distribution in the proximal part of a series of paired fresh human femurs using strain gauge rosettes to compare femoral stems with different geometrical designs and lengths. A prospective study revealed that changes in cortical stress before implantation and up to one year after implantation in 20 patients allowed for the prediction changes in periprosthetic BMD in the proximal part of the femur (Decking et al., 2008).

A biomechanical study noted that increasing the stem length of a femoral prosthesis could reduce the stress in the proximal part of the femur while increasing the stress in the distal part of the femur after implantation (Arno et al., 2012). A recent study proposed a contradictory opinion that the stress transfer at the proximal part of a femur implanted with cementless stems was affected by the underlying anatomy rather than the stem geometry (Schwarz et al., 2018). Femoral stem press-fit fixation depends on optimal proximal fit and stress transfer for long-term functionality (Stiehl, 1993). An experimental study using 12 cadaveric femurs with a hip simulator confirmed that load transfer in the proximal femur of an uncemented stem was overall equal to that of a cemented stem under single-leg or stair-climbing conditions when the stems had similar geometrical designs (Enoksen et al., 2017).

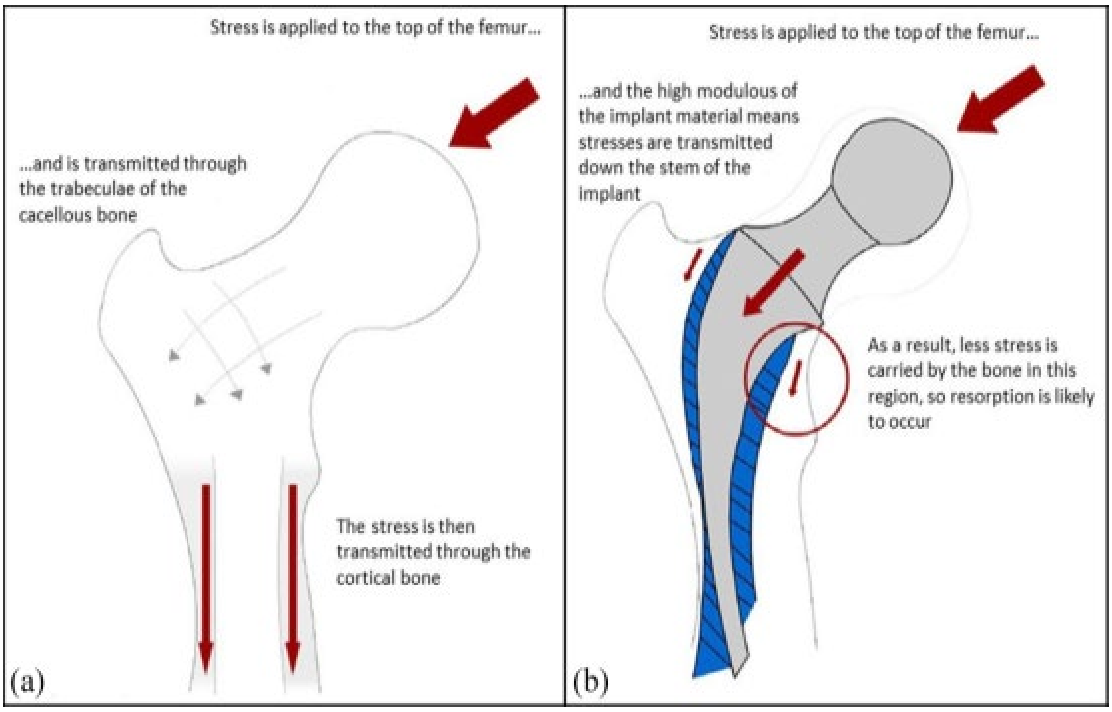

Figure 13. Diagrammatic sketch of the stress transfer in the proximal part of a healthy femur and the femur implanted with hip joint prosthesis (Arifin et al., 2014)

(a) Diagrammatic sketch of the stress transfer in the proximal part of a healthy femur;

(b) Diagrammatic sketch of the stress transfer in the proximal part of the femur implanted with a hip joint prosthesis.

2.9 Finite Element Analysis

FE analysis (FEA) is a numerical modeling method used to analyse products and systems built in a virtual environment to find and resolve possible (or existing) structural or performance issues by using mathematical approximations to simulate real physical systems (geometry and load cases). The basic principle of the FEA method is to discretize the continuous solution area of a research object into a finite set of interconnected units, simulate the solution area with different geometrical shapes, and then perform mechanical analysis on the units.

As a mathematical or numerical analysis approach, FEA is widely used to solve complicated structural, fluid and multiphysics issues of engineers and scientists by dividing a complex structure into many simple interacting elements (i.e., units) that can precisely represent the geometry of targeted objects. Hence, FEA yields approximate solutions rather than exact solutions by breaking down an actual complicated issue into many simpler problems. However, it is not easy to produce an accurate solution from multiple practical complicated problems. The advantage of the FEA method is that it can represent the total solution and achieve local effects by calling an adaptable definition of different material characteristics under various complex conditions (Reddy, 2006; Yan, 2019). Because of the excellent performance of FEA in the analysis of the physical properties of complex matters, the FEA method has been rapidly expanded from the analysis and calculation of structural engineering strength to almost all fields of science and technology (Keyak et al., 1990; Skinner et al., 1994; Yan, 2019).

FEA is a reliable method for evaluating and optimizing various geometrical designs and materials and improving the properties of products; moreover, the use of FEA could reduce the number of physical prototypes needed during product development and the time and material consumption of testing. In recent years, with the improvement of computer functions and the maturity of this technology, many people have used FE methods for mechanical analyses of hip joints, and multiple studies (Korhonen et al., 2005; Nadzadi et al., 2002; Radcliffe et al., 2007; Yan, 2019) have verified the practicality and scientific merits of FEA by comparing experimental and clinical results with the predicted outcomes obtained from FEA.

2.9.1 Types of FEA

To simulate various complete conditions, many types of FEA methods are commonly used, including linear statistics, nonlinear statistics and dynamics, normal mode, dynamic response, bending, and heat transfer. Among these types of FEA, linear and nonlinear statistics are often used in the field of Orthopaedics (Yan, 2019). Linear-elastic analysis obviously cannot be used to calculate the strength of bone as it is an anisotropic material with constitutive behavior and the initial conditions will be changed when simulating the actual failure process. Recent development and improvement of computer power and efficient solvers have made it possible to perform nonlinear analyses that provide better bone strength predictions than linear-elastic analyses (Arbenz et al., 2008; Christen et al., 2013; MacNeil and Boyd, 2008a; Yan, 2019).

2.9.2 Finite Element Model

An FE model includes the material and structural properties, the FE mesh formed by multiple nodes and different elements, such as triangular, tetrahedral or hexahedral elements (Yan, 2019). In the field of medicine, FE modeling of human bone can be created using medical scanning images involving computed tomography (CT) or magnetic resonance imaging (MRI).

CT-based FEA models typically based on bone microstructure (Lang, 2010) were developed and applied to CT images of skeletal structures to noninvasively investigate the stiffness and strength of bone from a patient (Keyak, 2001; Niebur et al., 2000; van Rietbergen et al., 1998). Keaveny et al. noted that advancements had been achieved in FEA models of vertebra created from section dimensions of CT images on the order of millimeters; however, no advancements were reported in the proximal femur (Keaveny et al., 2007). Two studies reported that in vivo imaging of bone microstructure was achieved via MRI (Chang et al., 2014; Han et al., 2015) which had been applied for the creation of an FEA model (Chang et al., 2014). A three-dimensional (3D) hip model (Akrami et al., 2018) of the entire pelvis and femur was generated from MRI scans of a healthy patient to analyse the various loads applied in the femoral head, and this FE model can be used as a new method to simulate THA with the minimum recurrence of dislocations and discomfort, and providing more available range of movement (ROM).

In addition to MRI, in vivo imaging of the bone microstructure was also achieved via micro-computed tomography (micro-CT). Scans from micro-CT or μCT, which is also called high-resolution CT (HRCT), produce data of targeted objects that can be processed into cross-sections using X-rays, and then a series of imaging can be used to reconstruct virtual 3D models without destroying the original objects (Dame Carroll et al., 2006; Duan et al., 2013; Hu et al., 2016). In the early 1980s, the first X-ray micro-CT images published by Jim Elliott were reconstructed slices of a small tropical snail, wherein the pixel size was approximately 50 micrometers (Elliott and Dover, 1982). The high-resolution images of presently available micro-FE analyses will significantly improve the quality of FEA (van Rietbergen, 2001).

2.9.3 Finite Element Modeling Steps

The FE modeling in this study includes the following steps: the creation of 3D models based on the geometrical design of bones, meshing of the models, assignment of various material properties (e.g., cortical bone, cancellous bone and artificial implants), and definition of boundary conditions and loading physiological forces. The use of high-quality medical scanning images to generate an FE model will provide more geometrical information during the modeling process. The density and quality of the FE mesh depends on the expected change in stress levels in a particular region. Regions with large stress variations typically require higher grid densities than regions with little or no stress change. The quality of the mesh step has a major influence on the precision of the final solution and convergence (Yan, 2019). The density of a mesh will directly influence the precision of the final solution but has to be limited to a reasonable number because of the limited time for calculation and random access memory (RAM) of computers.

For the definition of material properties, which mainly involve the Young's modulus and Poisson's ratio, implant elements were assigned based on the typical properties of Ti, whereas bone elements were attributed properties based on the bone site and bone types, as reported by previous published studies (Abdul-Kadir et al., 2008; Chevalier et al., 2009; Hengsberger et al., 2002; Mazza et al., 2008; Reggiani et al., 2008; Yan, 2019). According to the requirements of a real-world work environment, an FEA model will be applied with different loads involving nodal loads (e.g., force, moment, displacement, velocity and acceleration), base loads (e.g., distributed loads and pressure) and acceleration body loads (gravity).

2.9.4 Evaluation Indexes of FEA

In the medical field, the results calculated by the solver usually involve in nodal displacement, velocity and acceleration as well as natural forces, strain and stress.

2.9.4.1 Stability Measures of Total Hip Arthroplasty in FEA

Although numerous methods (Hefzy and Singh, 1997; Reggiani et al., 2007; Yan, 2019) are commonly used to measure the primary stability of THA through complex and expensive biomechanical settings with linear variable differential transformers (LVDTs) in biomechanical studies, these methods are still limited because they focus on a few special points. Fortunately, FEA provides the feasibility to investigate the primary stability of THA and the detailed information pertaining to the micromotions of the entire structure; moreover, the final results of FEA can be validated by biomechanical methods (Dammak et al., 1997; Hefzy and Singh, 1997; Reggiani et al., 2007; Tarala et al., 2011; Whiteside et al., 1993; Yan, 2019). Two studies confirmed the reliability of FEA for the measurement of micromotions at the bone-implant interface by comparing their results with experimental data (Hefzy and Singh, 1997; Reggiani et al., 2007; Yan, 2019). In addition, a biomechanical study (Reggiani et al., 2007) compared peak micromotion data from experiments and an FEA model and found that the error of the model was only 7%, indicating that FEA can accurately predict the primary stability of cementless stems.

Although it is common knowledge that the secondary stability is essential to the long-term behaviour of cementless femoral stems, to our knowledge, no experimental method have been proposed for the direct evaluation of 3D micromotions at the interface between bone and femoral stem. It seems impossible to measure the secondary stability of uncemented femoral stem using an experimental setting. Unlike the primary stability of uncemented femoral stems, several FEA studies have focused on the investigation of secondary stability and may make it possible. An FEA study (Orlik et al., 2003) using the homogenization technique was performed by Orlik et al. to measure secondary stability, and demonstrated that the frictional coefficient and normal contact surface were found to be most important parameters for secondary stability because these two parameters increased when the new bone grew into the femoral stem interface, thereby providing stronger secondary stability and reduced micromotions. Another biomechanical FEA study provided a purely numerical model of osseointegration and revealed clinically meaningful results (Viceconti et al., 2004).

2.9.4.2 Stress Transfer of Total Hip Arthroplasty in FEA

In addition to the assessment of primary and secondary stability of artificial femoral stems, FEA has also been used to measure local stress distributions in the proximal part of femurs before and after implantation.

In 1987, Rohlmann et al. constructed a 3D FEA model to investigate the impact of the essential aspects involving the length and elastic modulus of artificial stems on the stress distributions in cemented femoral hip endoprosthesis, and their results showed that the stem length had only a minor impact on the stress distribution, whereas the elastic modulus had a considerable influence (Rohlmann et al., 1987).

For cementless femoral stems, Huiskes et al. discussed the applicability of 3D FEA models in numerical theory of trabecular bone remodeling coupled with the issue of stress shielding and cortical bone remodeling (Huiskes et al., 1987). Rohlmann et al. created a geometrically simplified FEA model assuming both rigidly bonded and nonlinear interfaces to measure stress transfer between femoral stem prosthesis and a femur (Rohlmann et al., 1988). Another FEA study explored the influence of muscle forces on the strain distribution around the femoral stem, and the results indicated that ignoring muscle loads can lead to a considerable overestimation of strains (Duda et al., 1998).

Several studies were reported to systematically compare subject-specific FE models of femurs with experimental assessments. A combined numerical-experimental study involving eight cadaveric proximal femurs was conducted to compare strains predicted with the FE method to those obtained experimentally using strain gauge measurements under six different loading scenarios (Schileo et al., 2007). The study confirmed that the density-elasticity relationship had a strong impact on the accuracy of numerical predictions (Schileo et al., 2007).

Compared with experimental measurements of human cadaveric femurs before and after implantation using uncemented femoral stems under single-leg stance or stair-climbing configuration, the FE models were found to successfully reproduce the experimentally observed stress shielding (Pettersen et al., 2009; Yan, 2019). A good agreement of the stress shielding in total hip replacements between FEA and experiments was found in five other studies (Anderson et al., 2005; Barker et al., 2005; Gupta et al., 2004; Taddei et al., 2006; Weinans et al., 2000). Thus, these studies concluded that subject-specific FEA had good accuracy in the prediction of the stress distribution around the femoral stem.

2.9.4.3 Apparent Bone Density (BV/TV)

Bone quantity (tissue density), which is usually presented using bone density (g/cm^3), and bone quality, which reflects the natural properties, including the geometrical design, cortical bone thickness and trabecular microstructure, are the primary determinants of the mechanical integrity of bone (Alomari et al., 2018; Seeman, 2008; Seeman and Delmas, 2006). Several non-destructive and non-invasive in vivo methods have been put into practice, such as dual-energy X-ray absorptiometry (DEXA), which is widely used to evaluate bone density using BMD (Kanis and Johnell, 2005; Rachner et al., 2011; Schneider, 2013) and X-ray quantitative CT (QCT) to separately analyse cortical bone and trabecular microstructure (Bouxsein and Seeman, 2009; Guglielmi and Lang, 2002; Miller et al., 1999). In vitro micro-CT is known as the gold standard for the measurement of trabecular bone structure with a voxel size of 100 μm (Ruegsegger et al., 1996). However, standard 3D parameters (e.g., cortical thickness, trabecular microstructure, and geometrical design) (Dempster et al., 2013; Hildebrand et al., 1999; Hildebrand and Ruegsegger, 1997; Kabel et al., 1999; Laib et al., 2002; Muller et al., 1994; Odgaard, 1997; Odgaard and Gundersen, 1993; Parfitt et al., 1987) are used to evaluate the elastic properties of bone with limited values (Uchiyama et al., 1999).

Bone volume fraction (BV/TV) and various morphological variables from the output of a micro-CT analysis performed on human bone are potential determinants of the mechanical properties of trabecular bone. BV/TV, which is usually reported as a percentage value, is defined as the bone volume (BV) divided by total volume (TV). BV/TV is probably the best known index accessible via micro-CT, and this index indicates the fraction of a given volume of interest (VOI) occupied by mineralized bone (i.e., the BV). The specimen source (e.g., human, rat, rabbit and dog), bone type, bone geometry and bone status, and sample location (i.e., location within a bone) will affect the final calculation of BV/TV. Therefore, there is no doubt that the appropriate selection of the TV plays a key role in the calculation of BV/TV. BV/TV can be used to evaluate the effectiveness of anti-osteoporosis drugs by calculating relative changes in BV density and to determine the integration of implants into bone.

Two studies demonstrated that axial and plate BV/TV is better than BV/TV alone for determining the elastic and yield properties of trabecular bone (Liu et al., 2008; Zhou et al., 2014). Ding et al. suggested that BV/TV is the single most important parameter in describing the trabecular microstructure (Ding et al., 1999). A recent study analyzed a total of 743 cubic trabecular bone samples using micro-CT imaging, and the results revealed that the BV/TV was a better determinant of the trabecular microstructure than other morphological variables (Maquer et al., 2015).

2.9.4.4 Contact Surface at Bone-Implant Interface in THA

The contact area between the implant and host bone is called the bone-implant interface. Numerous studies (animal and human experiments) had investigated the risk factors for the implant stability, such as the femoral stem geometrical design and length, bone-to-implant contact ratio, bone-implant contact location, relative trabecular bone quality and density (Alsaadi et al., 2007; Meredith et al., 1996; Nkenke et al., 2003; Schliephake et al., 2006; Sennerby and Meredith, 2008; Yan, 2019). Insufficient direct contact at the bone-implant interface was identified as one of the main risks for the instability of implants by Viceconti et al. (Viceconti et al., 2006). Reimeringer and Nuno (Reimeringer and Nuno, 2016) noted that both the contact ratio and contact location at the bone-implant interface contributed to the primary stability of uncemented femoral stems.

2.10 Micro-Finite Element Analysis

The accuracy of FE model prediction relies on not only the appropriate definition of parameters, including the contact area, nodes, elements, frictional coefficient and interface fit but also the medical scanning image quality (Abdul-Kadir et al., 2008; Viceconti et al., 2001; Viceconti et al., 2000; Yan, 2019). Recently, high-resolution numerical models generated from 3D medical techniques, such as peripheral quantitative CT (HRpQCT) and MRI with high field intensity, have been proposed to assess the healing state of distal radius fracture (de Jong et al., 2014; Meyer et al., 2014) and to assess the implant stability of artificial devices, such as screws and bone anchors (Chevalier, 2015; Chevalier et al., 2018; Sano et al., 2013; Steiner et al., 2017; Steiner et al., 2015; Wirth et al., 2011; Yan, 2019). Some of these models demonstrated the association of implant stability with the local microstructure in trabecular bone tissue (Basler et al., 2013; Walker et al., 2011). Micro-FEA models are created by using medical 3D images with sufficiently high resolution to derive bone properties and microstructures, provided highly detailed information for the definition of the geometry.

A large number of studies based on the assessment of isolated bone tissues have investigated and confirmed the accuracy of the micro-FE method on analyzing the stiffness and strength of bone (Christen et al., 2013; MacNeil and Boyd, 2008a, b; Mueller et al., 2011; Pistoia et al., 2002, 2004). Moreover, several studies (Burghardt et al., 2013; Ellouz et al., 2014; MacNeil and Boyd, 2008b; Paggiosi et al., 2014) have evaluated the reproducibility of micro-FEA outcomes even though biomechanical studies were performed based on human cadaveric bones that provided more natural information. Several factors regarding misalignment and calibration errors, micromotions and other errors due to the image analyses by various implementers may have important impacts on the actual reproducibility of micro-FEA outcomes. However, for the micro-FEA outcomes involving the stiffness and strength of radius and tibia samples, these single-center studies indicated relatively low overall rates of errors (3.6% - 4.4% error in stiffness and 2.3% - 3.7% error in strength).

To date, numerous validations studies (Mueller et al., 2011; Pistoia et al., 2004; Varga et al., 2010) have revealed that when compared with the standard experimental measurements, the results of micro-FEA on the prediction of bone failure load were better than those of any DEXA or other bone density-based parameters. Micro-FEA has been introduced as a widely used tool to derive the stiffness and strength of bone tissue as well as the stresses and strains of bone in biomedical studies (Chevalier, 2015; Niebur et al., 2000; Steiner et al., 2017; Torcasio et al., 2012; van Rietbergen et al., 1995; Wirth et al., 2011; Yan, 2019).

Micro-FEA methods not only provide an alternative testing method that reduces the need for invasive mechanical testing by replacing such techniques with computational biomechanics to simulate in-vivo bone-loading conditions but also enable the assessment strength of bone using non-invasive methods, thereby reducing the cost, time and number of experiments. To our knowledge, such methods have yet to be used to quantify internal stress transfer around femoral stems in association of local bone density and the implant-to-bone contact area at their interfaces.

3 Purposes and Objectives of the Study

The present research aims to investigate the fixation characteristics of femoral stems using micro-CT and μFE models based on the assessment of contact area and the predicted stress transfer. To accomplish this aim, two designs of cementless femoral stems and three different coating porosities were implanted in 27 paired cadaveric specimens and scanned with an industrial nano-CT scanner. From these scans, a sub-selection of 3 paired images was converted to micro-FE models to provide a quantification of internal bone tissue stresses in simulated physiological loading conditions. This study came up from our industry partner Aesculap under the supervision of Prof. Thomas Grupp and Dr. Christoph Schilling, who wanted us to perform FEA analysis on two types of stems (Excia® T and Taperloc) to combine with experimental migration tests performed in Heidelberg (Prof J.P. Kretzer). All specimens were prepared for implantation externally and also scanned for BMD at Heidelberg. They were then scanned with a high-resolution QCT at (Prof. Hadi Mozaffari-Jovein, Furtwangen University, HFU · Faculty of Industrial Technologies, Tuttlingen). However, the creation of micro-FE model and micro-FE analysis were performed at LMU in our team. Therefore, this study mainly focused on the micro-FE analysis on the characteristics of contact ratio, regional apparent bone density and stress transfer around the femoral stem by creating the micro-FE model based on the micro-CT images.

4 Hypothesis of the Study

Our hypotheses were three-fold: 1) small differences in the geometry design can affect bone-implant interfacial contact ratio and stress transfer in the surrounding bone tissue; 2) Different surface coating porosities could affect the bone-implant interfacial contact ratio; 3) peak bone tissue stresses are correlated positively with decreasing interfacial contact and local apparent bone density around the femoral stem, but will increase the risk of fracture.

5 Materials and Methods

The preparation, implantation and scanning of specimens were conducted by external collaborators: Aesculap (Prof. T. Grupp and Dr. Christoph Schilling); Labor für Biomechanik und Implantatforschung, Heidelberg (Prof. Jan-Philippe Kretzer, Dr. S. Jäger) and Furtwangen University, HFU · Faculty of Industrial Technologies, Tuttlingen (Prof. Hadi Mozaffari-Jovein). Implantations were performed by Prof. Dr. med. Peter Aldinger (Diakonie Klinikum & Paulinenhilfe gGmbH, Stuttgart, Germany) and Prof. Dr. med. Michael Clarius (Department of Orthopaedic and Trauma Surgery, Vulpius Klinik, Bad Rappenau, Germany). This was done as part of a larger study, with our involvement in a sub-study conducted within our group under the supervision of Dr. Y. Chevalier (Project: Biomechanical assessment of stress transfer of femoral stems - a numerical study). For information about the initial material used prior to the high-resolution images that were included as the basis of our analyses, these external, preliminary steps are summarized below in sections 5.1 to 5.3.

5.1 Femoral Stem Implants

To investigate the impacts of several biomechanical characteristics, including the femoral stem geometrical design, coating porosity, implant-bone interfacial contact surface, and regional bone quality, on the predicted stress transfer through the proposed combination of micro-CT and μFE models, two cementless femoral stem designs were used for implantation in 27 paired cadaveric specimens. The Taperloc stem (Zimmer-Biomet), a long-term established proven implant design, as well as the newly developed Excia® T stem (Aesculap) were the two stems selected for the study. Both stems have comparable overall geometries, but were clinically observed in a case series by Prof. Dr. med. Peter Aldinger to differ in their fixation characteristics. Additionally, for the Excia® T stem, three different coating porosities were tested to evaluate how these affect primary contact interface after implantation.

5.1.1 Excia® T Standard Femoral Stem

The Excia® T Standard Femoral stem (B. Braun, Aesculap, Tuttlingen, Germany) is available with two designs: cemented and uncemented fixation (**Figure 14**). This study used the uncemented femoral stem, which is made of titanium alloy (Ti6Al4V) and coated with pure titanium Plasmapore® μ-CaP.

To meet a growing demand for bone conservation, the Excia® T Standard Hip Stem was designed with a minimal rounded shoulder and lateral wingless design, which can decrease disruption of the greater trochanter through a minimally invasive implantation. To accurately restore joint biomechanics with an uncemented femoral stem and achieve long-term survival, the Excia® T Standard Hip Stem was developed with a dual tapered design and proximal flanges to achieve good primary stability after implantation; furthermore, and the coating surface of the femoral stem using microporous Ti-plasma to ensure the secondary stability of biological osseointegration.

Figure 14. Excia® T Standard femoral stems (Aesculap Implant Systems, 2015)

(a) Excia® T femoral prosthesis with plasmapore;

(b) Excia® T femoral prosthesis without plasmapore.

5.1.2 Taperloc® Hip Stem

The Taperloc® stems (Zimmer Biomet, Warsaw, Indiana 46581 USA) were adopted in this current study (**Figure 15**). The implant features a flat tapered wedge geometry and a proximal anchorage to enhance proximal offloading and bone preservation; when coupled with the insertion hole, these features provide good primary and rotational stability for implantation. To achieve the secondary stability of the femoral stem, this stem is made of titanium alloy (Ti6AL4V alloy) with a microporous surface and porous plasma spray (PPS) coating, which illustrated the initial scratch-fit stability and bone fixation.

The Taperloc cementless hip stem was designed using a titanium substrate with the following features: wedge-shaped, straight, collarless and proximally circumferential titanium porous plasma sprayed. It took long time for the Taperloc® hip stem to be used as a clinically referenced hip stem with proven good long-term clinical outcomes for rheumatoid arthritis patients, obese and non-obese patients, patients 50 years old or older, and patients 80 years old or older) (Dolhain et al., 2002; Giliberty, 1983; Hozack, 1998; Hozack et al., 1994; Keisu et al., 2001a; Keisu et al., 2001b; Koutalos et al., 2017; Labek et al., 2011; McGrory et al., 1995; McLaughlin and Lee, 2008, 2016; Parvizi et al., 2004).

Figure 15. Taperloc® Complete Hip stems prosthesis (Biomet, 2013).

5.2 Specimens

Twenty-seven paired "fresh frozen" human femurs were collected from 27 donors, excluding soft tissue based on a study plan and ethical vote from the University of Heidelberg. These femurs were purchased anonymously by Science Care (Science Care, Inc., Phoenix, USA). All preparations were tested for their serological safety. The exclusion criteria were previous operations on the musculoskeletal system and any signs of fracture, femur deformity and malignant lesions that might alter the bone quality. The twenty-seven paired cadaveric femurs came from 6 female and 21 male donors, and these femurs were separated into three groups (Group A, Group B and Group C) with random grouping methods. The following results were collected from the preparation of the specimens: female-to-male ratio (6:21), age (mean age = 67.8 years, range from 42.0 to 89.0 years), height (mean height = 1.72 m, range from 1.47 to 1.85 m), weight (mean weight = 92.1 kg, range from 44.5 to 145.1 kg), and body mass index (BMI) (mean = 31.7 kg/m^2, range from 13.6 to 53.3 kg/m^2). The basic information of the 27 donors regarding BMI (kg/m^2), weight (kg) and height (m) are presented in **Table 1**.

ID	Group	Age (years)	BMI (kg/m^2)	Weight (kg)	Height (cm)
C080624	A	82	15.2	46.7	1.75
C130201	A	76	35.3	117.9	1.83
C130349	A	59	32.6	112.0	1.85
C130433	A	49	40.7	136.1	1.83
C130539	A	68	36.1	117.5	1.80
C130805	A	60	19.5	63.5	1.80
S130496	A	82	24.4	81.6	1.83
S130908	A	62	39.9	108.9	1.65
C080101	A	80	14.9	44.5	1.73
C080011	B	69	38.7	118.8	1.75
C130611	B	65	53.3	145.1	1.65
C130636	B	66	47.6	117.9	1.57
S040157	B	42	50.7	117.0	1.52
L141129	B	60	27.9	90.7	1.80
L130581	B	59	33.5	108.9	1.80
L130607	B	77	26.8	79.3	1.73
L140927	B	89	13.6	45.4	1.83
C130779	B	46	19.5	45.4	1.52
L130832	C	77	21.1	72.6	1.85
L152290	C	63	32.3	90.7	1.68
L141188	C	72	43.0	136.1	1.78
L141481	C	84	33.4	72.6	1.47
L150404	C	81	37.1	104.3	1.68
L150469	C	63	14.8	45.4	1.75
L140355	C	53	44.3	113.4	1.60
L160049	C	76	27.4	81.6	1.73
L152238	C	71	31.2	72.6	1.52

Table 1. Demographic information of the 27 donors in this current study

BMI, body mass index; kg, kilogram; g, gram; cm, centimeter

Compared with synthetic bones, human cadaveric femurs are uniquely positioned for experiments, as they are more clinically relevant due to good presentation of an expected natural variation in both geometry and bone material features (cortical bone and trabecular bone). Preservation of biomechanical properties outside the experimental period is ensured by fresh frozen storage (Linde and Sorensen, 1993, Yan, 2019).

5.3 Specimen Preparation

Each specimen was identified using laboratory serial numbers (femur ID), which was combined with the following notation for further specificity: L (left) and R (right). This research was authorized by the Local Medical Research Ethics Committee. Each femur was scanned using DEXA, and femurs were eliminated if any signs of fracture, deformity or malignant lesions were detected or any sign of operations on the musculoskeletal system were identified. The preoperative BMD measurement was conducted on a Hologic QDR®-2000 X-ray-bone-densitometer (Hologic, Inc., Bedford, USA). Bone density ≤ 0.600 g/cm^2 was defined as the exclusion criterion. The results of the BMD assessment of each specimen are listed in **Table 2**. The process of specimen preparation was performed in our collaboration lab in Heidelberg, Germany.

Donor ID	Group	BMD (g/cm^2)	
		R	L
C080624	A.1	0.785	0.755
C130201	A.2	1.004	0.943
C130349	A.3	0.652	0.704
C130433	A.4	1.015	1.083
C130539	A.5	0.836	0.835
C130805	A.6	0.838	0.804
S130496	A.7	0.992	0.955
S130908	A.8	0.828	0.882
C080101	A.9	0.600	0.633
C080011	B.1	0.861	0.859
C130611	B.2	0.846	0.809
C130636	B.3	0.846	0.875
S040157	B.4	1.035	1.018
L141129	B.5	0.911	1.018
L130581	B.6	0.805	0.841
L130607	B.7	0.856	0.889
L140927	B.8	0.996	1.024
C130779	B.9	0.577	0.575
L130832	C.1	0.982	0.971
L152290	C.2	0.661	0.685
L141188	C.3	0.935	0.985
L141481	C.4	0.848	0.831
L150404	C.5	0.953	0.936
L150469	C.6	0.679	0.720
L140355	C.7	0.772	0.779
L160049	C.8	0.707	0.680
L152238	C.9	0.567	0.513

Table 2. Results from BMD measurements of each paired femurs used in this current study

BMD, bone mineral density; g, gram; cm, centimeter; R, right; L, left

Three groups (A, B, C) with n = 9 specimens each were measured in the right-left comparison (A1 *vs.* A2, B1 *vs.* B2, C1 *vs.* C2). The classification of the sample preparations into the experimental group A1 (Excia® T) *vs.* A2 (Taperloc®), group B1 (Excia® T) *vs.* B2 (Ti-Groth® 500 µm), and group C1 (Excia® T) *vs.* C2 (Ti-Groth® 700 µm) was carried out in a randomized form using a computer-generated random list (RandList 1.2, DatInf GmbH, Tübingen). This randomization process was conducted in accordance to the report "Human Preparatory Workshop 2" with a document (NO.: SA-DE13-M-5-1-04-060-2-D-EN). Statistical evaluation was performed with IBM SPSS Statistics for Windows, 22.0 Version (IBM Germany GmbH, Ehningen, Germany). For statistical evaluation, the Wilcoxon-test was conducted, wherein a two-tailed $p < 0.05$ indicated statistical significance. Their differences in the BMD were no significant in the Excia® T/Taperloc® comparison ($p = 0.383$), the Excia® T/Ti-Groth® 500 µm comparison (p = 0.844) and the Excia® T/Ti-Groth® 700 µm comparison ($p = 0.906$).

The determination of implant sizes was carried out on the basis of preoperative radiological examination, and the preoperative plan was performed with TraumaCad software (Voyant Health, 2015) (**Figure 16**). According to the instructions of manufacturer and a standardized manner, experienced surgeons (Prof. Dr. med. Peter Aldinger from Diakonie Klinikum & Paulinenhilfe gGmbH, Stuttgart, Germany; and Prof. Dr. med. Michael Clarius from the Department of Orthopaedic and Trauma Surgery, Vulpius Klinik, Bad Rappenau, Germany) performed the implantation operation for 9 pairs of femurs using either an Excia® T stem (Stem 1a, normal 350 µm porosity coating, Aesculap, Tuttlingen, Germany) or a Taperloc® hip stem (stem 2, Biomet) in the first group (n = 9 for each stem). The nine pairs of femurs in the second group were implanted with Excia® T stems (Stem 1a or Stem 1b, 500 µm porosity coating Aesculap, Tuttlingen, Germany). Similarly, the last nine pairs of femurs in the third group were implanted with Excia® T (Stem 1a or Stem 1c, 700 µm porosity coating Aesculap, Tuttlingen, Germany). All implantations were performed in our collaboration laboratory in Heidelberg, Germany.

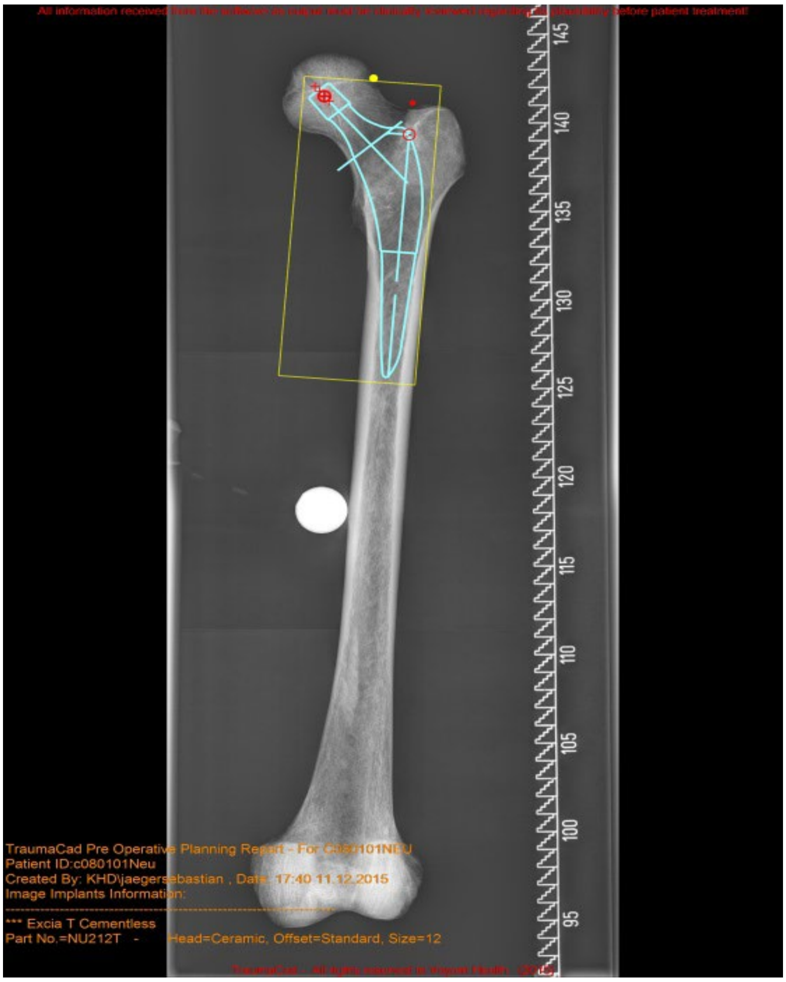

Figure 16. The preoperative plan for the determination of implant sizes was carried out on the basis of preoperative radiographs using the software TraumaCad

After implantation, the implanted femurs were scanned using a micro-CT (v | tome | x s 240, General Electrics, 160 kV, 580 µA) with an isometric resolution of 95 µm by our external collaborators (Prof. Hadi Mozaffari-Jovein, Furtwangen University, HFU · Faculty of Industrial Technologies, Tuttlingen). Due to the limitations of the physical dimensions of the scanner and the sizes of the specimens, the scanning process was performed in two parts, which were assembled after careful alignment and registration.

5.4 Finite Element Modeling Process

Figure 17 summarizes the process of the classical FE modeling. The FE models were created using the following steps:

(a) Creation of 3D models using micro-CT images of the femurs after implantation for the two femoral stem designs;

(b) Alignment of the two parts of images;

(c) Assignment of material properties;

(d) Assignment of boundary conditions.

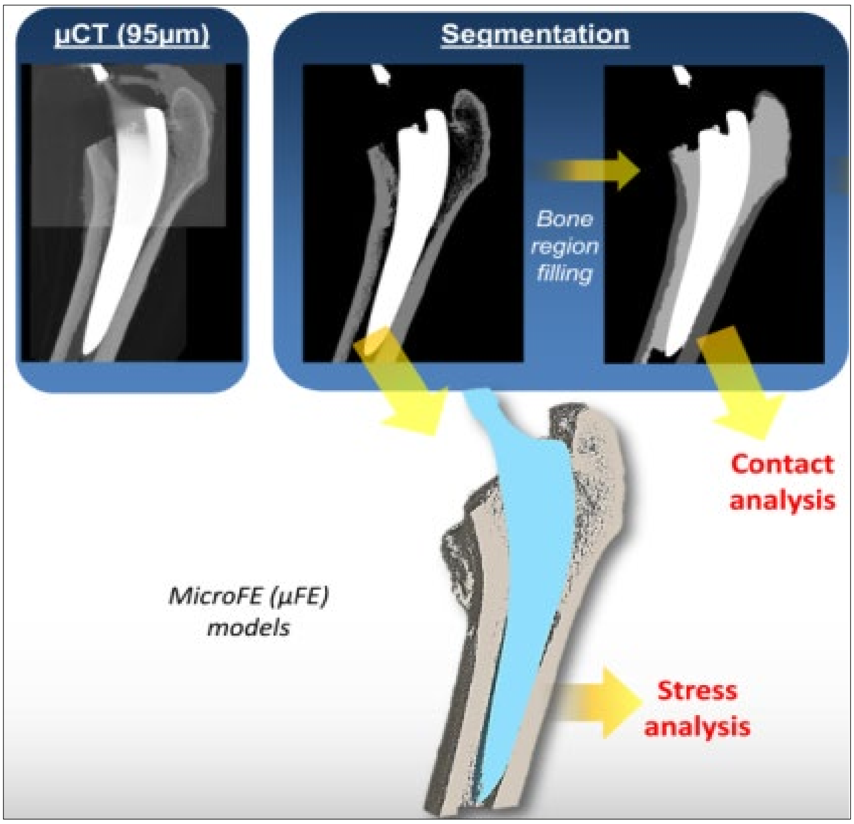

Figure 17. Flow chart summarizing the process of the contact analysis and micro FE modeling

5.5 Creation of 3D-model and Alignment of the Two Parts of Images

After scanning all specimens of the implanted femurs, a combination of Python, C++ and ITK scripts were used to align the two parts of the µCT images according to the anatomical axes and physiological loading orientation representing the position of the peak load in level walking (Chevalier et al., 2016; Heller et al., 2005; Yan, 2019) (**Figure 18**).

After finishing the alignment of the hip stems, the obtained images were carefully selected for segmentation, and the individual threshold was selected based on each specimen, which was visually adjusted to define the bone tissue and femoral stem. These µCT images were converted to the binarized images using the definition of three distinct regions including cortical bone, trabecular bone and femoral stem prosthesis. The different grey levels of the resulting composite binarized image were assigned and meshed with 8-noded hexahedral elements with 95 µm side lengths through a combination of Python and ITK scripts (Chevalier, 2015). These final images were used in the next step to define the micro-FE models of a selected amount of specimens.

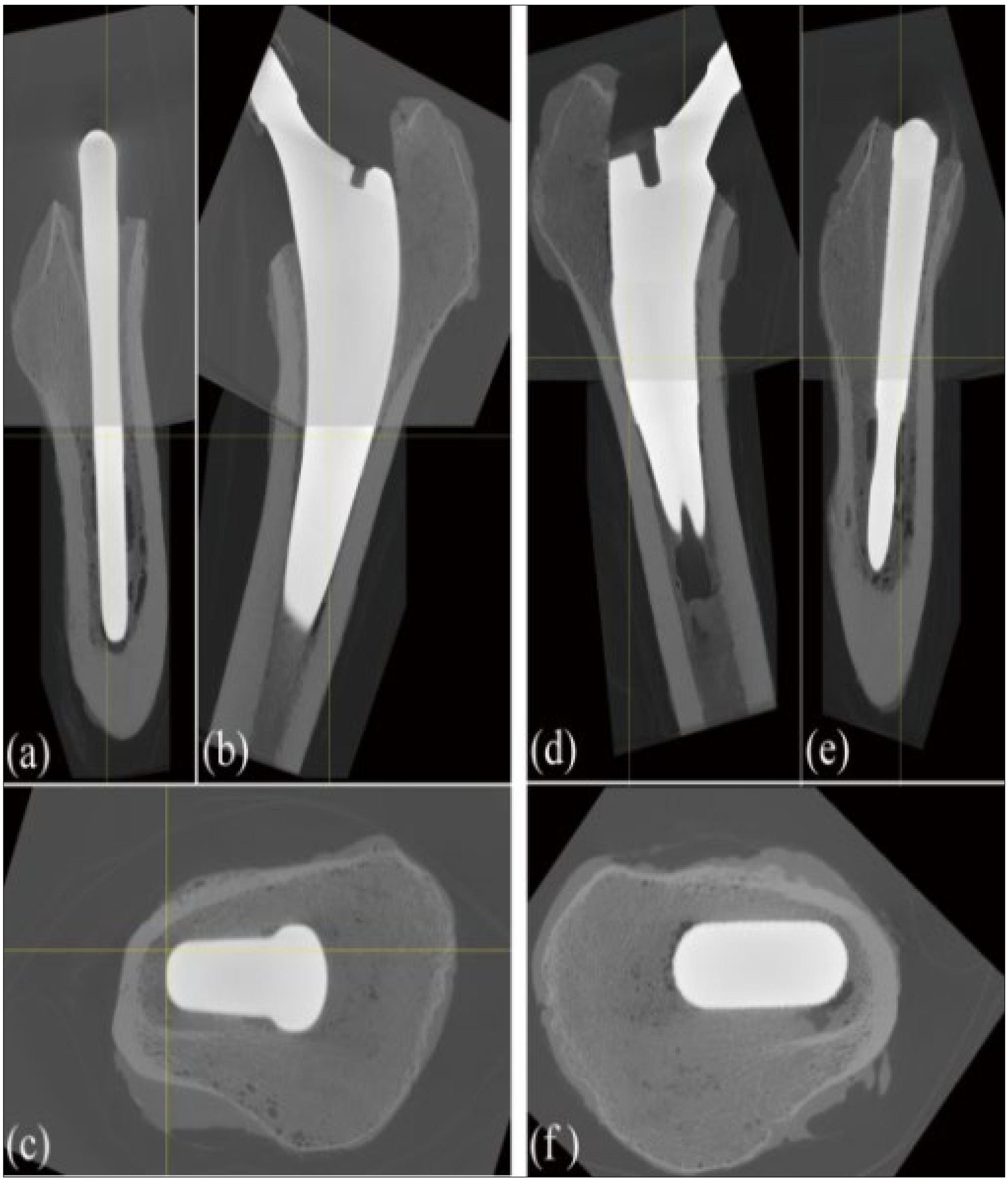

Figure 18. Assemble of the two femoral stem designs after careful alignment and registration of two parts imaging

(a) Sagittal section of a specimen implanted with the Excia® T femoral stem

(b) Coronal section of a specimen implanted with the Excia® T femoral stem

(c) Transverse section of a specimen implanted with the Excia® T femoral stem

(d) Coronal section of a specimen implanted with the Taperloc femoral stem

(e) Sagittal section of a specimen implanted with the Taperloc femoral stem

(f) Transverse section of a specimen implanted with the Taperloc femoral stem

Due to the extensive nature of the micro-FE simulations, only a limited amount of specimen pairs were included in the stress analysis study. The sub-selection of specimens for the micro-FE analyses was done based on experimental results by our collaborators. In essence, these were selected as representative specimen pairs that did not fail during dynamic loading conditions and with loading responses that were representative of the whole set of specimens. An additional selection criteria was the absence of image artifacts (such as missing bone after the final assembly of the images) that would have resulted in unacceptable errors in the simulation results.

Several methods have been reported to simulate complicated bone-implant interfaces in FE models. One previous FEA study performed by Viceconti et al. reported a direct contact method using gap elements to simulate the bone-implant interfaces (Viceconti et al., 2000).

Evidence suggested (Zachariah and Sanders, 2000) that the direct contact method had better performance than gap elements in reflecting local nodal displacement because it was more sensitive to the frictional coefficient and allowed interface discontinuity, separation and sliding between the bone and the implant. In our investigation, all shared nodes at the interfaces between implant and bone were bonded in the creation of micro-FE model, which did not allow the femoral stem to separate and slide. Therefore, only full bonding at the nodal interfaces was used to describe the bone-implant contact in this current FE analysis. The mesh steps were conducted with a combination of custom codes, which were written in Python, C++ and Fortran (Chevalier, 2015) (**Figure 19**).

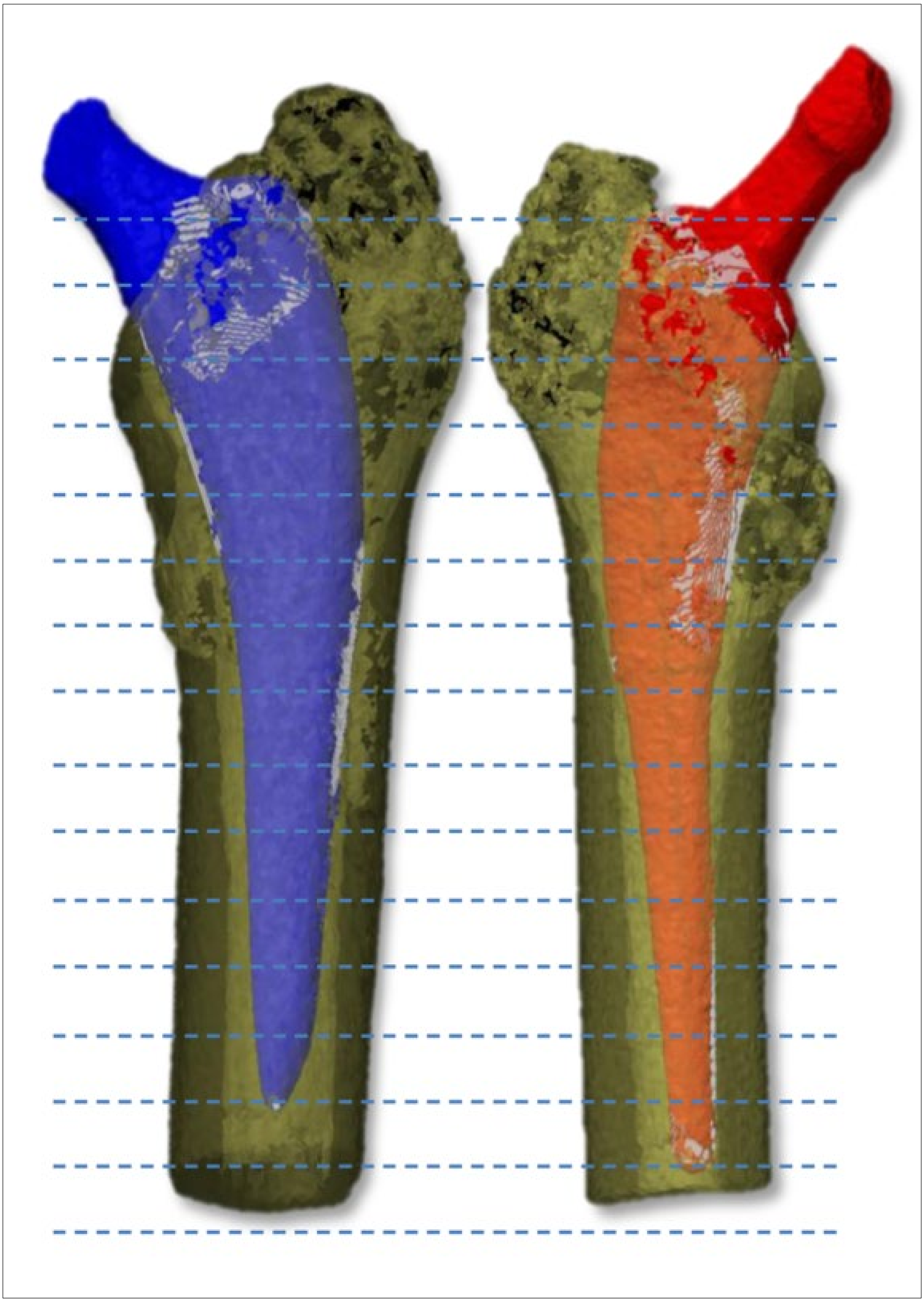

Figure 19. The results of creating the FE models for the femur implanted with Excia® T femoral stem (left) and Taperloc femoral stem (right)

5.6 Material Property Assignments

Custom codes (Chevalier, 2015; Chevalier et al., 2016) were used to convert the binarized implanted images into μFE models with approximately 150 million nodes and 200 million 8-noded hexahedral elements with 95 μm side lengths. According to previous published studies (Chevalier et al., 2009; Hengsberger et al., 2002; Mazza et al., 2008; Yan, 2019) regarding assessments of vertebral bone using nano indentation, the femoral stem elements were attributed properties of Ti alloy with a Young's modulus ($E_{implant}$) and Poisson's ratio ($\nu_{implant}$) of 110 GPa and 0.3, respectively, whereas the cortical bone elements and trabecular bone elements were assigned the properties of bone at the tissue scale wherein E_{bone} = 12 GPa and ν_{bone} = 0.3.

5.7 Boundary Conditions

The boundary conditions were defined to simulate physiological loading in accordance with Bergmann et al. (Bergmann et al., 2001), wherein the nodes of the outer distal bone edges were fully constrained, while a 0.1-mm vertical displacement was assigned to the top nodes of the stem. Pre- and post-processing was performed by running a combination of custom codes on a computer with high computing power. This computer has dual 10-core 2.30 GHz Intel Xeon E5-2650 processors with 128 Giga Byte (GB) of RAM and is equipped with a Linux cluster (Intel Westmere-EX sgi Ultra Violet) operating system. The FE models were solved through an open-source parallel solver (parFE, ETHZ, Switzerland) boarded operating environment on a computer with high computing power (Peeters et al., 2016).

5.8 Calculation of Regional BV/TV and Peak Bone Tissue Stress

TV was obtained by first filling the bone structure of the obtained imagines, subtracting the femoral voxels and then pooling the non-zero voxels. BV was obtained by pooling the bone tissue voxels of the corresponding unfilled images. Axial subregions for analysis of bone structural properties were created at intervals of 10 mm along the vertical loading axis of the femur, and the midpoint of the cut plane was used as the reference axis. BV/TV was calculated from the ratio of the resulting BV and TV in each zone. The bone-stem contact area was also calculated from the binarized, composite bone-implant images in these same subregions by summing the surface areas of implant voxel faces that intersected bone voxels. These values were then compared between the two stem designs.

5.9 Statistical Analysis

Visualization of bone tissue stresses (von Mises) was performed using Paraview v-3.14 (Utkarsch, 2015). Peak bone tissue stress was calculated in similar regions as those used for BV/TV calculations (e.g., in 10-mm axial zones along the loading axis), and the values were compared between stem designs (Stem 1a and Stem 2).

To test our first and second hypotheses, the mean and corresponding standard deviation (SD) were calculated, and the Kolmogorov-Smirnov test and Student's t-test were conducted to compare the regional BV/TV, contact surface, and eventual peak bone tissue stress for the restricted sub-selection used for the μFE models after implantation with the two designs of cementless femoral stems and three different coating porosities.

To test our third hypothesis, the Pearson correlation coefficient was adopted to establish the correlations between the contact surface, regional BV/TV and bone tissue stress. All plots were conducted using GraphPad Prism for Windows, 7.0 Version (GraphPad Software, California, USA). All statistical analyses were calculated using IBM SPSS Statistics for Windows, 22.0 Version (IBM Germany GmbH, Ehningen, Germany).

6 Results

6.1 Contact Surface

In this study, all 27 pairs of specimens, which were implanted with two designs of cementless femoral stems and three different coating porosities, were used to calculate the contact surface to evaluate whether geometrical designs and surface coating porosities can affect the bone-implant interfacial contact area.

For all 54 femoral specimens, the mean contact surface was 6.59% ± 4.72%, with a range from 1.21% to 25.69%. For the 27 femoral specimens implanted with Excia® T stems (Stem 1), the mean contact surface was 5.49% ± 3.70% with a range from 1.21% to 17.91%. For the other 27 femoral specimens, which were implanted with the Excia® T stems coated with Ti-Growth® (500 µm and 700 µm porosities) (Stem 1b and Stem 1c) and the Taperloc® stems (Stem 2), the mean contact surface values were 6.21% ± 7.91%, 8.39% ± 2.52% and 7.92% ± 4.64%, respectively.

Axial subregions for analysis of the contact surface were created at intervals of 10 mm along the vertical loading axis of the femur, and the midpoint of the cut plane was used as the reference axis. The results of the stem-cortex contact surface at the axial subregions generated from all specimens implanted with the two designs of cementless femoral stems and three different coating thicknesses (porosities) are presented in **Figure 20**.

No significant differences were found in any of the axial subregions of the stem-cortex contact surface after implantation of the two cementless femoral stem designs (Stem 1a vs. Stem 2, $p > 0.103$). Moreover, no significant differences were found between the standard Excia® T stem (Stem 1a) and Excia® T stem with a 500 μm thickness coating (Stem 1b) ($p > 0.411$). However, a further increase in coating produced significant differences between Stem 1a and 1c in the 10-mm and 20-mm subregions ($p = 0.025$ and $p = 0.024$, respectively).

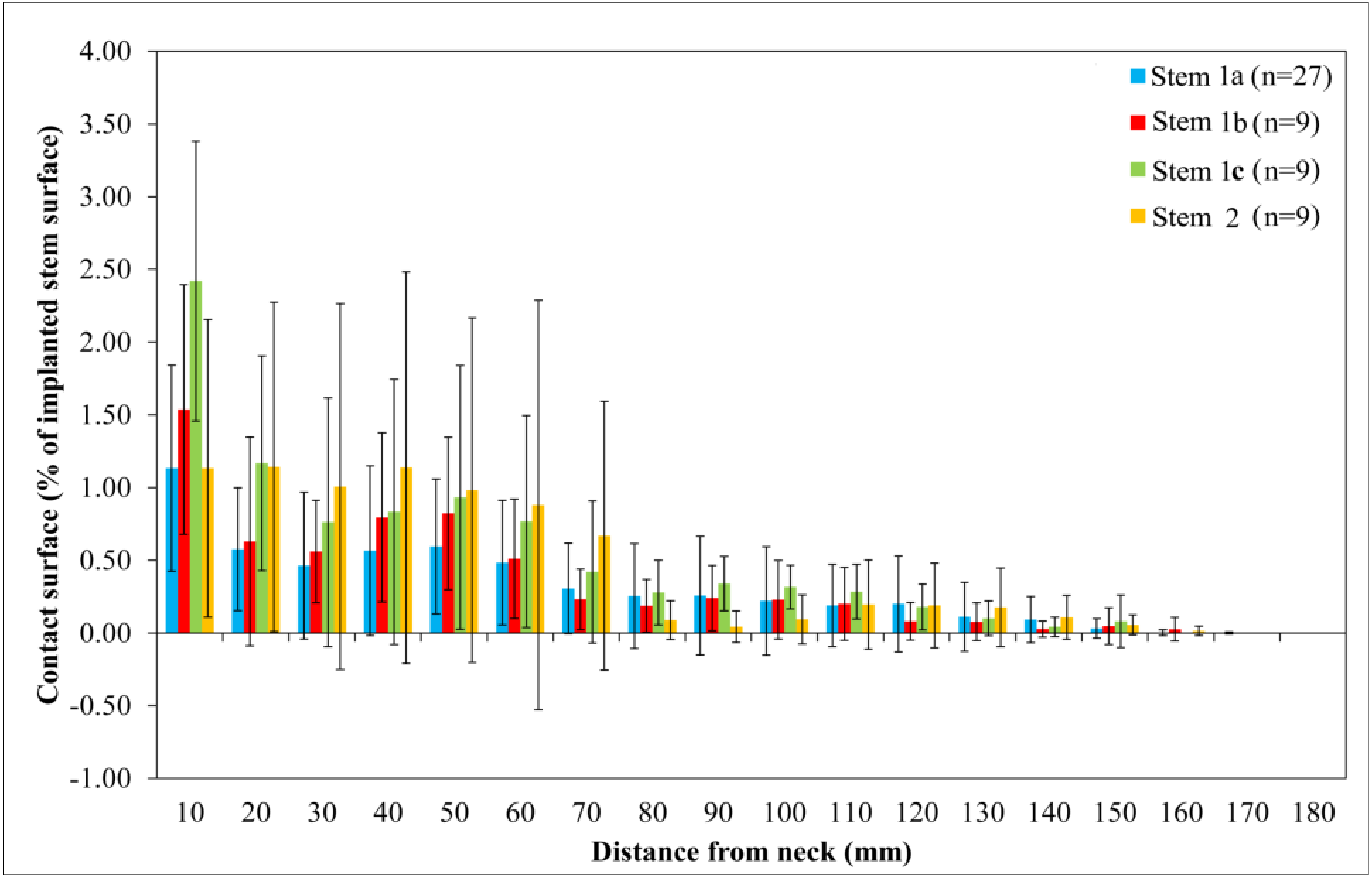

Figure 20. Contact surface in the axial subregions after implantation of the two designs of cementless femoral stems and three different coating thicknesses

A sub-selection of three paired images was converted to micro-FE models to provide a quantification of internal bone tissue stresses in simulated physiological loading conditions and to evaluate whether that geometrical design can affect load transfer in the surrounding bone tissue. The results of the contact surface for the two designs of femoral stem are shown in **Figure 21**. The results regarding the individual contact surface values of the three pairs of femurs and the mean value of the contact surface in the axial subregions after implantation of the two femoral stem designs are presented in **Figure 22**.

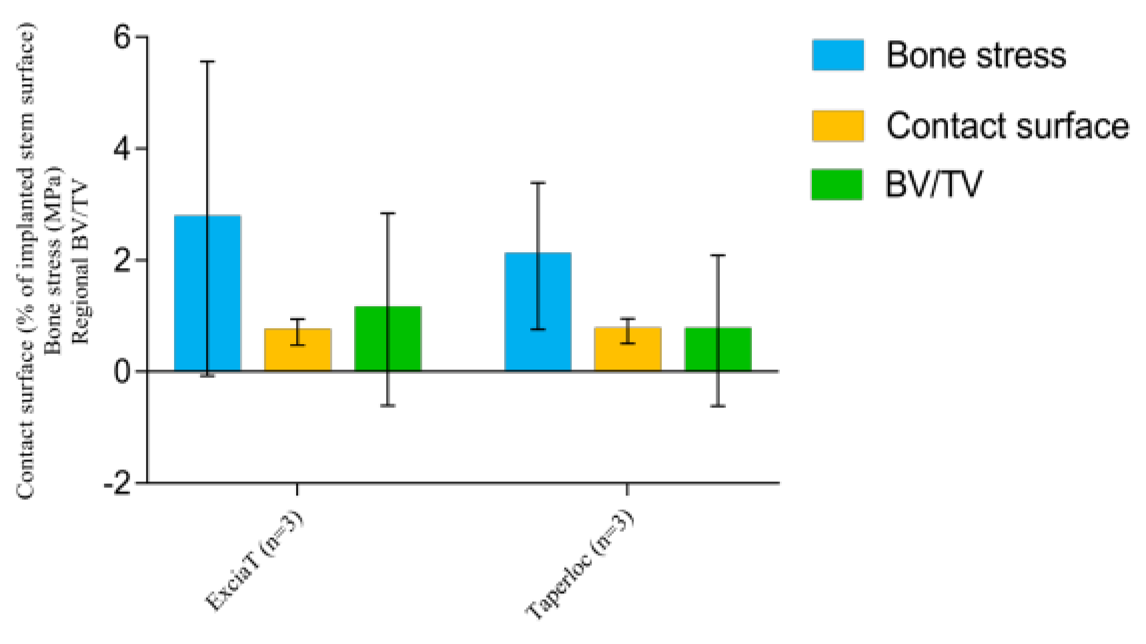

Figure 21. The regional BV/TV, contact surface and peak bone stress after implantation of the two femoral stem designs

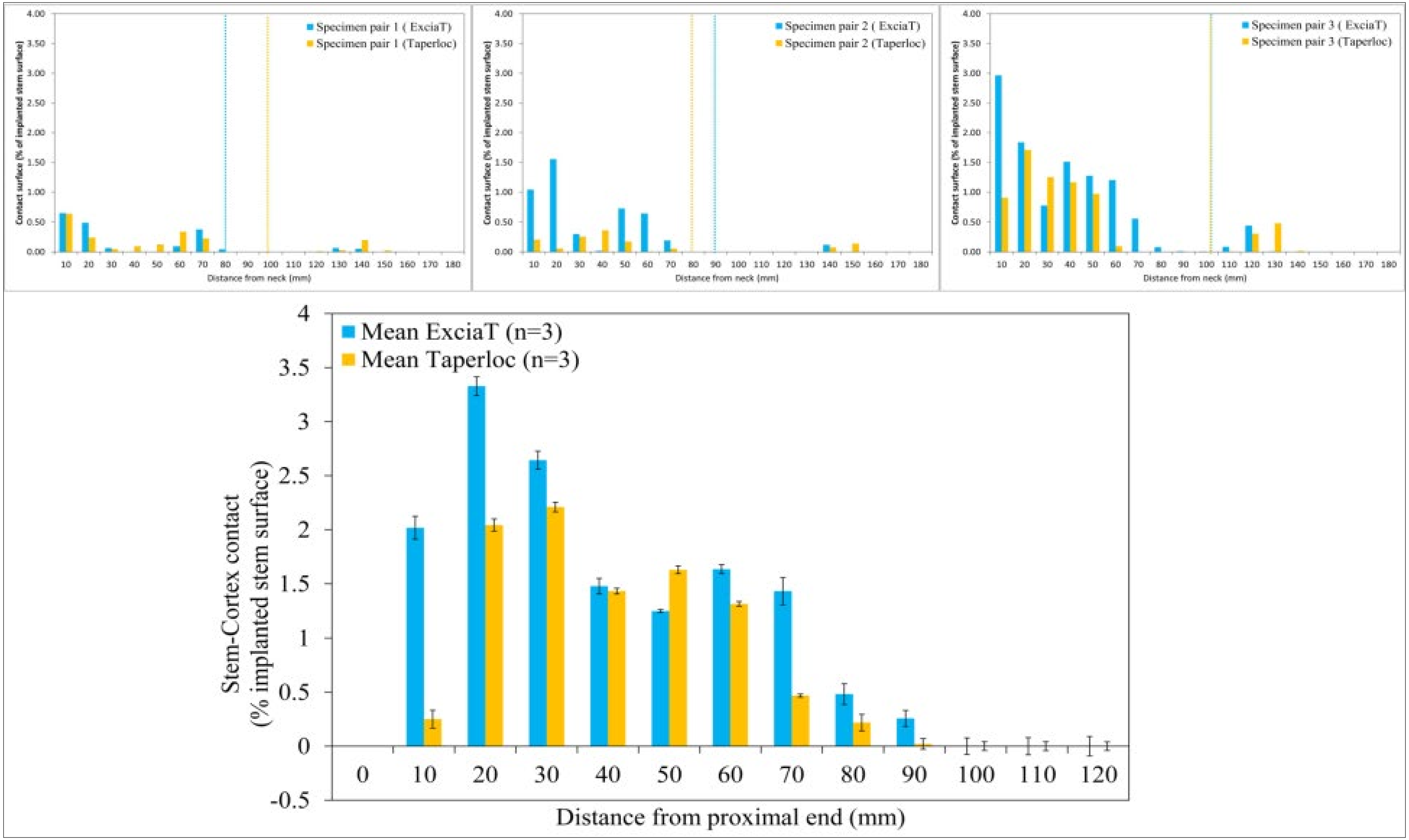

Figure 22. The results regarding individual contact surface of three pairs of femurs and the mean value of contact surface in the axial subregions after implantation of the two femoral stem designs

6.2 Regional BV/TV

Three paired images were converted to micro-FE models to quantify internal bone tissue stresses, and their results of regional BV/TV for the two stem designs are shown in **Figure 21**.

For all 6 femoral specimens, the mean regional BV/TV was 0.7408 ± 0.1971. For the 3 femoral specimens implanted with Excia® T stems (Stem 1a), the mean BV/TV was 1.3660 ± 0.2014 with a range from 0.0468 to 0.9392, whereas for the other 3 femoral specimens implanted with the Taperloc stem (Stem 2), mean BV/TV was 1.9386 ± 0.2311 with a range from 0.0473 to 0.9061.

The results regarding the individual regional BV/TV values of these three pairs specimens and the mean regional BV/TV value in the axial subregions after implantation of the two femoral stem designs are presented in **Figure 23**; the results were not statistically different between the Excia® T stem and Taperloc® stem ($p > 0.056$) or among any of the axial subregions ($p > 0.152$).

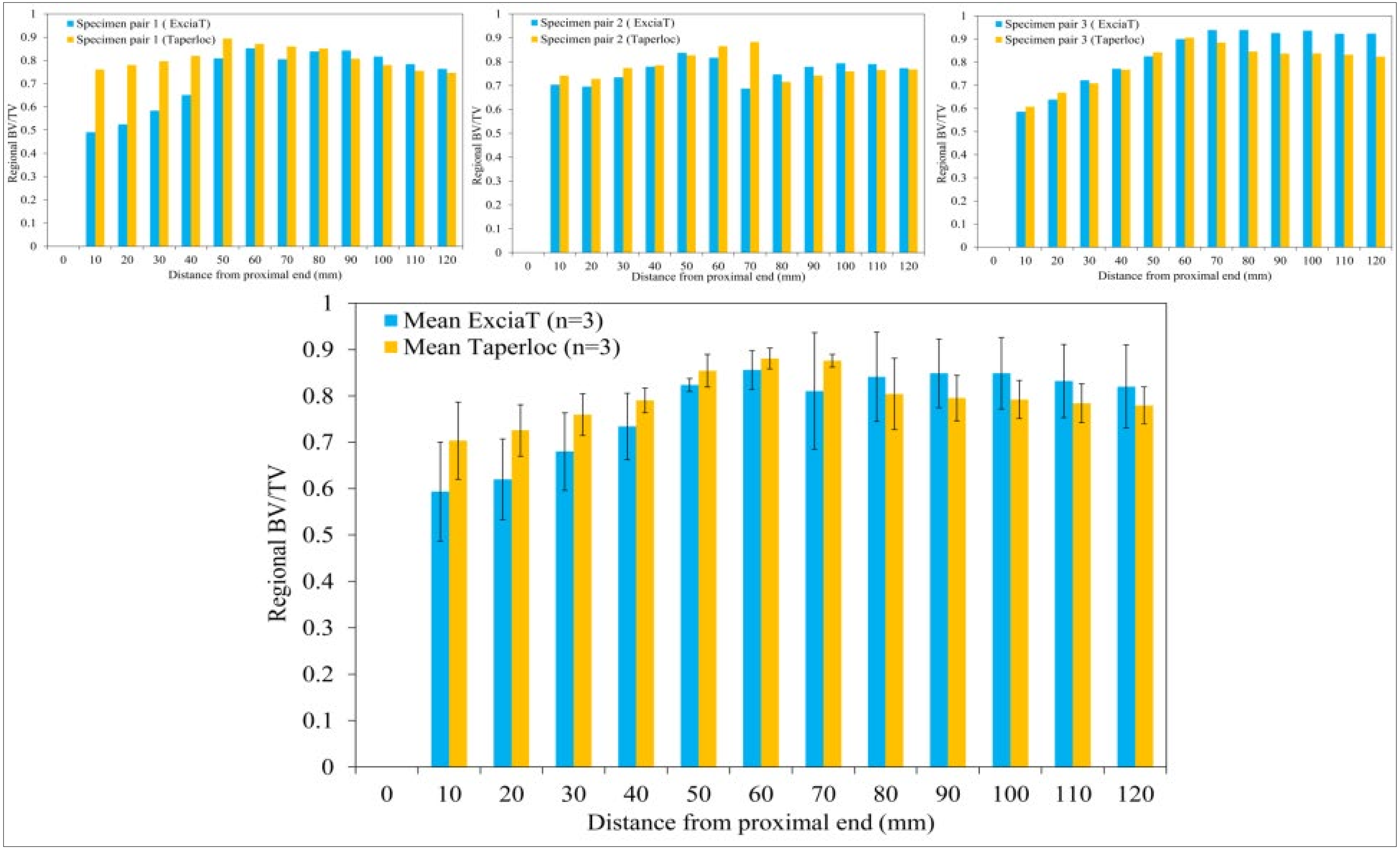

Figure 23. The results regarding individual regional BV/TV of three pairs of femurs and the mean value of apparent bone density (regional BV/TV) in the axial subregions after implantation of the two femoral stem designs

6.3 Bone Tissue Stresses

Three paired images were selected to quantify internal bone tissue stresses using FE models, and their results of peak bone stress for the two stem designs are shown in **Figure 21**.

For all 6 femoral specimens, the mean peak bone tissue stress was 40.0865 ± 10.0578 MPa with a range from 24.9097 to 49.0046 MPa. For the 3 femoral specimens implanted with Excia® T stems (Stem 1a), the mean peak bone tissue stress was 40.8065 ± 13.7621 MPa with a range from 24.9097 to 49.0046 MPa, whereas for the other 3 femoral specimens implanted with Taperloc stems (Stem 2), the mean bone tissue stress was 39.3750 ± 7.8731 MPa with a range from 31.9383 to 47.6218 MPa.

The results regarding the individual bone tissue stresses in the three pairs of images selected to quantify internal bone tissue stresses using FE models and the mean bone tissue stresses in the axial subregions after implantation of the two femoral stem designs are presented in **Figures 24** and **25**. No significant difference in the von Mises stresses were found between the two femoral stems ($p = 0.901$), among all axial subregions ($p > 0.067$), or in the comparison of peak bone tissue stresses with different femoral stem sizes ($p > 0.372$).

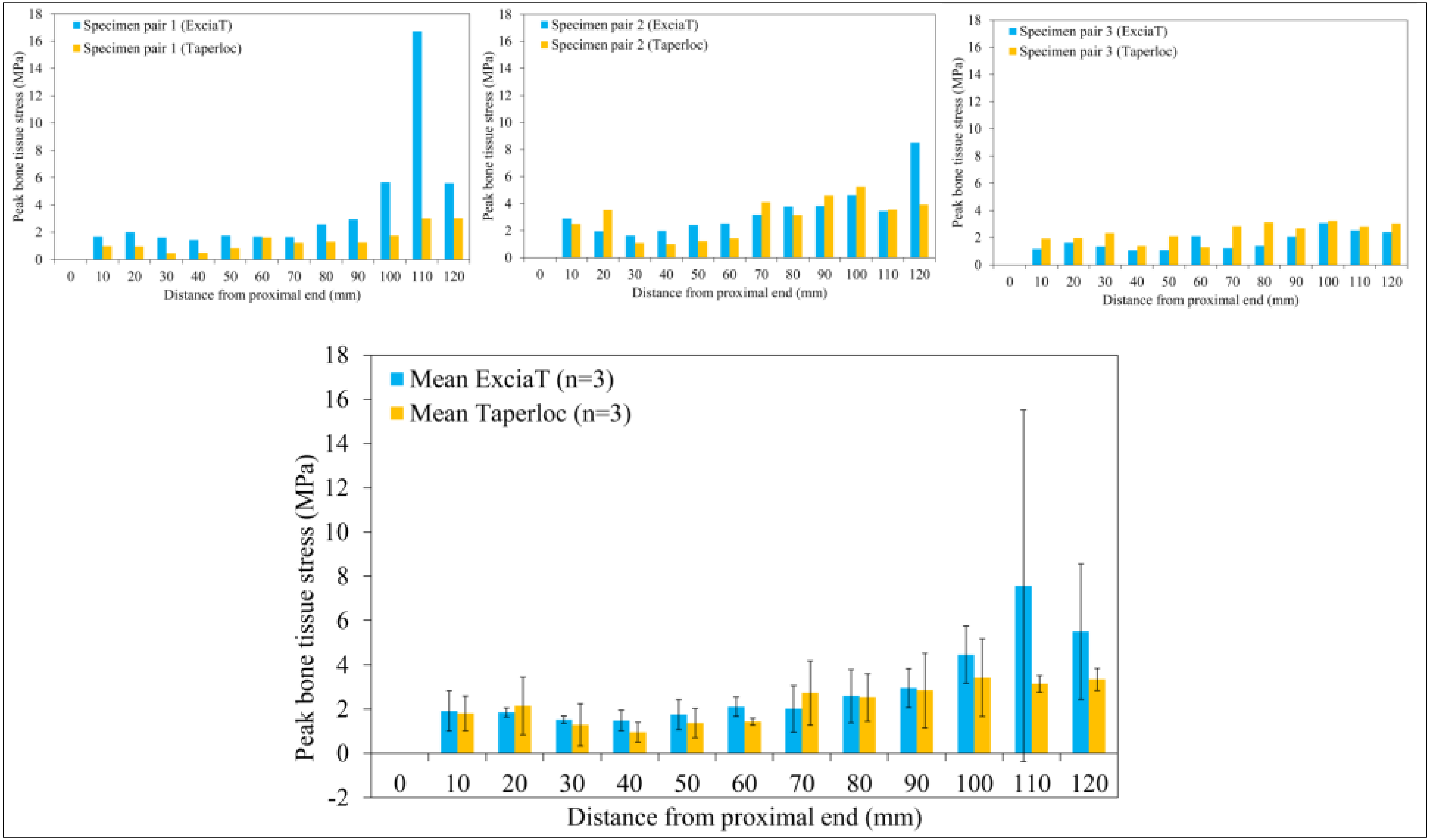

Figure 24. The results regarding individual peak bone tissue stress of three pairs of femurs and the mean value of peak bone tissue stress in the axial subregions after implantation of the two femoral stem designs

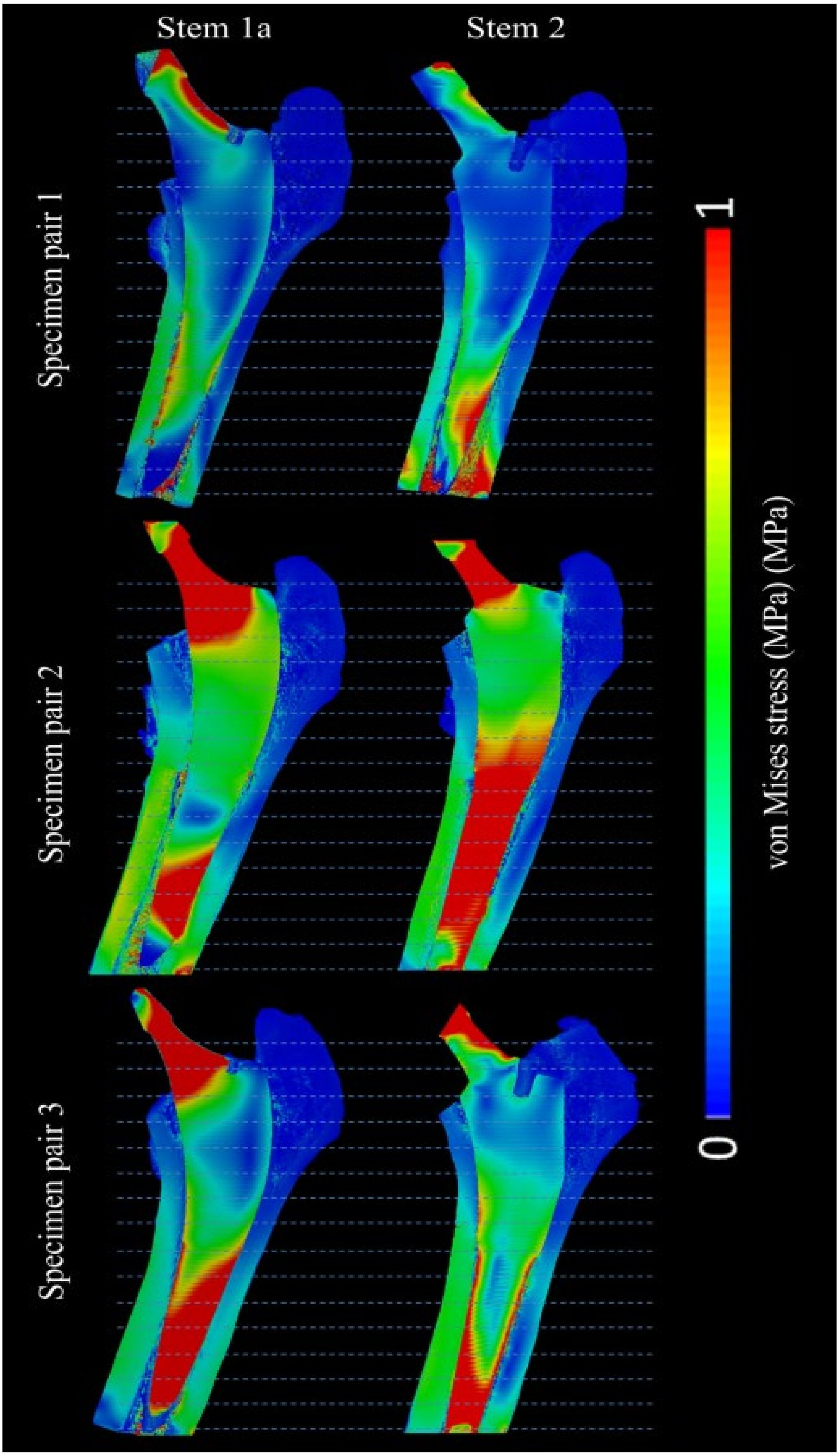

Figure 25. The von misses stress distribution of three pairs of specimens after implantation.

6.4 Role of the Contact Surface on the Stress Transfer

Three paired images were selected to quantify internal bone tissue stresses using FE models, and the role of the contact surface on the stress transfer in each pair of specimens for the two stem designs is shown in **Figure 26**. For all three specimens, the peak bone stresses are positively correlated with decreasing interfacial contact in the full regions (Excia® T: $R^2 = 0.511$, $p = 0.010$; Taperloc: $R^2 = 0.629$, $p = 0.003$) (**Figure 26**).

6.5 Role of the Regional BV/TV on the Stress Transfer

Three paired images were selected to quantify internal bone tissue stresses using FE models, and the role of regional BV/TV on the stress transfer in each pair of specimens for the two stem designs is shown in **Figure 27**. For all three pairs of specimens, the peak bone stresses are weakly correlated with the regional BV/TV (Excia® T: $R^2 = 0.285$, $p = 0.062$; Taperloc: $R^2 = 0.333$, $p = 0.041$) (**Figure 27**).

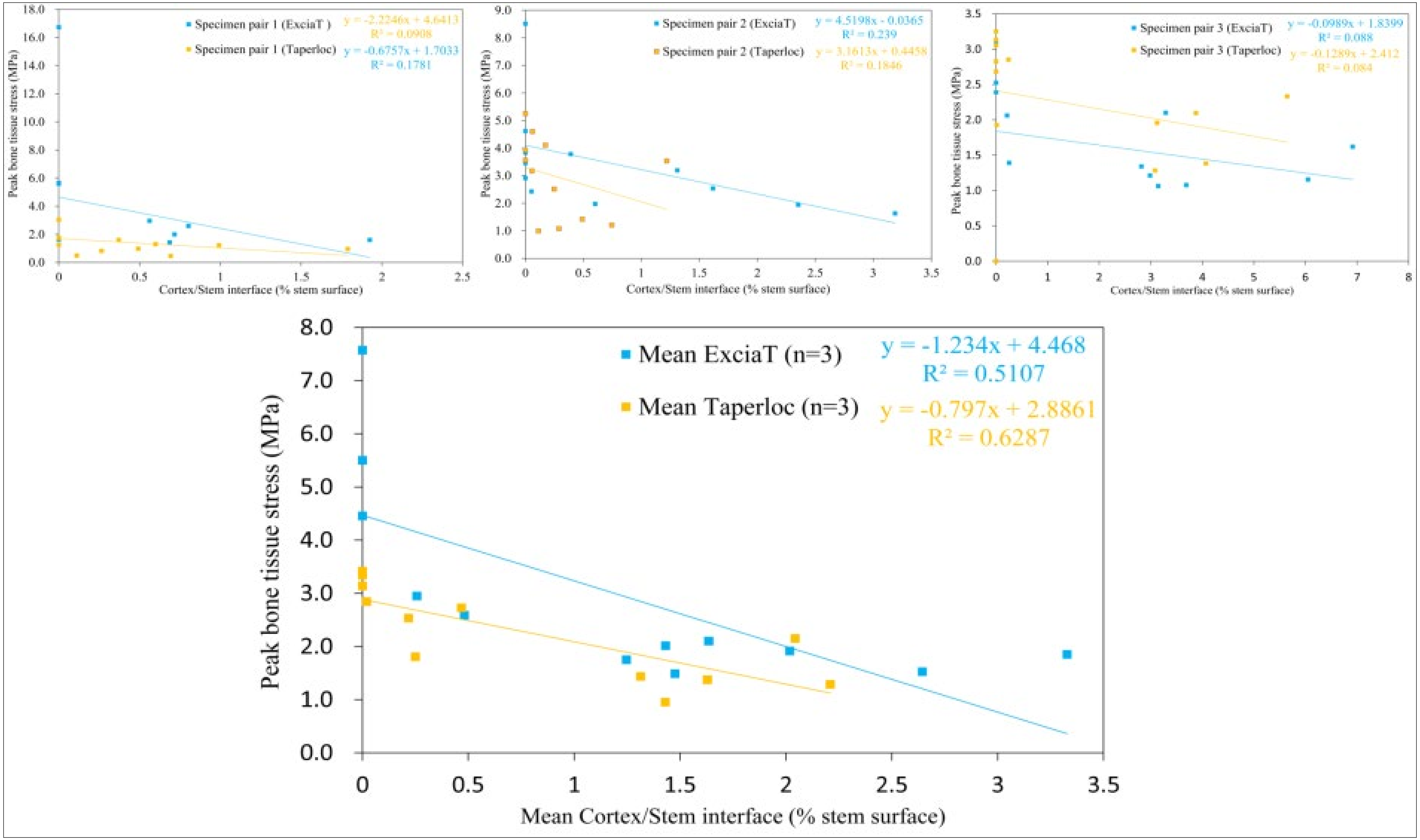

Figure 26. The results regarding the correlations between contact surface and peak bone tissue stresses of three pair of femurs after implantation of the two femoral stem designs

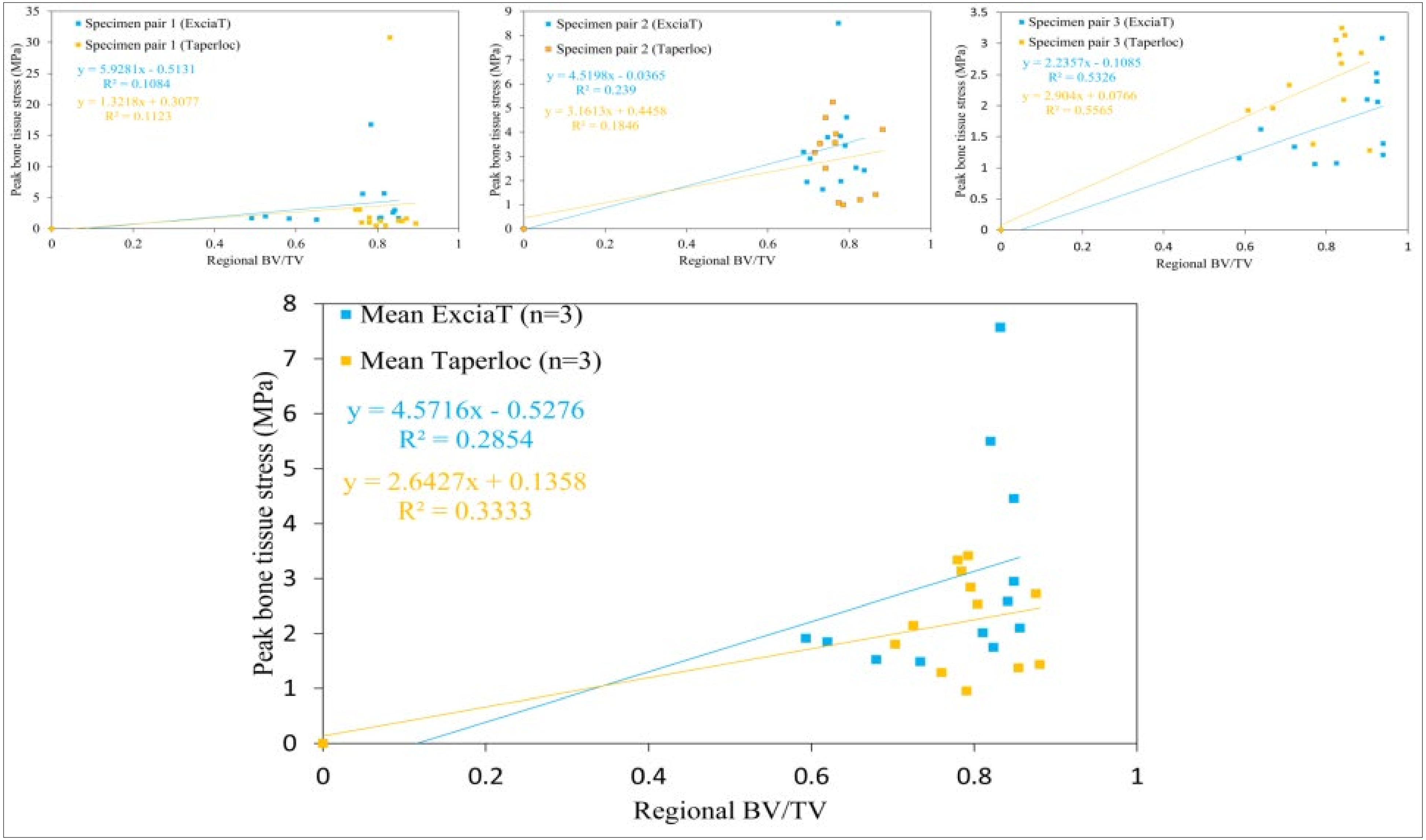

Figure 27. The results regarding the correlations between regional BV/TV and bone tissue stresses of three pairs of femurs after implantation of the two femoral stem designs

7 Discussion

Several biomechanical factors, including regional bone quality and bone-stem interfacial contact, may have an important effect on femoral stem stress transfer. The aim of this current research was to evaluate how regional bone quality (BV/TV) and bone-stem interfacial contact affect the stress transfer around cementless femoral stems and to explore the correlation of peak stresses with interfacial contact area by virtue of the combined use of micro-CT imaging and micro-FE models. Our results show that small differences in geometrical design of the femoral stem has little effect on load transfer, whereas the interfacial contact area significantly impacts the peak bone tissue stresses at the implant-bone interface, as demonstrated by the observed positive correlation of peak bone stresses with decreasing contact area at the implant-bone interface.

The effect of small geometrical differences in stem design on bone-stem contact ratio and stress transfer

Our first hypothesis was that small differences in the geometry design, such as the ones between the Excia® T and the Taperloc stems, can affect bone-stem contact ratio and stress transfer. Currently, uncemented fixation in THA presented excellent long-term survival and clinical outcomes, which is demonstrated with the increasing use in clinical routine procedure document in national requires. Uncemented femoral stems were designed to achieve maximal primary stability and promote bone ingrowth for secondary stability. There are various designs for cementless femoral stems that were developed and used in numerous conditions. The design and surface coating of a femoral stem implant had a strong influence on the final survival (Tuncay et al., 2016). The femoral anteversion before the THA operation using a standard uncemented femoral stem significantly decreased, whereas the neck-shaft angles slightly increased (Muller et al., 2015). One biomechanical study (Tuncay et al., 2016) was performed using 20 synthetic femurs to compare femoral stems with cylindrical cross-sections to those with rectangular cross-sections, and the results demonstrated that the former could provide a higher rotational stability of the transverse osteotomy than the latter.

Our numerical predictions demonstrated that, on average, for all specimen pairs (n = 3), the peak bone tissue stress did not show significant differences between stem designs (Excia® T & Taperloc). Meanwhile, no significant differences were revealed in all axial subregions of these two stems; however, in our study, we constructed a comparison in the same femur implanted with different sizes of cementless stems (Excia® T, n = 2). The results showed that the size of femoral stems in that swale range had no effect on the bone tissue stresses. The load transfer of cementless stems may depend on the underlying anatomical mechanisms and small interface changes rather than the geometrical design of the femoral stem based on the micro-CT image and micro-FE model. One previous study revealed that the stem geometry, particularly in uncemented THA, might be a key determinant of biological behaviour in the stress transfer around the femoral stem (Aamodt et al., 2001). However, a recent study proposed a contradictory opinion that the stress transfer at the proximal part of femur implanted with cementless stems was affected by the underlying anatomy rather than the geometrical design of the stem (Schwarz et al., 2018). An experimental study using 12 cadaveric femurs with a hip simulator confirmed that the load transfer in a proximal femur with an uncemented stem was overall equalent to the load transfer in a proximal femur with a cemented stem under single-leg or stair-climbing conditions if the stems had similar geometries (Enoksen et al., 2017). In addition, a biomechanical study conducted by Enoksen et al. revealed that minor differences in stress distribution between different femoral stems with various modular neck lengths, designs or necks shafts might not lead to severe bone resorption in the proximal part of the femur (Enoksen et al., 2016). Femoral stem press-fit fixation depends on optimal proximal fit and stress transfer for long-term functionality (Stiehl, 1993). The process of inserting the femoral stem into the femur can change the natural stress distribution in the proximal part of the femur (Jayasuriya et al., 2013; Stucinskas et al., 2012). Furthermore, the size of the femoral stem was selected to use by the surgeon during preoperative process, depending on the shape and size of the femoral medullary cavity.

Surface coating thickness and roughness affects the bone-stem contact ratio

The surface of the femoral stem is the first surface that contacts the host bone; therefore, the physicochemical properties of this surface are key determinants of primary stability (de Lima Cavalcanti et al., 2019). The design and surface coating of a femoral stem implant had a strong influence on the final survival (Tuncay et al., 2016). An interface between the femoral stem and the host bone was formed after a metal femoral stem was inserted into the proximal cavity, and the initial stability mainly relied on the surface coating, structures and nano-scale interactions (Renders et al., 2008; Zinger et al., 2004). The interface between the cementless femoral stem and the bone in THA ensured adequate fixation because it enabled bone modeling over time. The coating porosity of the femoral stem is important for the primary stability (Baltopoulos et al., 2008). In theory, coating HA on the surface of a femoral stem has the most compelling advantage because HA coatings offer the ability to increase the strength of bond between the femoral stem and host bone, thereby increasing the primary stability of binding fixation (Cook et al., 1992; Soballe et al., 1991). Several studies (Aksakal et al., 2014; Garcia Araujo et al., 1998; Soballe et al., 1993) confirmed that HA promoted the growth of bone. Uncemented stems with HA coatings have shown good clinical and radiological results with good long-term survival (Capello et al., 2006; Geesink, 2002; Lazarinis et al., 2011). One clinical study (Inoue et al., 2016) was conducted to evaluate the implant-femur interfacial contact ratio and cortical hypertrophy, which revealed that there was no relationship between the implant-femur interfacial contact ratio and regional bone hypertrophy. One FEA (Reimeringer and Nuno, 2016) was performed to explore the impact of implant-femur interfacial contact area on the stability of uncemented stem in THA. However, no study was conducted to investigate the effect of geometrical design and surface coating thickness (pressfit) and roughness on the bone-implant interfacial contact area. Our numerical predictions demonstrated that, on average, for all specimen pairs ($n = 9$), the contact area did not show significant statistical differences between the two geometrical designs (Stem 1a & Stem 2) or among all axial subregions in these two designs of stems. However, a further increase in surface thickness showed significant differences between Stem 1a and 1c in the 10-mm and 20-mm subregions, which may indicate that the pressfit will affect the bone-stem contact ratio.

Bone tissue stresses increased with reduced contact ratio but not regional BV/TV

Our third hypothesis that peak bone tissue stresses are positively correlated with decreasing interfacial contact was validated by our findings, which showed that the peak bone tissue stresses around both tested stem designs increased with decreasing interfacial contact. However, the peak bone stresses are weakly correlated with the regional BV/TV. Interfacial contact was measured by calculating the percentage/ratio of the femoral stem interface in contact with the femur (contact ratio). One recent study confirmed that the implant-bone interfacial contact ratio and its location contributed to the maximal primary stability of cementless femoral stems (Reimeringer and Nuno, 2016). Femoral stem press-fit fixation depends on optimal proximal fit and stress transfer for long-term functionality (Stiehl, 1993). An experimental study using 12 cadaveric femurs showed that an uncemented femoral stem had the same stress transfer as a cemented femoral stem with a similar geometry (Enoksen et al., 2017). Both studies confirmed that the load transfer of cementless stems was determined by the underlying anatomy. To our knowledge, our study is the first to assess the accurate geometrical interfacial contact area and load transfer using micro-CT and FEA. Our results revealed the relationship between peak bone stresses and interfacial contact.

Limitations

Several limitations within our study merit considerations. First, some sub-selection analyses for the extensive nature of bone were based on a relatively small number of samples (n = 6), which potentially led to a reduced range of apparent bone density and peak bone tissue stress and possibly limit the obtained associations of regional BV/TV or contact surface and peak bone tissue stresses. Second, the calculations of the regional BV/TV, peak bone tissue stress and contact surface based on the μFE models were unable to distinguish intact bone from bone debris after implantation, which are not expected to contribute mechanically to fixation and therefore to stress transfer. Our method does not either account for the local damage in bone tissue induced by stem implantation. Third, the μFE model was created according to the assumption that different sites in bone have constant properties, which cannot account for the regional differences and bone plasticity at the tissue level of trabeculae, thereby resulting in the overestimation of bone elastic properties (Paschalis et al., 1997; Renders et al., 2008). Finally, actual boundary conditions are difficult to mimic using more detailed configurations, and the simplified version might not account for the complex load transfer in such cases.

8 Conclusion

Summarizing the results from the contact analysis, the contact area did not show significant differences between the two geometrical designs or among all axial subregions in these two stems. Similar results were obtained for the surface coating thickness (pressfit) on the contact area. Our results show that small differences in geometrical design of femoral stem might have little effect on load transfer, but that interface contact area can on the other hand impact significantly on the peak stresses at implant-bone interface, as demonstrated by the observed positive correlation of peak bone stresses with decreasing contact area at implant-bone interface.

We further demonstrated that peak bone tissue stress did not show significant differences in relation to small differences in stem designs according to our micro-FE analyses (Excia® T & Taperloc). No differences were revealed among all axial subregions of these two stems; moreover, no significant differences were found in the comparison of bone tissue stress with two different cementless femoral stem sizes.

Furthermore, our study is the first to assess the accurate geometrical interfacial contact area and load transfer using micro-CT and micro-FEA. Our FE analysis revealed that peak bone tissue stresses around both tested stem designs increased with decreasing interfacial contact.

Our analyses based on the micro-FE models generated from micro-CT imaging highlight the role of structural effects of cementless femoral stems especially implant-bone interfacial contact surface as predominant factors influencing stress transfer, whereas only limited insights were observed involving the influences of regional apparent BV/TV, which implied the limitations of high-resolution numerical models when not interpreting contact ratio on stress transfer. Future work will relate these findings to experimental migration analyses performed on the corresponding specimens by our collaborative partners.

9 Summary

Primary stability of femoral stems in THA is crucial in the long-term behavior of these implants. The metaphyseal fit and implant design are decisive factors of primary fixation stability. Recently, high resolution numerical models using μFE analyses based on μCT scanning have been proposed to assess the fixation stability of numerous artificial prostheses. However, such methods have yet to be used to quantify bone-stem contact surface and the internal load transfer. Therefore, this study aims to assess the effects of several biomechanical factors on the stress transfer after implantation of femoral stems. In order to do this, two designs of cementless femoral stems and three different coating thicknesses (pressfit) were implanted in paired cadaveric specimens and scanned with an industrial nano-CT scanner. From these, a sub-selection of paired images was converted to micro finite element models to provide a quantification of internal bone tissue stresses in simulated physiological loading conditions.

A series of μFE models were created to evaluate the specific impact of stem design on local bone stresses. These were generated from μCT imaging (v | tome | x s 240, General Electrics, 160 kV, 580 μA, 95 μm resolution) of 27 paired cadaveric femurs implanted with two types of femoral stems (Excia® T, Aesculap; Taperloc, Biomet). Images were first segmented to evaluate stem-bone contact area along the diaphysis axis. From these scans, a selection of images was processed to generate μFE models composed of approximately 200 million hexahedral elements. These were attributed isotropic, linear elastic material properties based on numerous studies. Subjected to the simulated physiological loading and solved with a parallel solver on a Linux

Cluster, the resulting local bone tissue stresses were compared between stems and related to implantation bone-stem contact and local bone volume fraction (BV/TV).

Regional BV/TV was not statistically different in two stem designs as well as at any of the axial subregions. No significant difference of contact surface was found at any of the axial subregions in two stem designs. However, a further increase in surface porosity produced significant differences between Stem 1a and 1c in the 10-mm and 20-mm subregions. Peak bone stresses are correlated positively with decreasing interface contact in the full regions.

The aim of this present research was to analyze quantitatively how regional bone quality and interface contact of bone-stem affect femoral stem tress transfer, in particular accounting for structural effects of femoral stems on stress transfer, and explore the correlation of peak bone tissue stresses with interface contact. This investigation highlights the role of bone-stem contact as a predominant factor influencing stress transfer. Future work will relate these findings to experimental migration analysis performed on the corresponding specimens.

10 Zusammenfassung

Die Primärstabilität der Femurschäfte bei der totalen Hüftendoprothetik ist für das Langzeitverhalten dieser Implantate von entscheidender Bedeutung. Die metaphysäre Passform und das Implantatdesign sind entscheidende Faktoren für die Stabilität der primären Fixation. In letzter Zeit wurden hochauflösende numerische Modelle unter Verwendung von Mikro-Finite-Elemente-Analysen (µFE), basierend auf Mikrocomputertomographie, entwickelt (µCT), um die Fixationsstabilität verschiedener Prothesen zu bewerten. Solche Methoden müssen jedoch angewendet werden, um die Kontaktfläche zwischen Knochen und Schaft und die interne Lastübertragung zu quantifizieren. In dieser Studie sollten daher die Auswirkungen verschiedener biomechanischer Faktoren auf die Lockerung nach Implantation von Oberschenkelschäften untersucht werden. Zu diesem Zweck wurden zwei Modelle zementfreier Oberschenkelschäfte und drei verschiedene Beschichtungen mit unterschiedlichen Pornegrößen in gepaarte Leichenpräparate implantiert und mit einem industriellen Nano-CT-Scanner gescannt. Hieraus wurde eine Unterauswahl von gepaarten Bildern in Mikro-Finite-Elemente-Modelle umgewandelt, um eine Quantifizierung der inneren Knochengewebespannungen unter simulierten physiologischen Belastungsbedingungen zu erhalten.

Es wurde eine Serie von µFE-Modellen erstellt, um die spezifischen Auswirkungen des Schaftdesigns auf die lokale Knochenbelastung zu ermitteln. Dies wurden durch µCT-Bildgebung (v | tome | x s 240, General Electrics, 160 kV, 580 µA, 95 µm resolution) von 27 gepaarten Leichenfemura untersucht, in die zwei unterschiedliche Designs von Prothesenschäften implantiert waren. Die Bilder wurden zuerst segmentiert, um die Schaft-Knochen-Kontaktfläche entlang der Diaphysenachse ermitteln zu können. Aus diesen Scans wurde eine Auswahl von Bildern verarbeitet (Excia® T, Aesculap, Taperloc, Biomet) um µFE-Modelle zu erzeugen, die aus ungefähr 200 Millionen hexaedrischen Elementen zusammengesetzt waren. Diesen wurden auf der Grundlage zahlreicher Studien isotrope, linearelastische Materialeigenschaften zugeschrieben. Die resultierenden lokalen Knochengewebespannungen wurden unter simulierter physiologischer Belastung mit einem parallelen Rechner in einem Linux-Cluster verglichen und mit dem Knochen-Stamm-Kontakt der Implantation und dem lokalen Knochenvolumenanteil (BV/TV) in Verbindung gebracht.

Das regionale BV/TV unterschied sich statistisch nicht zwischen den beiden Prothesendesigns sowie in einer der axialen Subregionen. Kein Unterschied der wurde in einer der axialen Teilregionen der zwei Schaftdesigns festgestellt. Es konnte kein signifikanter Unterschied der Mises-Vergleichsspannung in den beiden Designs der Schäfte sowie in einem der axialen Teilbereiche festgestellt werden. Spitzenknochenspannungen korrelieren positiv mit abnehmendem Grenzflächenkontakt in allen Regionen.

Das Ziel der Studie war es zu Untersuchen wie sich die regionale Knochenqualität und der Grenzflächenkontakt zwischen Knochen und Schaft auf den Stresstransfer des Oberschenkelstamms auswirken. Dabei sollten insbesondere die strukturellen Auswirkungen des Femurschaftes auf den Stress-Transfer berücksichtigt und die Korrelation von Spitzenspannungen mit dem Grenzflächenkontakt untersucht werden. Diese Untersuchung hebt die Bedeutung des Knochen-Schaft-Kontakts als einen entscheidenden Faktor hervor, der die Spannungsübertragung beeinflusst. Zukünftige

Arbeiten werden diese Ergebnisse mit experimentellen Migrationsanalysen in Verbindung bringen, die an den entsprechenden Proben durchgeführt werden.

11 References

Aamodt, A., Lund-Larsen, J., Eine, J., Andersen, E., Benum, P., Husby, O.S., 2001. Changes in proximal femoral strain after insertion of uncemented standard and customised femoral stems. An experimental study in human femora. The Journal of bone and joint surgery. British volume 83, 921-929.

Abate, M., Pelotti, P., De Amicis, D., Di Iorio, A., Galletti, S., Salini, V., 2008. Viscosupplementation with hyaluronic acid in hip osteoarthritis (a review). Upsala journal of medical sciences 113, 261-277.

Abdul-Kadir, M.R., Hansen, U., Klabunde, R., Lucas, D., Amis, A., 2008. Finite element modelling of primary hip stem stability: the effect of interference fit. J Biomech 41, 587-594.

Acklin, Y.P., Jenni, R., Bereiter, H., Thalmann, C., Stoffel, K., 2016. Prospective clinical and radiostereometric analysis of the Fitmore short-stem total hip arthroplasty. Archives of orthopaedic and trauma surgery 136, 277-284.

Aesculap Implant Systems, 2015. Excia® T Standard Hip Stem System [Online]. Available: https://www.aesculapimplantsystems.com/en/healthcare-professionals/orthopaedics/excia-t.html [Accessed January 22, 2021].

Akrami, M., Craig, K., Dibaj, M., Javadi, A.A., Benattayallah, A., 2018. A three-dimensional finite element analysis of the human hip. Journal of medical engineering & technology 42, 546-552.

Aksakal, B., Kom, M., Tosun, H.B., Demirel, M., 2014. Influence of micro- and nano-hydroxyapatite coatings on the osteointegration of metallic (Ti6Al4 V) and bioabsorbable interference screws: an in vivo study. European journal of orthopaedic surgery & traumatology : orthopedie traumatologie 24, 813-819.

Alomari, A.H., Wille, M.L., Langton, C.M., 2018. Bone volume fraction and structural parameters for estimation of mechanical stiffness and failure load of human cancellous bone samples; in-vitro comparison of ultrasound transit time spectroscopy and X-ray muCT. Bone 107, 145-153.

Alsaadi, G., Quirynen, M., Michiels, K., Jacobs, R., van Steenberghe, D., 2007. A biomechanical assessment of the relation between the oral implant stability at insertion and subjective bone quality assessment. Journal of clinical periodontology 34, 359-366.

Ancelin, D., Reina, N., Cavaignac, E., Delclaux, S., Chiron, P., 2016. Total hip arthroplasty survival in femoral head avascular necrosis versus primary hip osteoarthritis: Case-control study with a mean 10-year follow-up after anatomical cementless metal-on-metal 28-mm replacement. Orthopaedics & traumatology, surgery & research : OTSR 102, 1029-1034.

Anderson, A.E., Peters, C.L., Tuttle, B.D., Weiss, J.A., 2005. Subject-specific finite element model of the pelvis: development, validation and sensitivity studies. Journal of biomechanical engineering 127, 364-373.

Arbenz, P., Lenthe, G.H.v., Mennel, U., Müller, R., Sala, M., 2008. A scalable multilevel preconditioner for matrix-free µ-finite element analysis of human bone structures. International Journal for Numerical Methods in Engineering 73, 21.

Arifin, A., Sulong, A.B., Muhamad, N., Syarif, J., Ramli, M.I., 2014. Material processing of hydroxyapatite and titanium alloy (HA/Ti) composite as implant materials using powder metallurgy: a review. Materials & Design 55, 165-175.

Arno, S., Fetto, J., Nguyen, N.Q., Kinariwala, N., Takemoto, R., Oh, C., Walker, P.S., 2012. Evaluation of femoral strains with cementless proximal-fill femoral implants of varied stem length. Clinical biomechanics 27, 680-685.

Baltopoulos, P., Tsintzos, C., Papadakou, E., Karagounis, P., Tsironi, M., 2008. Hydroxyapatite-coated total hip arthroplasty: the impact on thigh pain and arthroplasty survival. Acta orthopaedica Belgica 74, 323-331.

Barker, D.S., Netherway, D.J., Krishnan, J., Hearn, T.C., 2005. Validation of a finite element model of the human metacarpal. Medical engineering & physics 27, 103-113.

Basler, S.E., Traxler, J., Muller, R., van Lenthe, G.H., 2013. Peri-implant bone microstructure determines dynamic implant cut-out. Medical engineering & physics 35, 1442-1449.

Belmont, P.J., Jr., Powers, C.C., Beykirch, S.E., Hopper, R.H., Jr., Engh, C.A., Jr., Engh, C.A., 2008. Results of the anatomic medullary locking total hip arthroplasty at a minimum of twenty years. A concise follow-up of previous reports. The Journal of bone and joint surgery. American volume 90, 1524-1530.

Bennell, K.L., Egerton, T., Martin, J., Abbott, J.H., Metcalf, B., McManus, F., Sims, K., Pua, Y.H., Wrigley, T.V., Forbes, A., Smith, C., Harris, A., Buchbinder, R., 2014. Effect of physical therapy on pain and function in patients with hip osteoarthritis: a randomized clinical trial. Jama 311, 1987-1997.

Bergmann, G., Deuretzbacher, G., Heller, M., Graichen, F., Rohlmann, A., Strauss, J., Duda, G.N., 2001. Hip contact forces and gait patterns from routine activities. J Biomech 34, 859-871.

Berry, D.J., Harmsen, W.S., Cabanela, M.E., Morrey, B.F., 2002. Twenty-five-year survivorship of two thousand consecutive primary Charnley total hip replacements: factors affecting survivorship of acetabular and femoral components. The Journal of bone and joint surgery. American volume 84-A, 171-177.

Bieger, R., Ignatius, A., Decking, R., Claes, L., Reichel, H., Dürselen, L., 2012. Primary stability and strain distribution of cementless hip stems as a function of implant design. Clinical biomechanics 27, 158-164.

Biomet, Z., 2013. Taperloc® Complete Hip System [Online]. Available: https://www.zimmerbiomet.com/medical-professionals/hip/product/taperloc-complete-hip-system.html [Accessed January 22, 2021].

Bordini, B., Stea, S., De Clerico, M., Strazzari, S., Sasdelli, A., Toni, A., 2007. Factors affecting aseptic loosening of 4750 total hip arthroplasties: multivariate survival analysis. BMC musculoskeletal disorders 8, 69.

Bouxsein, M.L., Seeman, E., 2009. Quantifying the material and structural determinants of bone strength. Best practice & research. Clinical rheumatology 23, 741-753.

Bragdon, C.R., Burke, D., Lowenstein, J.D., O'Connor, D.O., Ramamurti, B., Jasty, M., Harris, W.H., 1996. Differences in stiffness of the interface between a cementless porous implant and cancellous bone in vivo in dogs due to varying amounts of implant motion. The Journal of arthroplasty 11, 945-951.

Brinkmann, V., Radetzki, F., Gutteck, N., Delank, S., Zeh, A., 2017. Influence of varus/valgus positioning of the Nanos(R) and Metha(R) short-stemmed prostheses on stress shielding of metaphyseal bone. Acta orthopaedica Belgica 83, 57-66.

Brown, T.E., Larson, B., Shen, F., Moskal, J.T., 2002. Thigh pain after cementless total hip arthroplasty: evaluation and management. J Am Acad Orthop Surg 10, 385-392.

Bugbee, W.D., Culpepper, W.J., 2nd, Engh, C.A., Jr., Engh, C.A., Sr., 1997. Long-term clinical consequences of stress-shielding after total hip arthroplasty without cement. The Journal of bone and joint surgery. American volume 79, 1007-1012.

Burghardt, A.J., Pialat, J.B., Kazakia, G.J., Boutroy, S., Engelke, K., Patsch, J.M., Valentinitsch, A., Liu, D., Szabo, E., Bogado, C.E., Zanchetta, M.B., McKay, H.A., Shane, E., Boyd, S.K., Bouxsein, M.L., Chapurlat, R., Khosla, S., Majumdar, S., 2013. Multicenter precision of cortical and trabecular bone quality measures assessed by high-resolution peripheral quantitative computed tomography. Journal of bone and mineral research : the official journal of the American Society for Bone and Mineral Research 28, 524-536.

Burke, D.W., O'Connor, D.O., Zalenski, E.B., Jasty, M., Harris, W.H., 1991. Micromotion of cemented and uncemented femoral components. The Journal of bone and joint surgery. British volume 73, 33-37.

Capello, W.N., D'Antonio, J.A., Jaffe, W.L., Geesink, R.G., Manley, M.T., Feinberg, J.R., 2006. Hydroxyapatite-coated femoral components: 15-year minimum followup. Clinical orthopaedics and related research 453, 75-80.

Chang, G., Deniz, C.M., Honig, S., Rajapakse, C.S., Egol, K., Regatte, R.R., Brown, R., 2014. Feasibility of three-dimensional MRI of proximal femur microarchitecture at 3 tesla using 26 receive elements without and with parallel imaging. Journal of magnetic resonance imaging : JMRI 40, 229-238.

Charnley, J., 1961. Arthroplasty of the hip. A new operation. Lancet 1, 1129-1132.

Chevalier, Y., 2015. Numerical Methodology to Evaluate the Effects of Bone Density and Cement Augmentation on Fixation Stiffness of Bone-Anchoring Devices. Journal of biomechanical engineering 137.

Chevalier, Y., Matsuura, M., Kruger, S., Fleege, C., Rickert, M., Rauschmann, M., Schilling, C., 2018. Micro-CT and micro-FE analysis of pedicle screw fixation under different loading conditions. J Biomech 70, 204-211.

Chevalier, Y., Pahr, D., Zysset, P.K., 2009. The role of cortical shell and trabecular fabric in finite element analysis of the human vertebral body. Journal of biomechanical engineering 131, 111003.

Chevalier, Y., Santos, I., Muller, P.E., Pietschmann, M.F., 2016. Bone density and anisotropy affect periprosthetic cement and bone stresses after anatomical glenoid replacement: A micro finite element analysis. J Biomech 49, 1724-1733.

Christen, D., Melton, L.J., 3rd, Zwahlen, A., Amin, S., Khosla, S., Muller, R., 2013. Improved fracture risk assessment based on nonlinear micro-finite element simulations from HRpQCT images at the distal radius. Journal of bone and mineral research : the official journal of the American Society for Bone and Mineral Research 28, 2601-2608.

Cook, S.D., Thomas, K.A., Dalton, J.E., Volkman, T.K., Whitecloud, T.S., 3rd, Kay, J.F., 1992. Hydroxylapatite coating of porous implants improves bone ingrowth and interface attachment strength. Journal of biomedical materials research 26, 989-1001.

Cross, M., Smith, E., Hoy, D., Nolte, S., Ackerman, I., Fransen, M., Bridgett, L., Williams, S., Guillemin, F., Hill, C.L., Laslett, L.L., Jones, G., Cicuttini, F., Osborne, R., Vos, T., Buchbinder, R., Woolf, A., March, L., 2014. The global burden of hip and knee osteoarthritis: estimates from the global burden of disease 2010 study. Annals of the rheumatic diseases 73, 1323-1330.

Dallari, D., Stagni, C., Rani, N., Sabbioni, G., Pelotti, P., Torricelli, P., Tschon, M., Giavaresi, G., 2016. Ultrasound-Guided Injection of Platelet-Rich Plasma and Hyaluronic Acid, Separately and in Combination, for Hip Osteoarthritis: A Randomized Controlled Study. The American journal of sports medicine 44, 664-671.

Dame Carroll, J.R., Chandra, A., Jones, A.S., Berend, N., Magnussen, J.S., King, G.G., 2006. Airway dimensions measured from micro-computed tomography and high-resolution computed tomography. The European respiratory journal 28, 712-720.

Dammak, M., Shirazi-Adl, A., Zukor, D.J., 1997. Analysis of cementless implants using interface nonlinear friction--experimental and finite element studies. J Biomech 30, 121-129.

Dawson, J., Linsell, L., Zondervan, K., Rose, P., Randall, T., Carr, A., Fitzpatrick, R., 2004. Epidemiology of hip and knee pain and its impact on overall health status in older adults. Rheumatology 43, 497-504.

de Jong, J.J., Willems, P.C., Arts, J.J., Bours, S.G., Brink, P.R., van Geel, T.A., Poeze, M., Geusens, P.P., van Rietbergen, B., van den Bergh, J.P., 2014. Assessment of the healing process in distal radius fractures by high resolution peripheral quantitative computed tomography. Bone 64, 65-74.

de Lima Cavalcanti, J.H., Matos, P.C., Depes de Gouvea, C.V., Carvalho, W., Calvo-Guirado, J.L., Aragoneses, J.M., Perez-Diaz, L., Gehrke, S.A., 2019. In Vitro Assessment of the Functional Dynamics of Titanium with Surface Coating of Hydroxyapatite Nanoparticles. Materials 12.

Decking, R., Rokahr, C., Zurstegge, M., Simon, U., Decking, J., 2008. Maintenance of bone mineral density after implantation of a femoral neck hip prosthesis. BMC musculoskeletal disorders 9, 17.

Dempster, D.W., Compston, J.E., Drezner, M.K., Glorieux, F.H., Kanis, J.A., Malluche, H., Meunier, P.J., Ott, S.M., Recker, R.R., Parfitt, A.M., 2013. Standardized nomenclature, symbols, and units for bone histomorphometry: a 2012 update of the report of the ASBMR Histomorphometry Nomenclature Committee. Journal of bone and mineral research : the official journal of the American Society for Bone and Mineral Research 28, 2-17.

Dickinson, A.S., Taylor, A.C., Browne, M., 2010. Performance of the resurfaced hip. Part 1: the influence of the prosthesis size and positioning on the remodelling and fracture of the femoral neck. Proceedings of the Institution of Mechanical Engineers. Part H, Journal of engineering in medicine 224, 427-439.

Ding, M., Odgaard, A., Hvid, I., 1999. Accuracy of cancellous bone volume fraction measured by micro-CT scanning. J Biomech 32, 323-326.

Dolhain, P., Tsigaras, H., Bourne, R.B., Rorabeck, C.H., Mac Donald, S., Mc Calden, R., 2002. The effectiveness of dual offset stems in restoring offset during total hip replacement. Acta orthopaedica Belgica 68, 490-499.

Duan, J., Hu, C., Chen, H., 2013. High-resolution micro-CT for morphologic and quantitative assessment of the sinusoid in human cavernous hemangioma of the liver. PloS one 8, e53507.

Duda, G.N., Heller, M., Albinger, J., Schulz, O., Schneider, E., Claes, L., 1998. Influence of muscle forces on femoral strain distribution. J Biomech 31, 841-846.

Elliott, J.C., Dover, S.D., 1982. X-ray microtomography. Journal of microscopy 126, 211-213.

Ellouz, R., Chapurlat, R., van Rietbergen, B., Christen, P., Pialat, J.B., Boutroy, S., 2014. Challenges in longitudinal measurements with HR-pQCT: evaluation of a 3D registration method to improve bone microarchitecture and strength measurement reproducibility. Bone 63, 147-157.

Engh, C.A., Jr., Claus, A.M., Hopper, R.H., Jr., Engh, C.A., Sr., 2002. Long-term results using the anatomic medullary locking hip prosthesis. Hip international : the journal of clinical and experimental research on hip pathology and therapy 12, 94.

Engh, C.A., Jr., Young, A.M., Engh, C.A., Sr., Hopper, R.H., Jr., 2003. Clinical consequences of stress shielding after porous-coated total hip arthroplasty. Clinical orthopaedics and related research, 157-163.

Enoksen, C.H., Gjerdet, N.R., Klaksvik, J., Arthursson, A.J., Schnell-Husby, O., Wik, T.S., 2016. Deformation pattern and load transfer of an uncemented femoral stem with modular necks. An experimental study in human cadaver femurs. Clinical biomechanics 32, 28-33.

Enoksen, C.H., Wik, T.S., Klaksvik, J., Arthursson, A.J., Husby, O.S., Gjerdet, N.R., 2017. Load transfer in the proximal femur and primary stability of a cemented and uncemented femoral stem: An experimental study on cadaver femurs. Proceedings of the Institution of Mechanical Engineers. Part H, Journal of engineering in medicine 231, 1195-1203.

Falez, F., Casella, F., Panegrossi, G., Favetti, F., Barresi, C., 2008. Perspectives on metaphyseal conservative stems. J Orthop Traumatol 9, 49-54.

Fottner, A., Schmid, M., Birkenmaier, C., Mazoochian, F., Plitz, W., Volkmar, J., 2009. Biomechanical evaluation of two types of short-stemmed hip prostheses compared to the trust plate prosthesis by three-dimensional measurement of micromotions. Clinical biomechanics 24, 429-434.

Frost, H.M., 1994. Wolff's Law and bone's structural adaptations to mechanical usage: an overview for clinicians. The Angle orthodontist 64, 175-188.

Garcia Araujo, C., Fernandez Gonzalez, J., Tonino, A., 1998. Rheumatoid arthritis and hydroxyapatite-coated hip prostheses: five-year results. International ABG Study Group. The Journal of arthroplasty 13, 660-667.

Geesink, R.G., 2002. Osteoconductive coatings for total joint arthroplasty. Clinical orthopaedics and related research, 53-65.

Giliberty, R.P., 1983. Hemiarthroplasty of the hip using a low-friction bipolar endoprosthesis. Clinical orthopaedics and related research, 86-92.

Glassman, A.H., Bobyn, J.D., Tanzer, M., 2006. New femoral designs: do they influence stress shielding? Clinical orthopaedics and related research 453, 64-74.

Gronewold, J., Berner, S., Olender, G., Hurschler, C., Windhagen, H., von Lewinski, G., Floerkemeier, T., 2014. Changes in strain patterns after implantation of a short stem with metaphyseal anchorage compared to a standard stem: an experimental study in synthetic bone. Orthop Rev (Pavia) 6, 5211.

Guglielmi, G., Lang, T.F., 2002. Quantitative computed tomography. Seminars in musculoskeletal radiology 6, 219-227.

Gupta, S., van der Helm, F.C., Sterk, J.C., van Keulen, F., Kaptein, B.L., 2004. Development and experimental validation of a three-dimensional finite element model of the human scapula. Proceedings of the Institution of Mechanical Engineers. Part H, Journal of engineering in medicine 218, 127-142.

Gustke, K., 2012. Short stems for total hip arthroplasty: initial experience with the Fitmore stem. The Journal of bone and joint surgery. British volume 94, 47-51.

Hailer, N.P., Garellick, G., Karrholm, J., 2010. Uncemented and cemented primary total hip arthroplasty in the Swedish Hip Arthroplasty Register. Acta orthopaedica 81, 34-41.

Han, M., Chiba, K., Banerjee, S., Carballido-Gamio, J., Krug, R., 2015. Variable flip angle three-dimensional fast spin-echo sequence combined with outer volume suppression for imaging trabecular bone structure of the proximal femur. Journal of magnetic resonance imaging: JMRI 41, 1300-1310.

Harris, W.H., McGann, W.A., 1986. Loosening of the femoral component after use of the medullary-plug cementing technique. Follow-up note with a minimum five-year follow-up. The Journal of bone and joint surgery. American volume 68, 1064-1066.

Hefzy, M.S., Singh, S.P., 1997. Comparison between two techniques for modeling interface conditions in a porous coated hip endoprosthesis. Medical engineering & physics 19, 50-62.

Heller, M.O., Bergmann, G., Kassi, J.P., Claes, L., Haas, N.P., Duda, G.N., 2005. Determination of muscle loading at the hip joint for use in pre-clinical testing. J Biomech 38, 1155-1163.

Hemmila, M., Karvonen, M., Laaksonen, I., Matilainen, M., Eskelinen, A., Haapakoski, J., Puhto, A.P., Kettunen, J., Manninen, M., Makela, K.T., 2019. Survival of 11,390 Continuum cups in primary total hip arthroplasty based on data from the Finnish Arthroplasty Register. Acta orthopaedica, 1-10.

Hengsberger, S., Kulik, A., Zysset, P., 2002. Nanoindentation discriminates the elastic properties of individual human bone lamellae under dry and physiological conditions. Bone 30, 178-184.

Hildebrand, T., Laib, A., Muller, R., Dequeker, J., Ruegsegger, P., 1999. Direct three-dimensional morphometric analysis of human cancellous bone: microstructural data from spine, femur, iliac crest, and calcaneus. Journal of bone and mineral research : the official journal of the American Society for Bone and Mineral Research 14, 1167-1174.

Hildebrand, T., Ruegsegger, P., 1997. Quantification of Bone Microarchitecture with the Structure Model Index. Computer methods in biomechanics and biomedical engineering 1, 15-23.

Hozack, W., 1998. Ten Year Experience with a Wedge-Fit Stem. Presentation. Crucial Decisions in Total Joint Replacement and Sports Medicine.

Hozack, W., Gardiner, R., Hearn, S., Eng, K., Rothman, R., 1994. Taperloc femoral component. A 2-6-year study of the first 100 consecutive cases. The Journal of arthroplasty 9, 489-493.

Hu, L., O'Neil, M., Erturun, V., Benitez, R., Proust, G., Karaman, I., Radovic, M., 2016. High-Performance Metal/Carbide Composites with Far-From-Equilibrium Compositions and Controlled Microstructures. Scientific reports 6, 35523.

Huddleston, H.D., 1988. Femoral lysis after cemented hip arthroplasty. The Journal of arthroplasty 3, 285-297.

Huiskes, R., Weinans, H., Grootenboer, H.J., Dalstra, M., Fudala, B., Slooff, T.J., 1987. Adaptive bone-remodeling theory applied to prosthetic-design analysis. J Biomech 20, 1135-1150.

Ibrahim, H., Esfahani, S.N., Poorganji, B., Dean, D., Elahinia, M., 2017. Resorbable bone fixation alloys, forming, and post-fabrication treatments. Materials science & engineering. C, Materials for biological applications 70, 870-888.

Inoue, D., Kabata, T., Maeda, T., Kajino, Y., Yamamoto, T., Takagi, T., Ohmori, T., Tsuchiya, H., 2016. The correlation between clinical radiological outcome and contact state of implant and femur using three-dimensional templating software in cementless total hip arthroplasty. European journal of orthopaedic surgery & traumatology : orthopedie traumatologie 26, 591-598.

Isaacson, B., Jeyapalina, S., 2014. Osseointegration: a review of the fundamentals for assuring cementless skeletal fixation. Orthop Res Rev 6, 55-65.

Jameson, S.S., Mason, J., Baker, P.N., Gregg, P.J., Deehan, D.J., Reed, M.R., 2015. Implant Optimisation for Primary Hip Replacement in Patients over 60 Years with Osteoarthritis: A Cohort Study of Clinical Outcomes and Implant Costs Using Data from England and Wales. PloS one 10, e0140309.

Jasty, M., Bragdon, C., Burke, D., O'Connor, D., Lowenstein, J., Harris, W.H., 1997. In vivo skeletal responses to porous-surfaced implants subjected to small induced motions. The Journal of bone and joint surgery. American volume 79, 707-714.

Jayasuriya, R.L., Buckley, S.C., Hamer, A.J., Kerry, R.M., Stockley, I., Tomouk, M.W., Wilkinson, J.M., 2013. Effect of sliding-taper compared with composite-beam cemented femoral prosthesis loading regime on proximal femoral bone remodeling: a randomized clinical trial. The Journal of bone and joint surgery. American volume 95, 19-27.

Jordan, J.M., Helmick, C.G., Renner, J.B., Luta, G., Dragomir, A.D., Woodard, J., Fang, F., Schwartz, T.A., Nelson, A.E., Abbate, L.M., Callahan, L.F., Kalsbeek, W.D., Hochberg, M.C., 2009. Prevalence of hip symptoms and radiographic and symptomatic hip osteoarthritis in African Americans and Caucasians: the Johnston County Osteoarthritis Project. The Journal of rheumatology 36, 809-815.

Julius, Wolff, 1886. The law of bone remodelling. (trans: Maquet P, Furlong R) Springer, Berlin.

Kabel, J., Odgaard, A., van Rietbergen, B., Huiskes, R., 1999. Connectivity and the elastic properties of cancellous bone. Bone 24, 115-120.

Kabukcuoglu, Y., Grimer, R.J., Tillman, R.M., Carter, S.R., 1999. Endoprosthetic replacement for primary malignant tumors of the proximal femur. Clinical orthopaedics and related research, 8-14.

Kaipel, M., Grabowiecki, P., Sinz, K., Farr, S., Sinz, G., 2015. Migration characteristics and early clinical results of the NANOS(R) short-stem hip arthroplasty. Wiener klinische Wochenschrift 127, 375-378.

Kanis, J.A., Johnell, O., 2005. Requirements for DXA for the management of osteoporosis in Europe. Osteoporosis international : a journal established as result of cooperation between the European Foundation for Osteoporosis and the National Osteoporosis Foundation of the USA 16, 229-238.

Keaveny, T.M., Donley, D.W., Hoffmann, P.F., Mitlak, B.H., Glass, E.V., San Martin, J.A., 2007. Effects of teriparatide and alendronate on vertebral strength as assessed by finite element modeling of QCT scans in women with osteoporosis. Journal of bone and mineral research : the official journal of the American Society for Bone and Mineral Research 22, 149-157.

Keisu, K.S., Orozco, F., McCallum, J.D., 3rd, Bissett, G., Hozack, W.J., Sharkey, P.F., Rothman, R.H., 2001a. Cementless femoral fixation in the rheumatoid patient undergoing total hip arthroplasty: minimum 5-year results. The Journal of arthroplasty 16, 415-421.

Keisu, K.S., Orozco, F., Sharkey, P.F., Hozack, W.J., Rothman, R.H., McGuigan, F.X., 2001b. Primary cementless total hip arthroplasty in octogenarians. Two to eleven-year follow-up. The Journal of bone and joint surgery. American volume 83-A, 359-363.

Keyak, J.H., 2001. Improved prediction of proximal femoral fracture load using nonlinear finite element models. Medical engineering & physics 23, 165-173.

Keyak, J.H., Meagher, J.M., Skinner, H.B., Mote, C.D., Jr., 1990. Automated three-dimensional finite element modelling of bone: a new method. J Biomed Eng 12, 389-397.

Khanuja, H.S., Banerjee, S., Jain, D., Pivec, R., Mont, M.A., 2014. Short bone-conserving stems in cementless hip arthroplasty. The Journal of bone and joint surgery. American volume 96, 1742-1752.

Khanuja, H.S., Vakil, J.J., Goddard, M.S., Mont, M.A., 2011. Cementless femoral fixation in total hip arthroplasty. The Journal of bone and joint surgery. American volume 93, 500-509.

Kim, C., Linsenmeyer, K.D., Vlad, S.C., Guermazi, A., Clancy, M.M., Niu, J., Felson, D.T., 2014. Prevalence of radiographic and symptomatic hip osteoarthritis in an urban United States community: the Framingham osteoarthritis study. Arthritis & rheumatology 66, 3013-3017.

Kim, J.T., Yoo, J.J., 2016. Implant Design in Cementless Hip Arthroplasty. Hip & pelvis 28, 65-75.

Korhonen, R.K., Koistinen, A., Konttinen, Y.T., Santavirta, S.S., Lappalainen, R., 2005. The effect of geometry and abduction angle on the stresses in cemented UHMWPE acetabular cups--finite element simulations and experimental tests. Biomedical engineering online 4, 32.

Koutalos, A.A., Kourtis, A., Clarke, I.C., Smith, E.J., 2017. Mid-term results of ReCap/Magnum/Taperloc metal-on-metal total hip arthroplasty with mean follow-up of 7.1 years. Hip international : the journal of clinical and experimental research on hip pathology and therapy 27, 226-234.

Labek, G., Frischhut, S., Schlichtherle, R., Williams, A., Thaler, M., 2011. Outcome of the cementless Taperloc stem: a comprehensive literature review including arthroplasty register data. Acta orthopaedica 82, 143-148.

Laib, A., Newitt, D.C., Lu, Y., Majumdar, S., 2002. New model-independent measures of trabecular bone structure applied to in vivo high-resolution MR images. Osteoporosis international : a journal established as result of cooperation between the European Foundation for Osteoporosis and the National Osteoporosis Foundation of the USA 13, 130-136.

Lang, T.F., 2010. Quantitative computed tomography. Radiologic clinics of North America 48, 589-600.

Lazarinis, S., Karrholm, J., Hailer, N.P., 2011. Effects of hydroxyapatite coating on survival of an uncemented femoral stem. A Swedish Hip Arthroplasty Register study on 4,772 hips. Acta orthopaedica 82, 399-404.

Learmonth, I.D., Young, C., Rorabeck, C., 2007. The operation of the century: total hip replacement. Lancet 370, 1508-1519.

Lee, S.H., Lee, G.W., Seol, Y.J., Park, K.S., Yoon, T.R., 2017. Comparison of Outcomes of Total Hip Arthroplasty between Patients with Ankylosing Spondylitis and Avascular Necrosis of the Femoral Head. Clinics in orthopedic surgery 9, 263-269.

Limongi, R.M., Tao, J., Borba, A., Pereira, F., Pimentel, A.R., Akaishi, P., Velasco e Cruz, A.A., 2016. Complications and Management of Polymethylmethacrylate (PMMA) Injections to the Midface. Aesthetic surgery journal 36, 132-135.

Linde, F., Sorensen, H.C., 1993. The effect of different storage methods on the mechanical properties of trabecular bone. J Biomech 26, 1249-1252.

Liu, X.S., Sajda, P., Saha, P.K., Wehrli, F.W., Bevill, G., Keaveny, T.M., Guo, X.E., 2008. Complete volumetric decomposition of individual trabecular plates and rods and its morphological correlations with anisotropic elastic moduli in human trabecular bone. Journal of bone and mineral research : the official journal of the American Society for Bone and Mineral Research 23, 223-235.

Lumen, 2008. Appendicular Muscles of the Pelvic Girdle and Lower Limbs [Online]. Available: https://courses.lumenlearning.com/ap1/chapter/appendicular-muscles-of-the-pelvic-girdle-and-lower-limbs [Accessed January 22, 2021].

Macneil, J.A., Boyd, S.K., 2008a. Bone strength at the distal radius can be estimated from high-resolution peripheral quantitative computed tomography and the finite element method. Bone 42, 1203-1213.

MacNeil, J.A., Boyd, S.K., 2008b. Improved reproducibility of high-resolution peripheral quantitative computed tomography for measurement of bone quality. Medical engineering & physics 30, 792-799.

Makela, K.T., Eskelinen, A., Pulkkinen, P., Paavolainen, P., Remes, V., 2008. Total hip arthroplasty for primary osteoarthritis in patients fifty-five years of age or older. An analysis of the Finnish arthroplasty registry. The Journal of bone and joint surgery. American volume 90, 2160-2170.

Malchau, H., Wang, Y.X., Karrholm, J., Herberts, P., 1997. Scandinavian multicenter porous coated anatomic total hip arthroplasty study. Clinical and radiographic results with 7- to 10-year follow-up evaluation. The Journal of arthroplasty 12, 133-148.

Maquer, G., Musy, S.N., Wandel, J., Gross, T., Zysset, P.K., 2015. Bone volume fraction and fabric anisotropy are better determinants of trabecular bone stiffness than other morphological variables. Journal of bone and mineral research : the official journal of the American Society for Bone and Mineral Research 30, 1000-1008.

Mariconda, M., Costa, G., Misasi, M., Recano, P., Balato, G., Rizzo, M., 2017. Ambulatory Ability and Personal Independence After Hemiarthroplasty and Total Arthroplasty for Intracapsular Hip Fracture: A Prospective Comparative Study. The Journal of arthroplasty 32, 447-452.

Mazza, G., Franzoso, G., Pretterklieber, M., Zysset, P., 2008. Anisotropic elastic properties of vertebral compact bone measured by microindentation. In: 16th Congress of the European Society of Biomechanics July 6-9, 2008. Lucerne, Switzerland.

McGrory, B.J., Morrey, B.F., Cahalan, T.D., An, K.N., Cabanela, M.E., 1995. Effect of femoral offset on range of motion and abductor muscle strength after total hip arthroplasty. The Journal of bone and joint surgery. British volume 77, 865-869.

McKellop, H., Ebramzadeh, E., Niederer, P.G., Sarmiento, A., 1991. Comparison of the stability of press-fit hip prosthesis femoral stems using a synthetic model femur. J Orthop Res 9, 297-305.

McLaughlin, J.R., Lee, K.R., 2008. Total hip arthroplasty with an uncemented tapered femoral component. The Journal of bone and joint surgery. American volume 90, 1290-1296.

McLaughlin, J.R., Lee, K.R., 2016. Long-term results of uncemented total hip arthroplasty with the Taperloc femoral component in patients with Dorr type C proximal femoral morphology. The bone & joint journal 98-B, 595-600.

McNally, S.A., Shepperd, J.A., Mann, C.V., Walczak, J.P., 2000. The results at nine to twelve years of the use of a hydroxyapatite-coated femoral stem. The Journal of bone and joint surgery. British volume 82, 378-382.

Meding, J.B., Keating, E.M., Ritter, M.A., Faris, P.M., Berend, M.E., 2004. Minimum ten-year follow-up of a straight-stemmed, plasma-sprayed, titanium-alloy, uncemented femoral component in primary total hip arthroplasty. The Journal of bone and joint surgery. American volume 86-A, 92-97.

Meding, J.B., Nassif, J.M., Ritter, M.A., 2000. Long-term survival of the T-28 versus the TR-28 cemented total hip arthroplasties. The Journal of arthroplasty 15, 928-933.

Meredith, N., Alleyne, D., Cawley, P., 1996. Quantitative determination of the stability of the implant-tissue interface using resonance frequency analysis. Clinical oral implants research 7, 261-267.

Meyer, U., de Jong, J.J., Bours, S.G., Keszei, A.P., Arts, J.J., Brink, P.R., Menheere, P., van Geel, T.A., van Rietbergen, B., van den Bergh, J.P., Geusens, P.P., Willems, P.C., 2014. Early changes in bone density, microarchitecture, bone resorption, and inflammation predict the clinical outcome 12 weeks after conservatively treated distal radius fractures: an exploratory study. Journal of bone and mineral research : the official journal of the American Society for Bone and Mineral Research 29, 2065-2073.

Miller, P.D., Zapalowski, C., Kulak, C.A., Bilezikian, J.P., 1999. Bone densitometry: the best way to detect osteoporosis and to monitor therapy. The Journal of clinical endocrinology and metabolism 84, 1867-1871.

Morrey, B.F., 1989. Short-stemmed uncemented femoral component for primary hip arthroplasty. Clinical orthopaedics and related research, 169-175.

Morrey, B.F., Adams, R.A., Kessler, M., 2000. A conservative femoral replacement for total hip arthroplasty. A prospective study. The Journal of bone and joint surgery. British volume 82, 952-958.

Mueller, T.L., Christen, D., Sandercott, S., Boyd, S.K., van Rietbergen, B., Eckstein, F., Lochmuller, E.M., Muller, R., van Lenthe, G.H., 2011. Computational finite element bone mechanics accurately predicts mechanical competence in the human radius of an elderly population. Bone 48, 1232-1238.

Muller, M., Abdel, M.P., Wassilew, G.I., Duda, G., Perka, C., 2015. Do post-operative changes of neck-shaft angle and femoral component anteversion have an effect on clinical outcome following uncemented total hip arthroplasty? The bone & joint journal 97-B, 1615-1622.

Muller, R., Hildebrand, T., Ruegsegger, P., 1994. Non-invasive bone biopsy: a new method to analyse and display the three-dimensional structure of trabecular bone. Physics in medicine and biology 39, 145-164.

Nadzadi, M.E., Pedersen, D.R., Callaghan, J.J., Brown, T.D., 2002. Effects of acetabular component orientation on dislocation propensity for small-head-size total hip arthroplasty. Clinical biomechanics 17, 32-40.

Nichols, C.I., Vose, J.G., Nunley, R.M., 2017. Clinical Outcomes and 90-Day Costs Following Hemiarthroplasty or Total Hip Arthroplasty for Hip Fracture. The Journal of arthroplasty 32, S128-S134.

Niebur, G.L., Feldstein, M.J., Yuen, J.C., Chen, T.J., Keaveny, T.M., 2000. High-resolution finite element models with tissue strength asymmetry accurately predict failure of trabecular bone. J Biomech 33, 1575-1583.

Nkenke, E., Hahn, M., Weinzierl, K., Radespiel-Troger, M., Neukam, F.W., Engelke, K., 2003. Implant stability and histomorphometry: a correlation study in human cadavers using stepped cylinder implants. Clinical oral implants research 14, 601-609.

Odgaard, A., 1997. Three-dimensional methods for quantification of cancellous bone architecture. Bone 20, 315-328.

Odgaard, A., Gundersen, H.J., 1993. Quantification of connectivity in cancellous bone, with special emphasis on 3-D reconstructions. Bone 14, 173-182.

Oliveria, S.A., Felson, D.T., Reed, J.I., Cirillo, P.A., Walker, A.M., 1995. Incidence of symptomatic hand, hip, and knee osteoarthritis among patients in a health maintenance organization. Arthritis and rheumatism 38, 1134-1141.

Orlik, J., Zhurov, A., Middleton, J., 2003. On the secondary stability of coated cementless hip replacement: parameters that affected interface strength. Medical engineering & physics 25, 825-831.

OrthoInfo, 2019. Hip Osteoarthritis [Online]. Available: https://orthoinfo.aaos.org/en/treatment/total-hip-replacement [Accessed January 22, 2021].

Ostbyhaug, P.O., Klaksvik, J., Romundstad, P., Aamodt, A., 2010. Primary stability of custom and anatomical uncemented femoral stems: a method for three-dimensional in vitro measurement of implant stability. Clinical biomechanics 25, 318-324.

Paggiosi, M.A., Eastell, R., Walsh, J.S., 2014. Precision of high-resolution peripheral quantitative computed tomography measurement variables: influence of gender, examination site, and age. Calcified tissue international 94, 191-201.

Pang, Q.J., Yu, X., Chen, X.J., Yin, Z.C., He, G.Z., 2013. The management of acetabular malunion with traumatic arthritis by total hip arthroplasty. Pakistan journal of medical sciences 29, 191-196.

Parfitt, A.M., Drezner, M.K., Glorieux, F.H., Kanis, J.A., Malluche, H., Meunier, P.J., Ott, S.M., Recker, R.R., 1987. Bone histomorphometry: standardization of nomenclature, symbols, and units. Report of the ASBMR Histomorphometry Nomenclature Committee. Journal of bone and mineral research : the official journal of the American Society for Bone and Mineral Research 2, 595-610.

Parvizi, J., Keisu, K.S., Hozack, W.J., Sharkey, P.F., Rothman, R.H., 2004. Primary total hip arthroplasty with an uncemented femoral component: a long-term study of the Taperloc stem. The Journal of arthroplasty 19, 151-156.

Paschalis, E.P., Betts, F., DiCarlo, E., Mendelsohn, R., Boskey, A.L., 1997. FTIR microspectroscopic analysis of human iliac crest biopsies from untreated osteoporotic bone. Calcified tissue international 61, 487-492.

Peeters, C.M., Visser, E., Van de Ree, C.L., Gosens, T., Den Oudsten, B.L., De Vries, J., 2016. Quality of life after hip fracture in the elderly: A systematic literature review. Injury 47, 1369-1382.

Pettersen, S.H., Wik, T.S., Skallerud, B., 2009. Subject specific finite element analysis of stress shielding around a cementless femoral stem. Clinical biomechanics 24, 196-202.

Pilliar, R.M., Lee, J.M., Maniatopoulos, C., 1986. Observations on the effect of movement on bone ingrowth into porous-surfaced implants. Clinical orthopaedics and related research, 108-113.

Pipino, F., 2004. CFP prosthetic stem in mini-invasive total hip arthroplasty. Journal of Orthopaedics and Traumatology 5, 165-171.

Pipino, F., Molfetta, L., Grandizio, M., 2000. Preservation of the femoral neck in hip arthroplasty: results of a 13-to 17-year follow-up. Journal of Orthopaedics and Traumatology 1, 31-39.

Pistoia, W., van Rietbergen, B., Lochmuller, E.M., Lill, C.A., Eckstein, F., Ruegsegger, P., 2004. Image-based micro-finite-element modeling for improved distal radius strength diagnosis: moving from bench to bedside. Journal of clinical densitometry : the official journal of the International Society for Clinical Densitometry 7, 153-160.

Pyda, M., Koczy, B., Widuchowski, W., Widuchowska, M., Stoltny, T., Mielnik, M., Hermanson, J., 2015. Hip resurfacing arthroplasty in treatment of avascular necrosis of the femoral head. Medical science monitor: international medical journal of experimental and clinical research 21, 304-309.

Rachner, T.D., Khosla, S., Hofbauer, L.C., 2011. Osteoporosis: now and the future. Lancet 377, 1276-1287.

Radcliffe, I.A., Prescott, P., Man, H.S., Taylor, M., 2007. Determination of suitable sample sizes for multi-patient based finite element studies. Medical engineering & physics 29, 1065-1072.

Ravi, B., Pincus, D., Khan, H., Wasserstein, D., Jenkinson, R., Kreder, H.J., 2019. Comparing Complications and Costs of Total Hip Arthroplasty and

Hemiarthroplasty for Femoral Neck Fractures: A Propensity Score-Matched, Population-Based Study. The Journal of bone and joint surgery. American volume 101, 572-579.

Reddy, J.N., 2006. An introduction to the finite element method, 3rd ed. McGraw-Hill Higher Education, New York, NY.

Reggiani, B., Cristofolini, L., Taddei, F., Viceconti, M., 2008. Sensitivity of the primary stability of a cementless hip stem to its position and orientation. Artif Organs 32, 555-560.

Reggiani, B., Cristofolini, L., Varini, E., Viceconti, M., 2007. Predicting the subject-specific primary stability of cementless implants during pre-operative planning: preliminary validation of subject-specific finite-element models. J Biomech 40, 2552-2558.

Reimeringer, M., Nuno, N., 2016. The influence of contact ratio and its location on the primary stability of cementless total hip arthroplasty: A finite element analysis. J Biomech 49, 1064-1070.

Renders, G.A., Mulder, L., Langenbach, G.E., van Ruijven, L.J., van Eijden, T.M., 2008. Biomechanical effect of mineral heterogeneity in trabecular bone. J Biomech 41, 2793-2798.

Ridzwan, M., Shuib, S., Hassan, A., Shokri, A., Ibrahim, M.M., 2007. Problem of stress shielding and improvement to the hip implant designs: a review. J. Med. Sci 7, 460-467.

Roache, P.B., 2012. Hip Joint Anatomy [Online]. Available: https://www.jasonyoga.com/2015/11/21/yoga-anatomy-of-hips [Accessed January 22, 2021].

Rohlmann, A., Cheal, E.J., Hayes, W.C., Bergmann, G., 1988. A nonlinear finite element analysis of interface conditions in porous coated hip endoprostheses. J Biomech 21, 605-611.

Rohlmann, A., Mossner, U., Bergmann, G., Hees, G., Kolbel, R., 1987. Effects of stem design and material properties on stresses in hip endoprostheses. J Biomed Eng 9, 77-83.

Rolfson, O., Donahue, G.S., Hallsten, M., Garellick, G., Karrholm, J., Nemes, S., 2016. Patient-reported outcomes in cemented and uncemented total hip replacements. Hip international : the journal of clinical and experimental research on hip pathology and therapy 26, 451-457.

Ruben, R.B., Fernandes, P.R., Folgado, J., 2012. On the optimal shape of hip implants. J Biomech 45, 239-246.

Ruegsegger, P., Koller, B., Muller, R., 1996. A microtomographic system for the nondestructive evaluation of bone architecture. Calcified tissue international 58, 24-29.

Ruff, C., Holt, B., Trinkaus, E., 2006. Who's afraid of the big bad Wolff?: "Wolff's law" and bone functional adaptation. American journal of physical anthropology 129, 484-498.

Sano, H., Takahashi, A., Chiba, D., Hatta, T., Yamamoto, N., Itoi, E., 2013. Stress distribution inside bone after suture anchor insertion: simulation using a three-dimensional finite element method. Knee surgery, sports traumatology, arthroscopy : official journal of the ESSKA 21, 1777-1782.

Schileo, E., Taddei, F., Malandrino, A., Cristofolini, L., Viceconti, M., 2007. Subject-specific finite element models can accurately predict strain levels in long bones. J Biomech 40, 2982-2989.

Schliephake, H., Sewing, A., Aref, A., 2006. Resonance frequency measurements of implant stability in the dog mandible: experimental comparison with histomorphometric data. International journal of oral and maxillofacial surgery 35, 941-946.

Schmidler, C., 2018. The Hip Joint Replacement Surgery. [Online]. Available: https://www.healthpages.org/surgical-care/hip-joint-replacement-surgery [Accessed January 22, 2021].

Schmidutz, F., Wanke-Jellinek, L., Jansson, V., Fottner, A., Mazoochian, F., 2012. Revision of hip resurfacing arthroplasty with a bone-conserving short-stem implant: a case report and review of the literature. J Med Case Rep 6, 249.

Schmidutz, F., Woiczinski, M., Kistler, M., Schroder, C., Jansson, V., Fottner, A., 2017. Influence of different sizes of composite femora on the biomechanical behavior of cementless hip prosthesis. Clinical biomechanics 41, 60-65.

Schneider, R., 2013. Imaging of osteoporosis. Rheumatic diseases clinics of North America 39, 609-631.

Schnurr C., Schellen B., Dargel J., Beckmann J., Eysel P., Steffen R., 2017. Low Short-Stem Revision Rates: 1-11 Year Results From 1888 Total Hip Arthroplasties. J Arthroplasty 32:487-493.

Schünke, M., Schulte, E., Schumacher, U., 2015. Thieme atlas of anatomy. General anatomy and musculoskeletal system, 2nd edition, Latin nomenclature. ed. Thieme, New York.

Schwarz, E., Reinisch, G., Brandauer, A., Aharinejad, S., Scharf, W., Trieb, K., 2018. Load transfer and periprosthetic fractures after total hip arthoplasty: Comparison of periprosthetic fractures of femora implanted with cementless distal-load or proximal-load femoral components and measurement of the femoral strain at the time of implantation. Clinical biomechanics 54, 137-142.

Seeman, E., 2008. Bone quality: the material and structural basis of bone strength. Journal of bone and mineral metabolism 26, 1-8.

Seeman, E., Delmas, P.D., 2006. Bone quality--the material and structural basis of bone strength and fragility. The New England journal of medicine 354, 2250-2261.

Sennerby, L., Meredith, N., 2008. Implant stability measurements using resonance frequency analysis: biological and biomechanical aspects and clinical implications. Periodontology 2000 47, 51-66.

Skinner, H.B., Kim, A.S., Keyak, J.H., Mote, C.D., Jr., 1994. Femoral prosthesis implantation induces changes in bone stress that depend on the extent of porous coating. J Orthop Res 12, 553-563.

Smith, A.J., Dieppe, P., Howard, P.W., Blom, A.W., National Joint Registry for, E., Wales, 2012. Failure rates of metal-on-metal hip resurfacings: analysis of data from the National Joint Registry for England and Wales. Lancet 380, 1759-1766.

Soballe, K., Brockstedt-Rasmussen, H., Hansen, E.S., Bunger, C., 1992a. Hydroxyapatite coating modifies implant membrane formation. Controlled micromotion studied in dogs. Acta orthopaedica Scandinavica 63, 128-140.

Soballe, K., Hansen, E.S., Brockstedt-Rasmussen, H., Bunger, C., 1993. Hydroxyapatite coating converts fibrous tissue to bone around loaded implants. The Journal of bone and joint surgery. British volume 75, 270-278.

Soballe, K., Hansen, E.S., Brockstedt-Rasmussen, H., Hjortdal, V.E., Juhl, G.I., Pedersen, C.M., Hvid, I., Bunger, C., 1991. Gap healing enhanced by hydroxyapatite coating in dogs. Clinical orthopaedics and related research, 300-307.

Soballe, K., Hansen, E.S., H, B.R., Jorgensen, P.H., Bunger, C., 1992b. Tissue ingrowth into titanium and hydroxyapatite-coated implants during stable and unstable mechanical conditions. J Orthop Res 10, 285-299.

Sokolove, J., Lepus, C.M., 2013. Role of inflammation in the pathogenesis of osteoarthritis: latest findings and interpretations. Therapeutic advances in musculoskeletal disease 5, 77-94.

Sophia Fox, A.J., Bedi, A., Rodeo, S.A., 2009. The basic science of articular cartilage: structure, composition, and function. Sports Health 1, 461-468.

Statistisches Bundesamt, 2005 to 2016. Fallpauschalenbezogene Krankenhausstatistik (DRG-Statistik). Operationen und Prozeduren der vollstationären Patientinnen und Patienten in Krankenhäusern - Ausführliche Darstellung. Wiesbaden.

Steinberg, M.E., Corces, A., Fallon, M., 1999. Acetabular involvement in osteonecrosis of the femoral head. The Journal of bone and joint surgery. American volume 81, 60-65.

Steiner, J.A., Christen, P., Affentranger, R., Ferguson, S.J., van Lenthe, G.H., 2017. A novel in silico method to quantify primary stability of screws in trabecular bone. J Orthop Res 35, 2415-2424.

Steiner, J.A., Ferguson, S.J., van Lenthe, G.H., 2015. Computational analysis of primary implant stability in trabecular bone. J Biomech 48, 807-815.

Steultjens, M.P., Dekker, J., van Baar, M.E., Oostendorp, R.A., Bijlsma, J.W., 2000. Range of joint motion and disability in patients with osteoarthritis of the knee or hip. Rheumatology 39, 955-961.

Steultjens, M.P., Dekker, J., van Baar, M.E., Oostendorp, R.A., Bijlsma, J.W., 2001. Muscle strength, pain and disability in patients with osteoarthritis. Clinical rehabilitation 15, 331-341.

Stiehl, J.B., 1993. Optimum pressfit and proximal stress transfer with an improved modular design in total hip arthroplasty. Seminars in arthroplasty 4, 167-171.

Stirton, J.B., Maier, J.C., Nandi, S., 2019. Total hip arthroplasty for the management of hip fracture: A review of the literature. Journal of orthopaedics 16, 141-144.

Streit, M.R., Innmann, M.M., Merle, C., Bruckner, T., Aldinger, P.R., Gotterbarm, T., 2013. Long-term (20- to 25-year) results of an uncemented tapered titanium femoral component and factors affecting survivorship. Clinical orthopaedics and related research 471, 3262-3269.

Stucinskas, J., Clauss, M., Tarasevicius, S., Wingstrand, H., Ilchmann, T., 2012. Long-term femoral bone remodeling after cemented hip arthroplasty with the Muller straight stem in the operated and nonoperated femora. The Journal of arthroplasty 27, 927-933.

Stukenborg-Colsman, C.M., von der Haar-Tran, A., Windhagen, H., Bouguecha, A., Wefstaedt, P., Lerch, M., 2012. Bone remodelling around a cementless straight THA stem: a prospective dual-energy X-ray absorptiometry study. Hip international : the journal of clinical and experimental research on hip pathology and therapy 22, 166-171.

Taddei, F., Cristofolini, L., Martelli, S., Gill, H.S., Viceconti, M., 2006. Subject-specific finite element models of long bones: An in vitro evaluation of the overall accuracy. J Biomech 39, 2457-2467.

Tahim, A.S., Stokes, O.M., Vedi, V., 2012. The effect of femoral stem length on duration of hospital stay. Hip international : the journal of clinical and experimental research on hip pathology and therapy 22, 56-61.

Tarala, M., Janssen, D., Telka, A., Waanders, D., Verdonschot, N., 2011. Experimental versus computational analysis of micromotions at the implant-bone interface. Proceedings of the Institution of Mechanical Engineers. Part H, Journal of engineering in medicine 225, 8-15.

Toni A., Giardina F., Guerra G., Sudanese A., Montalti M., Stea S., Bordini B., 2017. 3rd generation alumina-on-alumina in modular hip prosthesis: 13 to 18 years follow-up results. Hip Int 27:8-13.

Torcasio, A., Zhang, X., Van Oosterwyck, H., Duyck, J., van Lenthe, G.H., 2012. Use of micro-CT-based finite element analysis to accurately quantify peri-implant bone strains: a validation in rat tibiae. Biomechanics and modeling in mechanobiology 11, 743-750.

Tsertsvadze, A., Grove, A., Freeman, K., Court, R., Johnson, S., Connock, M., Clarke, A., Sutcliffe, P., 2014. Total hip replacement for the treatment of end stage arthritis of the hip: a systematic review and meta-analysis. PloS one 9, e99804.

Tudor, F.S., Donaldson, J.R., Rodriguez-Elizalde, S.R., Cameron, H.U., 2015. Long-Term Comparison of Porous Versus Hydroxyapatite Coated Sleeve of a Modular Cementless Femoral Stem (SROM) in Primary Total Hip Arthroplasty. The Journal of arthroplasty 30, 1777-1780.

Tuncay, I., Yildiz, F., Bilsel, K., Uzer, G., Elmadag, M., Erden, T., Bozdag, E., 2016. Biomechanical Comparison of 2 Different Femoral Stems in the Shortening Osteotomy of the High-Riding Hip. The Journal of arthroplasty 31, 1346-1351.

Uchiyama, T., Tanizawa, T., Muramatsu, H., Endo, N., Takahashi, H.E., Hara, T., 1999. Three-dimensional microstructural analysis of human trabecular bone in relation to its mechanical properties. Bone 25, 487-491.

Unnanuntana, A., Dimitroulias, A., Bolognesi, M.P., Hwang, K.L., Goodman, S.B., Marcus, R.E., 2009. Cementless femoral prostheses cost more to implant than cemented femoral prostheses. Clinical orthopaedics and related research 467, 1546-1551.

van Oldenrijk, J., Molleman, J., Klaver, M., Poolman, R.W., Haverkamp, D., 2014. Revision rate after short-stem total hip arthroplasty: a systematic review of 49 studies. Acta orthopaedica 85, 250-258.

van Rietbergen, B., 2001. Micro-FE analyses of bone: state of the art. Advances in experimental medicine and biology 496, 21-30.

van Rietbergen, B., Majumdar, S., Pistoia, W., Newitt, D.C., Kothari, M., Laib, A., Ruegsegger, P., 1998. Assessment of cancellous bone mechanical properties from micro-FE models based on micro-CT, pQCT and MR images. Technology and health care : official journal of the European Society for Engineering and Medicine 6, 413-420.

van Rietbergen, B., Weinans, H., Huiskes, R., Odgaard, A., 1995. A new method to determine trabecular bone elastic properties and loading using micromechanical finite-element models. J Biomech 28, 69-81.

Varga, P., Pahr, D.H., Baumbach, S., Zysset, P.K., 2010. HR-pQCT based FE analysis of the most distal radius section provides an improved prediction of Colles' fracture load in vitro. Bone 47, 982-988.

Viceconti, M., Monti, L., Muccini, R., Bernakiewicz, M., Toni, A., 2001. Even a thin layer of soft tissue may compromise the primary stability of cementless hip stems. Clinical biomechanics 16, 765-775.

Viceconti, M., Muccini, R., Bernakiewicz, M., Baleani, M., Cristofolini, L., 2000. Large-sliding contact elements accurately predict levels of bone-implant micromotion relevant to osseointegration. J Biomech 33, 1611-1618.

Viceconti, M., Pancanti, A., Dotti, M., Traina, F., Cristofolini, L., 2004. Effect of the initial implant fitting on the predicted secondary stability of a cementless stem. Medical & biological engineering & computing 42, 222-229.

Viceconti, M., Pancanti, A., Varini, E., Traina, F., Cristofolini, L., 2006. On the biomechanical stability of cementless straight conical hip stems. Proceedings of the Institution of Mechanical Engineers. Part H, Journal of engineering in medicine 220, 473-480.

Walker, M.D., Liu, X.S., Stein, E., Zhou, B., Bezati, E., McMahon, D.J., Udesky, J., Liu, G., Shane, E., Guo, X.E., Bilezikian, J.P., 2011. Differences in bone microarchitecture between postmenopausal Chinese-American and white women. Journal of bone and mineral research: the official journal of the American Society for Bone and Mineral Research 26, 1392-1398.

Wang, Z., Bhattacharyya, T., 2017. Outcomes of Hemiarthroplasty and Total Hip Arthroplasty for Femoral Neck Fracture: A Medicare Cohort Study. Journal of orthopaedic trauma 31, 260-263.

Weinans, H., Sumner, D.R., Igloria, R., Natarajan, R.N., 2000. Sensitivity of periprosthetic stress-shielding to load and the bone density-modulus relationship in subject-specific finite element models. J Biomech 33, 809-817.

Westphal, F.M., Bishop, N., Honl, M., Hille, E., Puschel, K., Morlock, M.M., 2006. Migration and cyclic motion of a new short-stemmed hip prosthesis--a biomechanical in vitro study. Clinical biomechanics 21, 834-840.

Whiteside, L.A., White, S.E., Engh, C.A., Head, W., 1993. Mechanical evaluation of cadaver retrieval specimens of cementless bone-ingrown total hip arthroplasty femoral components. The Journal of arthroplasty 8, 147-155.

Whittle, M., 2003. Gait analysis: an introduction, 3rd ed. Butterworth-Heinemann, Edinburgh; New York.

Wilkinson, J.M., Hamer, A.J., Rogers, A., Stockley, I., Eastell, R., 2003. Bone mineral density and biochemical markers of bone turnover in aseptic loosening after total hip arthroplasty. J Orthop Res 21, 691-696.

Wirth, A.J., Goldhahn, J., Flaig, C., Arbenz, P., Muller, R., van Lenthe, G.H., 2011. Implant stability is affected by local bone microstructural quality. Bone 49, 473-478.

Woolf, A.D., Erwin, J., March, L., 2012. The need to address the burden of musculoskeletal conditions. Best practice & research. Clinical rheumatology 26, 183-224.

Yan, S., 2019. Evaluation of the initial fixation, stress distribution and revision of short stem hip arthroplasty: A biomechanical study and finite element analysis.

Yan, S.G., Woiczinski, M., Schmidutz, T.F., Weber, P., Paulus, A.C., Steinbruck, A., Jansson, V., Schmidutz, F., 2017. Can the metaphyseal anchored Metha short stem safely be revised with a standard CLS stem? A biomechanical analysis. International orthopaedics 41, 2471-2477.

Yuasa, T., Maezawa, K., Nozawa, M., Kaneko, K., 2016. Cementless total hip arthroplasty for patients with rheumatoid arthritis: a more than 10-year follow-up. European journal of orthopaedic surgery & traumatology: orthopedie traumatologie 26, 599-603.

Zachariah, S.G., Sanders, J.E., 2000. Finite element estimates of interface stress in the trans-tibial prosthesis using gap elements are different from those using automated contact. J Biomech 33, 895-899.

Zhou, B., Liu, X.S., Wang, J., Lu, X.L., Fields, A.J., Guo, X.E., 2014. Dependence of mechanical properties of trabecular bone on plate-rod microstructure determined by individual trabecula segmentation (ITS). J Biomech 47, 702-708.

Zinger, O., Anselme, K., Denzer, A., Habersetzer, P., Wieland, M., Jeanfils, J., Hardouin, P., Landolt, D., 2004. Time-dependent morphology and adhesion of osteoblastic cells on titanium model surfaces featuring scale-resolved topography. Biomaterials 25, 2695-2711.

12 List of Figures and Tables

13 Abbreviations

3D	Three dimensional
AMA	Abductor moment arm
AMF	Abductor muscle force
BMA	Body weight moment arm
BMD	Bone mineral density
BMI	Body mass index
BV	Bone volume
BV/TV	Bone volume fraction
BWF	Body weight force
CGAL	Computational Geometry Algorithms Library
cm	Centimeter
CT	Computed tomography
DXA	Dual energy X-ray absorptiometry
FE	Finite element
FEA	Finite element analysis
g	Gram
GB	Giga Byte
HA	Hydroxyapatite
HRCT	High-resolution CT
ITK	Insight Toolkit
JCF	Joint contact force
Kg	Kilogram
L	Left

LVDTs	Linear variable differential transformers
m	Meter
mm	Millimeter
MR	Magnetic resonance
MRI	Magnetic resonance imaging
PMMA	Polymethylmethacrylate
PPS	Porous plasma spray
QCT	Quantitative CT
R	Right
RAM	Random access memory
ROM	Range of motion
SD	Standard deviation
THA	Total hip arthroplasty
TV	Total bone volume
µm	Micrometer
VOI	Volume of interest

14 Acknowledgements

First and foremost, I would like to thank Prof. Dr. med. Dipl.-Ing. Volkmar Jansson and my supervisor Prof. Dr. med. Peter E. Müller, respectively, Director and Deputy Director of the Orthopädischen Klinik der Ludwig-Maximilians-Universität am Klinikum Großhadern, who provided me many precious opportunities and constant support during my Doctorate thesis at their institute and under their supervisions.

I would also like to acknowledge the contributions of several collaborators who contributed to some of the technical aspects of this work, especially in the planning phases prior to our work on image-based analyses. In particular, I would like to thank Prof. Thomas Grupp and Dr. Christoph Schilling, from Aesculap, for having provided financial support for the study which allowed me to perform these analyses. Additional thanks to Prof. Jan-Philippe Kretzer and Dr. Sebastian Jäger at the Labor für Biomechanik und Implantatforschung, Heidelberg, for specimen preparation and testing; Prof. Hadi Mozaffari-Jovein at the Furtwangen University, HFU · Faculty of Industrial Technologies, Tuttlingen for the micro-CT scanning; Prof. Dr. med. Peter Aldinger (Diakonie Klinikum & Paulinenhilfe gGmbH, Stuttgart, Germany) and Prof. Dr. med. Michael Clarius (Department of Orthopaedic and Trauma Surgery, Vulpius Klinik, Bad Rappenau, Germany) for the implantations. I also would like to thank Mrs Maiko Fertmann-Matsuura for her initial involvement in this work.

Grateful thanks go to my co-supervisor, Dr. techn. Yan Chevalier, who supported my work in this way and helped me get results of better quality for his precious assistances in my project and articles. There are many things he has taught me, but nothing was more precious than his enthusiasm and attitudes towards the science and project.

A similar gratitude belongs to the warm-hearted staffs in department of Orthopaedic surgery, Physical Medicine and Rehabilitation in the Grosshadern hospital of the University of Munich.

I also appreciate all the helps from the staffs in the Lab of Biomechanics and Experimental Orthopedics, Roland Manfred Klar, PhD, Dipl.-Ing. Ines Santos, Dr. rer. biol. hum. Matthias Woiczinski, Dipl.-Ing. Michael Kraxenberger, Dr. biol. hum. Oliver Betz, Christoph Thorwächter, Anna-Katharina Krombholz, Felix Uhlemann, Christian Vahrson, Toffey, Ute Brooks, Chi Chak, because they have lent a hand to me whenever I need help with their more enthusiasms, chariness and patience.

I would like to thank my brothers and friends from China, Shuanggen Yan, Fei Xiong, Xiangyun Cheng, Tao He, Yijiang Huang, Ren Bin, Qingyu Zhang, etc, because I think that they treat me is like to treat friends with full of enthusiasm and thoughtful.

I would like to thank my family: parents, wife, daughter, brother, niece and nephew for their continuous support. There is too much I want to say but so little that can be expressed. Last but not the least, I would like to thank China Scholarship Council for her providing funding to support my life, study and work.